Report No: 24000/8/14

Date 26 November 2014

For: Department for Transport

Department for Transport Technical Assessment of Petroleum Tankers: Work Package 2 – Detailed Engineering Critical Assessment

TWI Ltd

TWI is one of the world's foremost independent research and technology organisations, with expertise in solving problems in all aspects of manufacturing, fabrication and whole-life integrity management technologies.

Established at Abington, Cambridge, UK in 1946 and with facilities across the globe, the company has a first-class reputation for service through its teams of internationally respected consultants, scientists, engineers and support staff. The company employs over 900 staff, serving over 700 Member companies across 4500 sites in 80 countries.

TWI is a non-profit distributing company, limited by guarantee and owned by its Members. It can therefore offer confidential, independent advice and is internationally renowned for employing multidisciplinary teams to implement established or advanced joining technology or to address issues associated with initial design, materials selection, production and quality assurance, through to service performance and repair.

Supported by a successful international training and examinations network, TWI also takes technical and practical knowhow to regions looking for growth through skills development.

TWI houses the National Structural Integrity Research Centre for postgraduate education, and a professional institution, The Welding Institute, which has a separate membership of over 6000 individuals.

The company operates a management system certificated by LRQA to BS EN ISO 9001:2008. It also has certificated management systems for health and safety (BS OHSAS 18001) and environment (BS EN ISO 14001).

(See inside back cover TWI Management System.)

TWI Ltd, Granta Park, Great Abington, Cambridge CB21 6AL, United Kingdom. Tel: +44 (0)1223 899000

TWI Report: Department for Transport Technical Assessment of Petroleum Tankers: Work Package 2 – Detailed Engineering Critical Assessment

Report No: 24000/8/14

Date: 26 November 2014

Prepared for: **Department for Transport**

c/o Zone 2/31
Great Minster House
33 Horseferry Road
London
SW1P 4DR

Contact: Steve Gillingham

Author(s) Tyler London, Isabel Hadley and Emily Hutchinson

TWI Endorsement

This report has been reviewed in accordance with TWI Policy

Project Leader (Signature) Tyler London

Print name: Tyler London

Approved by..... Ian Norris
Product Manager
(Signature)

Print name: Ian Norris

Administrator..... C P Knight
(Signature)

Print name: Caroline Knight

Technical Reviewer.....
(Signature)

Print name: Marcus Warwick

Approved by.....
Group Commercial Manager
(Signature)

Print name: Andrew Carey

Published Version History

Date	Version	Reason
November 2014	001	Incorporation of revisions from peer review and metallographic examination

Contents

Executive Summary

Background

TWI Ltd (TWI) has been commissioned by the Department for Transport (DfT) to undertake a detailed engineering critical assessment (ECA) as part of a wider technical assessment of petroleum tankers. This report covers the activities of Work Package 2 (WP2). The specific tasks in Work Package 2 (WP2) are to:

- Task 1: Determine the typical in-service life cycle fatigue loadings at worst case locations on the circumferential weld seam, including, when appropriate, the effects of filling and dispensing from compartments;
- Task 2: Review a proprietary finite element model of the GRW tanker as well as the crack growth and leak-before-break and associated technical documents and studies undertaken by GRW and TWI;
- Task 3: Address deficiencies as appropriate (such as fracture toughness properties, fatigue crack growth rates and weld residual stresses), wherever possible using strength and fatigue tests of samples taken from tankers to validate the model;
- Task 4: Engage with GRW to solicit and incorporate views as appropriate;
- Task 5: Undertake a detailed engineering critical assessment to predict crack growth, likely fatigue life of weld seams and defect sizes under suitable loading conditions, incorporating geometric variability;

Additional optional tasks include detailed post-mortems of damaged tankers and peer review activities.

The project plan consists of two distinct phases. Phase 1 comprises tasks 1 and 2 above, whereas Phase 2 comprises tasks 3 through 5.

Objectives

The objectives of this report are to:

- Document, describe and report on the determination of representative duty cycle stresses obtained from the tanker fatigue data collection exercise;
- Review relevant technical documents related to investigations on the integrity of circumferential seam welds of GRW tankers;
- Perform a detailed engineering critical assessment, taking into account the geometric variability of the GRW tanker band joint, to assess the fracture and fatigue integrity of the joint.

Work Carried Out

TWI has critically reviewed a significant number of technical documents concerning the integrity of GRW tanker circumferential seam welds in the context of current best practice (as dictated by relevant codes and standards). Additional supporting material has been made available to TWI by DfT to complement this exercise where appropriate.

Additionally, TWI has undertaken both laden and corresponding unladen testing of GRW tanker J3857 whilst instrumented with strain gauges and accelerometers. For each circumferential seam weld and each instrumented position around the circumference, the strain data has been converted into stresses acting transverse (normal) to the weld seams. The resulting stress time-series were used to calculate the number of cycles per stress range at each location. These stress-range histograms were then used in fatigue crack growth calculations.

Finally, an engineering critical assessment has been performed to assess the fracture and fatigue integrity of crack-like defects in the circumferential seam welds of GRW tankers. The ECA takes into consideration the geometric variability of the tanker band joint; the fatigue stress spectra measured from the full-scale fatigue data collection exercise; likely residual stress profiles as obtained from a thermo-elastic-plastic welding simulation based on the GRW weld procedure specification; material properties obtained through previous and current mechanical testing, and information and insight obtained from the review of previous analyses.

Conclusions

Based upon review of the GRW documents and supporting material referenced herein, the following conclusions have been reached:

1 The methods GRW used to investigate fatigue crack growth are not sufficient to absolutely determine the absence of fatigue cracks in J2297.
2 The engineering critical assessment performed by GRW concludes that a 2.0mm deep flaw is acceptable under roll over conditions. Different conclusions have been reached by an HSE study (2013) and TWI work (2013a-b). A sensitivity-study is required to determine the margin of acceptability of the 2.0mm deep flaw considered by GRW, due to the evidence provided by HSE that flaws with depths greater than 2.0mm exist.
3 The review, carried out by Prof Issler on behalf of GRW, of the significance of the GRW studies in comparison with the HSE's findings demonstrates that there is a gap between experimental observations and testing and theoretical calculations. TWI agrees with several of Prof Issler's observations about methods to reconcile these differences; however, unlike Prof Issler, from the contrasting evidence presented, TWI cannot draw a definitive conclusion about the acceptability of a 2.0mm deep flaw.
4 The review of TWI work by Prof Issler on behalf of GRW highlights potential sources of over-conservatism in the ECAs conducted by TWI. The assumptions made by TWI were explicitly stated and documented in the TWI reports and scope of work. Within the current work programme, specific tasks have been designed to further study these potentially over-conservative assumptions through experimental testing and advanced numerical modelling.
5 GRW have developed a detailed finite element model of a ten-banded tanker and performed a stress analysis of this tanker subjected to various loads to derive inputs for their ECA calculations. Based on a review of the model and the post-processed results, it is recommended that a more consistent stress extraction method is used in order to ensure that the stresses obtained from the model are in line with the guidelines for stress extraction recommended in BS 7608.

In addition to the main conclusions above, TWI has also discussed several aspects of the work reviewed where additional detail could be provided to further substantiate the argument.

On the evidence provided, therefore, TWI does not conclude that the GRW analyses have demonstrated that:

- Under normal operations, GRW tankers will definitely remain safe after six years of use;
- The critical flaw depth in roll over conditions exceeds 2.0mm rather than 1.2mm.

Note that TWI is not concluding that these statements are incorrect, merely that they have not been demonstrated to the satisfaction of the relevant standards.

The conclusions from the ECA related to the safe operating life of the circumferential welds found that:

1 Provided an initial defect is present, the fatigue data (for a ten-banded tanker) identified the cradle positions above the fifth wheel coupling and above the front of the rear longitudinal support members as most susceptible to fatigue crack growth.
2 Under normal operating conditions, the minimum critical defect height is greater than 2.0mm and may be as large as 4.0mm or more. Variation in this defect height will depend on three factors: the presence of an internal fillet weld between the toe of the extrusion band and the inner surface of the tanker shell; the magnitude of the misalignment between the shell and extrusion band; and the size of the weld cap.
3 Assuming an initial defect size of 2x100mm (ie a 2mm deep by 100mm long surface-breaking flaw) based on observations from the post-mortem examination of sections from GRW tankers that such a flaw would not be unexpected, the fatigue life of the joint (ie the time required to grow the 2x100mm defect to a critical size) is greater than 20 years when an internal fillet weld is present and continuous.
4 When a continuous (or potentially intermittent) internal fillet weld is not present, the fatigue life of the joint is influenced significantly by the misalignment and weld cap geometry. For this case, a parametric study involving over 300 simulations was used to derive a quadratic relationship between the fatigue life (assuming an initial 2x100mm flaw) and a geometry parameter that incorporates the weld cap height and misalignment. This allows a conservative estimate of the fatigue life of a joint (without the internal fillet weld) to be easily determined from a look-up table (derived from the quadratic relationship) using measurements of misalignment and weld cap height, which can be taken relatively quickly with a profile/laser gauge. A sensitivity study was undertaken to highlight the influence of bending stresses in the fatigue spectrum and initial flaw size assumptions on the calculated fatigue life.

The ECA of the circumferential welds related to the rollover conditions found that:

1 For the rollover case derived from the topple test, and from associated FE modelling with fuel oil undertaken by the Health and Safety Laboratory (HSL), and allowing for some ductile tearing to occur, the critical defect height in an 'average' weld geometry is 1.1mm when no internal fillet weld is present. Here the 'average' weld geometry relates to measurements from GRW tanker J3910 and may, therefore, not be truly representative of all non-compliant tanker joints.
2 Taking into account geometric differences (ie smaller weld cap height in the test than in the average joint simulation), the predicted critical defect height of 1.1mm agrees well with the experimental observation of the through-wall rupture of a circumferential weld resulting from a 1.0mm deep lack of fusion defect that was over 230mm long in a section of the impacted side of GRW tanker J2580. Although the contained fluid and the impact velocity in the HSL topple test simulation were different to those in the actual J2580 test that involved water and a lower impact velocity, the moment acting on the joint was similar.
3 Considering the rollover load case derived from the pressure-impulse simulation, and allowing for some ductile tearing to occur, the critical defect height in the 'average' weld geometry is 2.5mm when no internal fillet weld is present.
4 When a well-made and suitable internal fillet weld is present, the integrity of the tank in a rollover is not governed by the quality of the circumferential weld, but by the strength of the parent metal of the tank shell or other factors such as the bulkhead to extrusion band joint(s), which were seen to fail in topple tests.

The metallographic examination of multiple sections removed from three GRW tankers found that:

1 A 320mm long, through-wall rupture of a circumferential weld was observed in a section of the impacted side from J2580. The rupture was due to an initial lack of fusion defect at the positioner lip on the extrusion band. The height of the initial defect was approximately 1.0mm and over 230mm long.
2 Examination of a section from J3910 revealed only relatively small (total height less than 1.0mm) lack of side wall fusion, embedded-type defects. This class of defect is not of as significant concern as the surface-breaking flaws analysed in the report.
3 Examination of sections from J3564 revealed both a 2.19mm and a 2.04mm deep surface-breaking defect. These defects were not located directly at the positioner lip but at a small distance offset. The length of these defects was between 40mm and 50mm. Such defects could be critical under rollover conditions if an additional internal fillet weld was not present, however further analysis is required to conclusively determine the criticality of these defects.
4 No evidence of fatigue crack growth was observed. The samples taken from J2580 and J3910 were removed from the sides of the tanker and therefore the samples were not in locations particularly susceptible to fatigue damage. The samples taken from J3564 were located along the cradle welds where fatigue crack growth may be expected. Most samples prepared had additional internal fillet welds present and therefore, fatigue crack growth was not expected. However, even for samples without additional internal fillet welds, no fatigue crack growth was observed.

1 Introduction

Mistras Group Ltd, on behalf of some owners and operators of road tank vehicles manufactured by GRW, has undertaken computed radiography of a small number of tankers to the fullest extent possible. Amongst other things, these examinations have found that the tankers exhibit extensive lack of fusion defects in the circumferential weld seams. Consequently, some petroleum road fuel tankers are not fully compliant with the provisions of Chapter 6.8 of the European Agreement on the Carriage of Dangerous Goods by Road (ADR, 2013).

In light of these findings, TWI Ltd (TWI) was commissioned by the Department for Transport (DfT) to assess the likelihood of a rupture failure of the circumferential weld seams on road tankers manufactured by GRW. As a consequence of the preliminary findings by TWI (2013a-b) and a parallel HSE study (2013), further research is now being conducted to refine the initial analyses, to more closely examine the effects of fatigue, to undertake full-scale testing and to assess the safety of non-compliant road tankers in their current condition.

TWI has been commissioned by the Department for Transport (DfT) to undertake a detailed engineering critical assessment (ECA) as part of a wider technical assessment of petroleum tankers. This report covers the activities of Work Package 2 (WP2). The specific tasks in Work Package 2 (WP2) are to:

- Task 1: Determine the typical in-service life cycle fatigue loadings at worst case locations on circumferential weld seam, including, when appropriate, the effects of filling and dispensing from compartments;
- Task 2: Review proprietary finite element model of the GRW tanker as well as the crack growth and leak-before-break and associated technical documents and studies undertaken by GRW and TWI;
- Task 3: Address deficiencies as appropriate (such as fracture toughness properties, fatigue crack growth rates and weld residual stresses, wherever possible using strength and fatigue tests of samples taken from tankers to validate the model);
- Task 4: Engage with GRW to solicit and incorporate views as appropriate;
- Task 5: Undertake a detailed engineering critical assessment to predict crack growth, likely fatigue life of weld seams and defect sizes under suitable loading conditions, incorporating geometric variability;

Additional optional tasks include detailed post-mortems of damaged tankers and peer review activities.

The project plan consists of two distinct phases. Phase 1 comprises tasks 1 and 2 above, whereas Phase 2 comprises tasks 3 through 5.

The report is structured as follows:

Section 1 provides an introduction to the research project.

In Section 2, a significant number of technical reports, experimental measurements and expert commentary documents concerning the integrity of the GRW circumferential seam welds are reviewed. In particular, the reports under consideration have been provided to TWI by DfT and concern:

- The presence and evidence of fatigue crack growth in a tanker after extensive service;
- An ECA to establish the acceptability of flaws;
- Reviews on behalf of GRW by Prof Issler of University of Applied Sciences, Esslingen, Germany;
- Reviews of the previous TWI ECA reports;
- Experimental residual stress measurements.

Specifically, in the context of the reports considered within this document, consideration is given to whether or not the GRW analyses demonstrate sufficiently that, under normal operations, GRW tankers will definitely remain safe after six years of use and that the critical flaw depth in roll over conditions exceeds 2.0mm rather than 1.2mm as HSE have reported (2013). Additionally, TWI has reviewed the proprietary GRW finite element model of a 10-banded tanker.

In Section 3, the details about the tanker fatigue data collection exercise are provided. The ten-banded, six-compartment, GRW tanker J3857 was provided to TWI for the purpose of collecting realistic fatigue loadings on the circumferential seam welds of the tanker representative of UK roads. To that end, TWI applied 62 strain gauges and two accelerometers to the tanker and recorded approximately five hours of unladen (empty) data; approximately five hours of corresponding laden data, and the filling and emptying of the tanker. For the laden test, the tanker was filled with water having a mass equivalent to the normal petrol capacity. This data was then processed to obtain stress range histograms for each band at various positions around the circumference.

In Section 4, a detailed engineering critical assessment is performed. The fracture and fatigue integrity of GRW tanker circumferential seam welds is analysed by taking into account a range of geometric variability. In order to reduce the previous overly conservative assumption of full yield-magnitude, tensile residual stresses, a detailed thermo-elastic-plastic welding simulation has been performed to predict the transverse welding residual stresses acting on hypothetical flaws in the GRW tanker band joint. Additionally, Section 4 details the metallographic examination of sections removed from three GRW tankers.

2 Review of Previous Analyses

2.1 Overview

In order to provide insight and guidance for the Phase 2 activities of WP2, TWI has been requested to review previous technical reports concerning the integrity of the circumferential weld seams of GRW-manufactured tankers, as well as any appropriate supporting documents and material.

This section is structured as follows:

- Sections 2.3-2.8 primarily address technical reports and reviews of GRW documents related to the fatigue crack growth, engineering critical assessments, residual stresses and the conclusions that can be obtained from these reports. When appropriate, comparisons are made to existing HSE and TWI reports and findings.
- Section 2.9 specifically addresses a review of the finite element model employed by GRW to provide input for the technical reports described above.

2.2 Objective

The objective of this section is to comprehensively review technical documents, where appropriate, generated before May 2014, by GRW, TWI, DfT and other technical bodies in relation to the integrity of the circumferential weld seams of GRW-manufactured tankers.

2.3 Fatigue crack growth

2.3.1 Overview

GRW report (2014a) concerns the sectioning of GRW Tanker J2297. In particular, it aims to check for the presence of fatigue cracks after seven years of service. The report notes that tanker J2297 has a service history of almost 1 million kilometres; however, the report does not specifically state that J2297 has a service history of seven years.

2.3.2 Sectioning and inspection

In order to determine if fatigue cracks were present, regions likely to be affected by high cyclic stresses, identified by finite element analysis (FEA), were cut out of the tanker. The locations of these cut-outs were also used (in conjunction with other evidence) for the derivation of the strain gauge plan detailed in Appendix B). These cut-outs were along the cradle of the tanker as shown in Figure 1. All cut-outs were radiographed and documented in (GRW, 2014b). Where geometric indications were found, further examination by sectioning was conducted. These sections were investigated to search for and size both lack-of-fusion defects arising from the manufacture of the tanker band welds and fatigue cracks emanating from the weld flaws at the location of the radiographic indications.

The report notes that:

'At these locations cross cuts were made in the joint and the joint profile was inspected after the cross section was suitably polished and acid etched to highlight the weld boundaries and other material boundaries. The geometry was inspected with a 15x magnifying loupe. From the magnified geometry the depths of any flaws that intruded into the plate thickness was noted.' (Section 5, GRW 2014a).

Only Figure 17 of the report is of sufficient resolution and magnification (this figure has been reproduced in this report as Figure 2). It is unclear from this figure how the actual flaw depth was measured. It seems that the flaw depth was based upon the dissimilar colouring of the weld metal and base metal after etching. This type of measurement is not wholly appropriate for the detection of crack-like defects along the fusion boundary.

It would have been preferable to provide full details of the etching, polishing and inspection procedure. In particular the report should quote the applicable standards or codes followed. Although large, macroscopic fatigue cracks could potentially have been detected using the methods described in the report, more refined methods should have been employed to determine the absolute absence of fatigue cracks. For example, Pearson (1975) used x130 magnification to identify fatigue initiation in commercial aluminium alloys.

In general, examination of metallographic sections to determine whether fatigue crack extension has occurred is not covered by standardised procedures. However, given that the objective is to detect a few

micrometres of crack extension, it is necessary to use a preparation technique which enables the samples to be observed at a few hundred times magnification, ie for examination using a metallurgical microscope. For aluminium alloys, this involves a grinding and polishing sequence, which terminates with polishing media with a size of a fraction of a micrometre.

Note that these considerations do not preclude the possibility that, upon further examination, there may be no evidence of fatigue crack growth; however, to reach such a conclusion a more refined analysis such as the one described above is required.

GRW note that, of the samples cut out from the tanker, 55% of the length of inspected welds contained radiographic indications (2014a). This figure is consistent with a previous DfT report on J2297 (DfT, 2013a) where 60% by length of inspected welds contained unacceptable geometric indications. This statistic suggests that the small sample of welds cut out from J2297 is a representative sample. However, based upon the cross-sectioning exercise, GRW claimed that only 16% of the total length of radiographed welds contained actual flaws, and the maximum flaw depth was 2.0mm. The precise definition of a flaw (or as noted before, how such a flaw is measured) is not described. Therefore it is difficult to use this percentage for the assessment of the safety of the tankers.

GRW argue (2013a and 2014a) that the maximum flaw depth is 2.0mm. This arises from the presence of a positioning lip on the extrusion profile shown in Figure 3 that is not fully removed during weld preparation. HSE (2013), sectioned GRW tanker J3025 and found flaws with depths of over 2mm, (the largest reported depth was 2.4mm).

The GRW report (2014a) gives no description of the other 39% of indications that were not classified as crack-like defects. GRW state (2013a) that the interpretation of radiographic test results for this particular joint geometry is difficult. Nevertheless, GRW do not suggest whether these regions are porosity, voids or a geometric feature of the joint geometry itself.

2.3.3 Conclusions

The conclusions from reviewing this report (GRW, 2014a) are therefore as follows:

1 There is insufficient detail in the report of the cross-section sample preparation and the method for measuring and identifying crack-like defects.
2 Although an attempt has been made to establish the percentage of radiographic indications that arise from crack-like defects, no explanation is made for the indications that are not classified as lack of fusion defects.
3 There is not enough evidence to support the claim that there was absolutely no sign of fatigue crack growth. A more refined investigation as described in this section would be recommended by TWI.
4 The largest depth of a flaw recorded was 2.0mm. GRW claim this is because of the geometry of the lip on the extrusion band. However, previous HSE work (2013) found a 2.4mm deep flaw on sample 10787 of tanker J3025. This may be because of issues raised in conclusions 1 and 2.

2.4 Flaw depth calculations

2.4.1 Overview

GRW report (2014c) and supplementary material (GRW 2014d-e) describe their engineering critical assessment to establish the acceptability of flaws in GRW tankers. To perform the engineering critical assessment, GRW followed the methods outlined in BS 7910 (2005). They concluded that 'a 2.0mm deep long surface flaw in a typical GRW tanker circumferential weld is acceptable from a structural strength point of view to withstand a[n] HSE-specified roll-over load case'. It is also claimed that even larger flaws could be acceptable, but no evidence of this is provided.

GRW conducted a series of finite element analyses to establish the stress intensity factors and collapse loads for a number of long surface flaws with varying depths in the typical GRW banded tanker joint. Additionally, GRW conducted experimental investigations to determine the plastic collapse load of the joint by machining notches into cut-outs from the tanker.

2.4.2 Sensitivity analysis

The ultimate conclusion of the flaw size acceptability study is presented in the GRW failure assessment diagram shown in Figure 4. In an ECA, an assessment point within the failure assessment line is considered 'acceptable' whilst a point outside of the failure assessment line is considered 'unacceptable'. The 2.0mm deep flaw analysed by GRW, is close to the failure assessment line. The maximum depth of 2.0mm was chosen by GRW for reasons described in Section 2 above. However, in light of the 2.4mm deep flaw found by the HSE (2013), it is possible that an assessment of this deeper flaw might result in an unacceptable assessment point. BS 7910 recommends that 'a sensitivity analysis, determining the sensitivity of the results to credible variations in input parameters, should normally be performed as part of an engineering critical assessment, especially where the results are marginal' (Clause 7.1.10, BS 7910, 2013). A sensitivity study is recommended for the following reasons:

1. The assumption employed by GRW to show that a 2.0mm deep flaw is acceptable may not be wholly conservative;
2. The GRW conclusion that flaw depths are less than or equal to 2.0mm;
3. The maximum tolerable flaw depth, not the safety of only one flaw depth should be established;
4. The HSE have found defects of greater depth than 2.0mm (2.4mm).

2.4.3 Welded joint geometry

GRW studied 90 weld cross sections at locations of typical weld flaw indications from tankers J3025 and J2297 and identified the weld cap height at the flaw location, maximum weld cap height; weld cap width; horizontal distance from weld toe to flaw; and the flaw depth as important geometric variables (Section 6.5, GRW 2014c). The weld cap geometry was raised by the GRW review of TWI's previous work (GRW, 2013c). This is addressed in Section 3.8.

2.4.4 Finite element analysis

Regarding the use of FEA to determine the stress intensity factor for the assumed flaws, the GRW report appears to employ sound and appropriate modelling conventions as described in Section 6.2 (GRW, 2014c). However, specific details of the actual geometric dimensions, boundary conditions,

load cases and finite element mesh properties are not provided. In particular, GRW have not stated explicitly the size of the weld cap that has been used in the model, although this parameter is identified as being one of the most important in the analysis. The size of the weld cap employed in the HSE and GRW studies, although not explicitly recorded, could result in the different values of acceptable flaw depths.
TWI calculated stress intensity magnification factors (referred to as M_K in BS 7910) for the extrusion profile joint containing hypothetical flaws (see Section 3.1.7 of the TWI report (2013a)). The M_K factors were evaluated for flaws with a normalised depth ratio 0.2, 0.4 and 0.6 only. GRW has extrapolated the TWI values as shown in Figure 5 (for bending stress) and Figure 6 (for membrane stress). The method used to perform the extrapolation is unclear and TWI cannot comment on its validity.

Although the terminology that GRW employ to discuss linear elastic fracture mechanics is inconsistent with the usual terminology of BS 7910, it does not appear that this leads to an inappropriate use of the values calculated.

2.4.5 Collapse load simulation and derivation of L_r

An engineering critical assessment uses the parameter L_r to determine the proximity of a defect to failure by plastic collapse. The load ratio, L_r is equal to the applied load (moment or stress) divided by the collapse load (moment or stress) of the joint geometry containing a specified flaw. GRW have provided both numerical methods and experimental methods for determining the collapse load, and thus L_r, for their assessment point.

The GRW numerical method employed to determine the collapse load appears to be sound. GRW employed an elastic-perfectly-plastic material definition for the joint and increased the applied loads until plastic collapse occurred. For the 2.0mm defect, plastic collapse of the tanker shell (yielding through thickness), remote from the defect, occurred before local plastic collapse in the section containing the flaw. According to GRW, it was determined that the collapse load occurred 'at a remote (linear elastic) bending stress of 215MPa', which was converted 'with the consideration of strain hardening, to a joint bending moment of 930 N.mm/mm' (Section 7.2, GRW, 2013c). TWI has attempted to verify this calculation and has obtained similar but not identical results. It would be valuable for GRW to supply the method for deriving the collapse moment. From the roll-over load case, GRW deduce that a remote (elastic-plastic) bending stress of 145MPa acts on the section containing the flaw. This is again converted to a moment resulting in an applied moment of 856N.mm/mm. Consequently, an L_r value of 856/930 or 0.92 is calculated by GRW.

However, by definition, L_r is the ratio of the real applied moment (including the full strain-hardening portion of the stress-strain curve) to the plastic moment from an elastic-perfectly-plastic analysis. Thus, the 215MPa bending stress should not have been converted 'with consideration of strain hardening' to obtain the plastic collapse moment. Likewise, therefore, the plastic collapse moment cannot be measured in a test when the material strain hardens.

2.4.6 Collapse load experiments

In order to provide some experimental verification of the finite element analysis predictions of the joint collapse load, GRW conducted a series of experiments on samples of the tanker band containing machined notches representing the hypothetical flaws under consideration (see Figure 7). The

test procedure is described at length (GRW, 2013c) and supporting information about the results and test specimen geometry is provided (GRW, 2013d-e).

These novel experiments seem to provide sound evidence of an experimental method for assessing the load bearing capacity of the GRW joint. It is important to note, in light of the comments from the previous section, some care should be taken in employing the results of this series of tests in an ECA. This is due to considerable geometric variability between samples, the interpretation of the flaw depth measurements (see section 2 above), and the clamping arrangement for the cantilever bend tests. Nevertheless, TWI is of the opinion that the results presented are valuable and could be refined to provide experimental verification of numerical modelling predictions of the load bearing capacity of the joint.

2.4.7 Assessment point

GRW predicted that a 2.0mm deep, fully circumferential (long) flaw is acceptable. GRW assumed full yield magnitude, tensile residual stresses incorporating some relief of residual stresses as a result of primary loading (ie Q_m from 7.3.4.2 of BS 7910:2005). GRW calculated a K_r of 0.68, and L_r was calculated to be 0.92 (see section 3.5). The assessment point is shown in Figure 4.

A sensitivity analysis should be performed (see section 3.2 above). For example, a 2.4mm flaw could be assessed using Figures 4 and 5 from the GRW report (2014c) to give M_b and M_m values of 0.75 and 2.2. K_r then changes from 0.68 (the initial calculation for a 2.0mm flaw) to 0.8. With the information available, it is difficult to determine how the load ratio (L_r) would change for this new flaw size. However, assuming that L_r does not change (ie the assumption that remote collapse is still occurring before local collapse due to the flaw), the new approximate assessment point is shown in Figure 8. This is still safe, but it is closer to the unsafe region and shows that a more complete sensitivity study should be undertaken.

2.4.8 Conclusions

To summarise, the conclusions from the review of this document are:

1. A sensitivity study, as recommended in BS 7910, on flaw depth should be performed in order to establish the critical flaw depth.
2. The limit load experiments used within the study provide a useful method for determining the limit load for the joint.
3. The L_r value used in the ECA by GRW may not be correct as it potentially incorporates strain-hardening. The information available is not sufficiently detailed to determine whether the calculation for L_r is correct.

2.5 Safety aspects of fuel tankers manufactured by GRW by Prof Issler

2.5.1 Overview

GRW asked Prof Issler to provide an opinion on the safety aspects of fuel tankers manufactured by GRW (GRW, 2014f). His report addresses three points:

1. His opinion on GRW's technical analysis, numerical and experimental methods and assessment procedures;
2. The difference in conclusions drawn by GRW and HSE;

3. Recommendations for further work to enable a reliable view of the safety of GRW's tankers to be formed.

2.5.2 GRW's technical analysis

Prof Issler stated that the GRW reports and supporting material (GRW, 2014a-e) appear to be correct. He noted a general consensus that the dominant failure mode for the flaws under consideration would be plastic collapse. He assessed the difference between the HSE predicted critical flaw depth of 1.2mm and the GRW conclusion that 2.0mm depth is acceptable (but not critical). He attributes the differences to be due to input materials, tensile properties and weld dimensions. TWI agrees that local weld dimensions, including the specific weld cap/overfill height used in the model will have an influence on the critical crack size.

Prof Issler notes that GRW has verified the collapse load calculations for the joints through a series of quasi-static bending tests on specimens with machined notches (see Section 2.4.6). He observed that 'the collapse load for a crack with depth 2.6mm exceeded that predicted by GRW's theoretical results'. However, whilst this is true, the reason for the result might not be as useful as it first appears. For example, there was significant geometric variability between each specimen tested; in fact, the lowest collapse load reported in (GRW, 2014c-e) did not come from the sample containing the deepest notch (2.6mm), but from a sample containing a 2.15mm deep notch. For this reason, although the GRW bend tests provide very useful experimental verification of model predictions, care is required in applying their results.

As a final assessment of GRW's technical analysis, he reiterates that GRW observed a maximum defect depth of 2.0mm in tanker J2297 and found no evidence of fatigue crack growth. Prof Issler states that he finds the methods employed by GRW to be sound. Although TWI does not contradict the evidence presented, the discussion in Section 2 (above) highlights several ways that the methods employed by GRW could be improved.

2.5.3 Significance of GRW's results for the HSE's conclusions

Prof Issler's also compares the GRW and HSE conclusions. The important points to note are that HSE (2013) concluded that:

1. The remnant life for a tanker exhibiting flaws with a depth of 2.4mm (and length of 100mm) was likely to be 1.5 years.
2. The fatigue life of a 1.5mm deep flaw was likely to be nine years.

Prof Issler provides several possible explanations for this discrepancy between theoretical predictions of the HSE and actual GRW observations (see section 2.2 above). TWI agrees that further work should be performed in order to clarify this difference (see Section 2).

Prof Issler claims that GRW's analysis of roll over 'suggests that HSE's assessment of the critical flaw depth in GRW's tankers is incorrect and that the critical flaw depth clearly exceeds 2mm'. This assertion is made without 'the details of … the input parameters' (GRW, 2014f) of the HSE study. Engineering critical assessments rely on the underlying assumptions made, and therefore two different critical defect sizes need not be mutually exclusive. Although the bend tests performed by GRW are significant and provide a valuable tool for model verification, the determination of critical crack depth is made in conjunction with other factors such as material

fracture toughness, presence of residual stress and the quality of the weld. For this reason, TWI cannot, on the basis of the evidence provided, agree with Prof Issler that a 2.0mm flaw is acceptable.

2.5.4 Recommendations for further work

Prof Issler also provides several recommendations for further work in his report (GRW, 2014f). Although his recommendations are not critical to this review, it is important to highlight that work at TWI is ongoing. For example, in the current work programme (TWI, 2014), the following suggestions for additional analysis will be explored:

1. Determination of load and stress spectra for tankers operating in UK conditions using strain gauges and accelerometer measurements;
2. Fracture toughness and material testing on specimens taken from tankers;
3. Fracture mechanics tests on defective welds.

2.5.5 Conclusions

The conclusions obtained from reviewing this report are as follows:

1. TWI agrees that there is a discrepancy between the HSE report and the GRW analysis. However, this discrepancy does not necessarily mean that either report is incorrect. The assumptions in each report must be reviewed.
2. TWI agrees that there is a gap between theoretical predictions of the fatigue life of the cracked tanker band welds and the GRW conclusions from welding sectioning. However, the GRW practical study of the fatigue cracks is not considered to be extensive. A more thorough demonstration of the absence of fatigue cracks and of the size of the existing defects is needed.

2.6 Review of DfT and TWI reports by Prof Issler

2.6.1 Overview

Prof. Issler was also asked by GRW to evaluate the TWI reports (2013a-b) and the DfT technical assessment (2013b). His report (GRW, 2013b) focusses on the following:

1. Review and commentary on TWI reports;
2. Proposal for experimental assessment;
3. Proposal for analytical assessment.

Only the first point above is considered in this review report as the other two are not relevant to the technical findings and conclusions of GRW.

2.6.2 Review and commentary on TWI reports

Prof Issler's main conclusion is that there is insufficient technical information to substantiate the DfT decisions (or authorisations) that have been partially based on results produced by TWI. His main comment was about the TWI use of yield-magnitude, tensile welding residual stresses and of fully-circumferential, partially through-thickness flaws.

In the absence of experimental or analytical measurements of welding residual stresses, TWI followed BS 7910 procedures and assumed yield-magnitude, tensile residual stresses were present and acting on the

hypothetical tanker flaws. The potential over-conservatism of this assumption was also clearly highlighted and discussed in the TWI reports (for example, Section 5 (TWI, 2013a)). In particular, a sensitivity analysis was performed. The current programme of work (PR23024-2) has specific tasks in which both experimental residual stress measurements and welding simulations will be performed.

TWI reports (2013a-b) described the shape of the assumed flaw to analyse. This shape was chosen because a full leak-before-break assessment (including fatigue crack growth) was beyond the scope of work within the time constraints of the initial TWI study. TWI agrees that it is appropriate to question the suitability of the crack front geometry modelled; however, a sensitivity analysis was also performed in order to ensure that certain crack front geometry parameters did not affect the results. This found, for example, that the maximum stress intensity factor was only weakly dependent on the radius of the circular arc where the crack front transitioned from an inner surface flaw to a through-thickness flaw.

The current work programme has a specific task related to the prediction of 'realistic' crack front: growing from an initial lack of fusion flaw by fatigue to a through-thickness flaw. Modelling will be used to predict the shape of the crack. This will capture the actual geometry of a partially through-thickness, 'leaking' flaw.

Prof Issler mentions the TWI use of cyclic stress data derived from South African road conditions in an ECA for UK road conditions. He notes that using the cyclic stress data may 'overstate the actual stress and fatigue exposure of the tankers representative of actual road conditions in the UK'. Although this may be the case, this, to date, has not been experimentally demonstrated or quantified. TWI used the information that was available through the DfT and clearly discussed any potential shortcomings in the report.

2.6.3 Conclusions

Prof Issler's review of the TWI reports highlights assumptions made by TWI ECAs. These were already known, acknowledged and documented by TWI. The conclusions reached in the TWI reports (2013a-b), were based upon these explicitly stated assumptions and on information available at the time. For this reason, the conclusions reached by the ECA can be considered to be appropriate when they were made.

2.7 Review of DfT and TWI reports by GRW

2.7.1 Overview

In this section, the GRW report (2013c), reviewing the draft reports arising from the short-term fitness for service assessment of GRW road tankers performed by TWI for DfT are discussed. This GRW report comprises two main sections: one reviewing the initial ECA report by TWI and one reviewing the additional FEA work. Below, only sections from this GRW report that address disagreements or concern with the TWI work are discussed.

2.7.2 Comments on document 'Draft: TWI Report 23437/1/13 Short-term Fitness for Service Assessment of GRW Road Tankers'

2.7.2.1 Stress analysis of modified ADR load cases (Point a.)

The GRW finite element model was provided as an Abaqus output database (.odb) file for a stress analysis. In an odb file, only limited information about the step definitions, load cases and boundary conditions can be obtained. When the step definitions were queried, the step names all began with the description 'ADR' and ended with 'modified'. GRW further provide a Microsoft excel sheet describing the load cases. It was not clear from the descriptions that the load cases were strictly ADR load cases, as they included both braking forces for certain cases, and did not include the full 2g scaling for certain load cases. Additionally, the maximum acceleration information that was provided by GRW to TWI in terms of accelerations in the x-, y- and z-directions were defined in a coordinate system not consistent to that of their finite element model. TWI did indeed misinterpret the acceleration scaling values; however, as GRW note 'this misinterpretation does not affect the TWI results because the load cases were used in permutations of all possible combinations. Email correspondence between TWI and GRW occurred in which the load directions were clarified'. Therefore, this point is not considered to be a point of contention.

GRW then discuss an over-conservatism of TWI's interpretation of the maximum acceleration information provided by GRW. GRW provided a table of maximum and minimum accelerometer readings from their laden and unladen road measurements. To ensure a conservative assessment, TWI considered all possible permutations of these maximum and minimum accelerations in the three principal directions as possible 'worst case' loads. GRW explain that the TWI combinations considered represented unrealistic cases that could not occur in practice. However, their data is from a limited sample, 45km laden and 45km unladen that was recorded on a different GRW tanker (a tridem refrigerated semi-trailer with similar mass and suspension). From this evidence, it is not possible to conclude that their measurements represent absolute maximum values. In order to ensure conservatism for the short-term assessment, TWI considered all possible 'maximal' combinations.

2.7.2.2 Considerations of the weld cap geometry (Point b.)

GRW discussed the nominal wall thickness 5.2mm employed in the TWI finite element models and calculations. They observe that 'the reinforcement effect of the weld cap would then have been ignored, although GRW is of the opinion that it contributes to a large extent to the weld's resistance against through-plate bending stresses'. TWI does not disagree with the fact that the presence of a weld cap would indeed increase the joint's resistance to through-wall bending, but the following issues should be considered:

- The value of 5.2mm was agreed with DfT in the statement of work contained in the proposal for the TWI work (TWI, 2013a). This proposal also described how an idealised cylinder model of the joint would be made, not taking into account the weld cap.
- GRW note that they have measured the size of the cap for various sections in terms of its height protruding above the shell plate's outer surface (≥1.5mm) and the weld cap width from toe to toe (≥ 18mm). These values, although indicative and illustrative, were not available at the time of TWI's analyses. Furthermore, they do not indicate lower bound values or statistical variation. The objective of the TWI ECA was

to provide conservative estimates of the acceptability of the flaws under consideration; considering a flush ground weld is conservative, whereas employing weld geometrical parameters without sound evidence of their statistical evidence would not necessary have been. Discussions involving TWI, DfT and GRW since the review (GRW, 2013c) was written have indicated that the values referenced above (1.5mm for the cap and 18mm for the width) are not fixed and do indeed vary significantly with other joint parameters (such as axial misalignment) that can have a deleterious effect on the load-bearing capacity of the joints.

- Design procedures do not usually take advantage of the weld overfill (eg AWS, 2010).

2.7.2.3 Considerations of the partial through-thickness flaw geometry (Point c.)

GRW discuss the shape of the fully-circumferential flaw with a super-imposed through-thickness flaw (partial through-thickness flaw) modelled by TWI. Their main point is that the geometry was not realistic or may not arise in practice. The shape of the flaws modelled by TWI were again (as with the weld cap geometry) explicitly defined in the TWI Proposal statement of work. This shape was chosen because it provided an effective, straight-forward geometry for modelling partial through-thickness flaws, without modelling a full leak-before-break assessment involving differential fatigue crack growth from a surface-breaking flaw to a break-through flaw. A sensitivity study was performed to assess the influence of the fillet radius and a negligible influence was observed.

2.7.2.4 Influence of residual stress (Point d.)

GRW note that TWI has considered secondary (residual) stresses in the ECA in accordance with BS 7910; however 'GRW believes that a more realistic magnitude is available'. Reference is made to Appendix Q, that for butt welds, the residual stress is likely to be lower than yield within the plate thickness. Further reference is also made to the self-balancing nature of residual stresses for through-thickness cracks. TWI does not refute these statements; however, this geometry is not strictly a butt weld as the bulkhead/baffle provides additional stiffness that may result in residual stresses not being balanced across the shell wall thickness. Again, the main objective of the TWI ECA was to provide a conservative approximation of the acceptability of the defects defined and agreed in the statement of work and timescales. Thus, the standard yield magnitude tensile residual stress assumption was employed in the absence of any evidence or additional information about the welding procedure or measurements of residual stresses for the GRW joint under consideration. Finally, note is made of the residual stress relief equations that can be employed when uniform residual stresses are assumed in the presence of high primary stresses; this was not included in some early draft versions of the report provided to DfT but was included in all later versions.

2.7.2.5 Weld misalignment (Point f.)

GRW comment on the negative effect of misalignment that TWI has reported. GRW note that 'as misalignment increases, the maximum initial surface flaw depth decreases'. This argument is based on the assumption that the maximum as-manufactured weld defect height is 2mm, based on geometric reasoning previously discussed. As highlighted earlier, it is not clear that the basis for the maximum initial defect height of 2mm is fully justified.

2.7.3 Comments on document 'Draft: TWI Report 23437/2/13 Project 23437 Contract Amendment: Additional FEA for Assessment of GRW Road Tankers'

The comments concerning the second TWI report related to the short-term fitness for service project (TWI, 2013b), primarily address the points discussed above: weld cap size, residual stresses and crack front shape. These points have all been discussed, and therefore are not re-addressed in this section.

2.8 Residual stress measurements

2.8.1 Overview

GRW contracted Sheffield Hallam University to conduct residual stress measurements using the X-ray diffraction, $\sin^2\psi$ method for the extrusion band joint under consideration (2013d). The resulting report discusses the experimental technique, the measurements made and recommendations.

2.8.2 Review of residual stress measurement report

The author describes a standard technique for the measurement of surface residual stresses using X-ray diffraction. The technique involves monitoring the change in lattice spacing of a crystalline solid as it is rotated through an off-axis angle ψ. The technique assumes plane stress conditions, ie zero residual stress in the through-thickness (radial) direction. A reduction in lattice spacing with increasing $\sin^2\psi$ (as observed in this case) denotes compressive residual stresses.

The National Physical Laboratory (NPL, 2005) has provided a detailed and clear summary of the technique as a contribution to a European standard. However, neither this nor any other method statement is referenced by the author.

The author describes having applied grinding and polishing to remove silver paint from the test specimen. This is specifically warned against in the aforementioned NPL best practice guide (2005) because of the fact that it is liable to produce an additional spurious source of stress. The author provides arguments to the effect that the grinding and polishing will have a limited influence on the measurements. However, he notes that 'such grinding and polishing treatment was applied only … because of the urgent request by the client. In normal stress analysis work, we would use a preparation-free (as-welded) surface' (GRW, 2013d).

The hardness of the plate is correlated with ultimate tensile strength (UTS) in order to derive a value of UTS around 240-280MPa. The specific hardness correlation that was employed is not provided. Although this information is not critical, since the UTS is only used to put the residual stress measurements into proportional context, it is good practice to provide the reader with sufficient information to reproduce the results when necessary. No additional information is provided on the hardness or tensile properties of the weld, although it is common for aluminium weldments to show substantial strength mismatch between parent and weld metal.

The surface residual stress measurements reveal compressive stresses in both the weld region and the parent plate. It is not clear how these results should be interpreted. Aside from the possible effects of cold work (polishing and grinding) on the residual stress measurements (as described above), there is the problem that the defects of interest in this case are sub-surface,

typically deeper than 1.0mm, but the measurements only extend 1.0mm from the surface; the residual stress distribution in deeper sub-surface regions is thus unknown.

This discussion is not a criticism of the author of the report or the findings. The author may not have been aware of the reasons for carrying out the residual stress measurements (the report only notes that the client (GRW) 'requested to measure the surface residual stress'. In this context, it is worth noting that R6 (EDF Energy, 2001), the UK nuclear industry's procedure for flaw assessment (equivalent of BS 7910 for nuclear plant), has recently proposed withdrawing the current data on surface residual stresses from its residual stress compendium, in part because it was potentially being misused by analysts who required a through-thickness distribution of residual stress.

Finally, the author recommends 'more detailed testing and analyses', rather than concluding that the residual stresses can reliably be assumed to be compressive. From a quality stand point, the report provided to TWI (GRW, 2013d) does not contain any signatures or evidence of peer review.

2.8.3 Conclusions

The report (GRW, 2013d) on residual surface stress measurements, conducted by Sheffield Hallam University on behalf of GRW, describes the X-ray diffraction residual stress measurements performed on a sample of the GRW extrusion band joint under consideration. Although the measurements indicated that the weld surface exhibits small compressive stresses, the sample was cold worked before the measurements were made, which is not recommended by the NPL good practice guide (2005) for carrying out X-ray diffraction measurements. Additionally, the measurements do not cover the entire region of interest, and therefore their applicability for use in an ECA performed according to the guidelines in BS 7910 is minimal.

2.9 Review of the GRW finite element model

2.9.1 Overview

GRW have conducted finite element analysis (FEA) of a model of a ten-banded tanker, in order to perform fracture and fatigue engineering critical assessment calculations using BS 7910. The largest magnitude stresses were extracted from the model from three different load cases: vertical, lateral and longitudinal unit load accelerations. The stresses predicted from the FEA model were then scaled by real acceleration measurements in order to produce stress-time histories for use in a fatigue analysis.

2.9.2 Geometry

The tanker geometry was modelled in detail, including the tanker shell, baffles and bulkheads, extrusion bands, valance, undercarriage and suspension system. The tanker was predominantly modelled with shells, which is appropriate for a thin-walled vessel. The suspension system was modelled using a combination of beams, linear springs, hinges, ball joints and bushings.

Lack of fusion indications have been observed in the tankers between the extrusion bands and the tanker shell. Therefore, this is the most critical part of the geometry, where stresses would be extracted from the model. This

means that any key features of the geometry around these locations that may affect the stresses should be included in the model. Overall, inspection of the geometry compared to engineering drawings provided by GRW for tanker J3857 (note that the FE model provided by GRW is not of J3857), revealed that all key features have been included.

2.9.3 Finite element mesh

The tanker was meshed with 630,000 linear quadrilateral elements (type S4R in Abaqus) and 18,000 linear triangular elements (type S3 in Abaqus) as well as 18,000 linear beam/line elements (type B31 in Abaqus) for the suspension and bolts. Linear elements are acceptable for an explicit analysis, such as the pressure impulse simulation performed by GRW. However, linear elements may not predict stresses accurately enough in the static 1g stress analyses without significant mesh refinement. The global mesh size at the intersection between the extrusion band and the shell tanker was 25mm. This is larger than the extrusion band thickness of 15mm, and much larger than the tanker shell thickness of 5mm. Elements of the order of the shell thickness would be recommended for accurate stress prediction.

GRW used some local mesh refinement around local stress raisers, where the highest stresses were predicted. However, evidence of mesh sensitivity studies to ensure that the stress predictions from these areas were mesh-independent was not provided. Quadratic integration elements in the regions of interest near the extrusion bands would be recommended for more accurate stress predictions. A structured mesh with characteristic element size 't', where t = 5mm, the nominal wall thickness, would be recommended. It was noted that although the static model is symmetric, it was not meshed symmetrically, and therefore the resulting stresses were not symmetric (or anti-symmetric for some load cases) as would be expected.

2.9.4 Boundary conditions

The king pin was fixed in all directions and the wheels fixed in the vertical direction (z-axis) to simulate the grounded wheels. A single wheel was also fixed in the lateral direction (y-axis) to prevent rigid body motion. For the lateral acceleration (y-axis) load case, all wheels were fixed in the lateral direction (y-axis).

Although the primary model under consideration was the FE model for the static, 1g acceleration load cases, it was observed that an incorrect boundary condition had been applied in the pressure impulse simulation. In particular, a significant portion of the edges of the rear dish had not had the symmetry plane boundary conditions applied to them. This is shown in Figure 9 where black lines have been added to show the absence of the appropriate boundary condition. This omission led to the potential incorrect identification of a potential critical location.

2.9.5 Loads

For the static model, unit acceleration loads were applied in the longitudinal direction (x-axis), lateral direction (y-axis) and vertical direction (z-axis) in three separate steps of the analysis. For the roll-over simulation, a 2 bar pressure-impulse was applied to all internal surfaces.

2.9.6 Stress extraction

GRW extracted nominal stresses from the FEA model, by using the stresses 'one to two plate thicknesses' (GRW, 2013c) away from the shell to extrusion band connection. The shell thickness is 5mm, so the mesh was locally refined to 5mm elements near these areas. The stress was then extracted two elements from the shell to extrusion band connection. Generally, the mesh was well-refined in regions of peak stresses.

However, in some areas, the transition from 5mm elements to 25mm occurs over very short distances. Therefore, when the stress was extracted two elements from the extrusion band joint, this may have been taken at any distance from 10mm to 50mm. The combination of linear integration elements and mesh size may result in an inaccurate evaluation of the stresses acting on the joint. There is also a risk that extracting stresses at these distances may not pick up any secondary bending effects due to the local joint geometry. The highest stresses in the model were often found where the undercarriage was attached to the tanker shell, where secondary bending is likely to occur.

A surface stress extrapolation technique would be recommended for extracting stresses more accurately, as described in BS 7608 (2014). This involves extracting the stresses at distances of 0.4t and t from the weld toe, where t is the shell thickness. The structural stress at the weld toe can then be found by extrapolating the stresses from these two locations.

2.9.7 Conclusions

GRW have produced a detailed finite element model of a ten-banded fuel tanker, representing the global geometry well. However, GRW have used linear elements with a global size of 25mm near the extrusion bands, and some local refinement of 5mm where the stresses were highest. TWI would recommend quadratic elements, with 5mm elements throughout all extrusion band regions. Additionally, more consistent stress extraction is required. GRW have extracted stresses one-to-two elements away from the extrusion band to represent the nominal stresses. TWI would recommend using the surface stress extraction technique described in BS 7608 (2014) for more accurate structural stress extraction.

2.10 Conclusions on review of previous analyses

Based upon review of the GRW documents and supporting material referenced herein, the following conclusions have been reached:

1 The methods GRW used to investigate fatigue crack growth are not sufficient to absolutely determine the absence of fatigue cracks in J2297.
2 The engineering critical assessment performed by GRW concludes that a 2.0mm deep flaw is acceptable under roll over conditions. Different conclusions have been reached by an HSE study (2013) and TWI work (2013a-b). A sensitivity-study is required to determine the margin of acceptability of the 2.0mm deep flaw considered by GRW, due to the evidence provided by HSE that flaws with depths greater than 2.0mm exist.
3 The review of the significance of the GRW studies in comparison with the HSE's findings carried out by Prof Issler on behalf of GRW demonstrates that there is a gap between experimental observations and testing and theoretical calculations. TWI agrees with several of Prof Issler's observations about methods to reconcile these differences; however,

unlike Prof Issler, from the contrasting evidence presented, TWI cannot draw a definitive conclusion about the acceptability of a 2.0mm deep flaw.

4 The review of TWI work by Prof Issler on behalf of GRW highlights potential sources of over-conservatism in the ECAs conducted by TWI. The assumptions made by TWI were explicitly stated and documented in the TWI reports and scope of work. Within the current work programme, specific tasks have been designed to further study these potentially over-conservative assumptions through experimental testing and advanced numerical modelling.

5 GRW have developed a detailed finite element model of a ten-banded tanker and performed a stress analysis of this tanker subjected to various loads to derive inputs for their ECA calculations. Based on a review of the model and the post-processed results, it is recommended that a more consistent stress extraction method is used in order to ensure that the stresses obtained from the model are in line with the guidelines for stress extraction recommended in BS 7608.

In addition to the main conclusions above, TWI has also discussed several aspects of the work reviewed where additional detail could be provided to further substantiate the arguments.

On the evidence provided, therefore, TWI does not conclude that the GRW analyses have demonstrated that:

- Under normal operations, GRW tankers will definitely remain safe after six years of use;
- The critical flaw depth in roll over conditions exceeds 2.0mm rather than 1.2mm.

Note that TWI is not concluding that these statements are incorrect, merely that they have not been demonstrated to the satisfaction of the relevant standards.

3 Tanker Instrumentation and Fatigue Data Collection

3.1 Overview

In order to determine typical in-service life cycle fatigue loadings on the circumferential weld seams of GRW tankers, DfT provided GRW Tanker J3857 for testing within WP2. DfT requested TWI to perform the fatigue data collection exercise using Wincanton Group Ltd premises in Thurrock. The tanker was instrumented with electrical resistance strain gauges on the outer surface of the tanker adjacent to the circumferential welds, and with two accelerometers, one each on the front and rear of the chassis. Data was recorded with the tanker unladen while the vehicle was driven on a route representative of a typical tanker journey (sections of motorway, Class A and B roads), and put through a series of manoeuvres. The vehicle was then filled with water of an appropriate volume to represent the mass when fully laden with petrol. Data was recorded during the filling operation. The route was repeated and the tanker was then emptied, again with data recording. The data was then post-processed to determine the frequency of occurrences of stress ranges of interest at each instrumented position.

3.2 Objectives

- Record data during road testing with the tanker, both unladen and laden, and collect strain data during filling and dispensing from compartments to derive representative fatigue stresses.
- Provide experimental measurements for later calibration and validation of the GRW tanker finite element model.

3.3 GRW tanker for fatigue data collection

The ten-banded, six-compartment GRW Tanker J3857 was provided by DfT for the tanker fatigue data collection exercise. Two illustrations of the tanker are shown in Figure 10 and Figure 11.

The following naming convention is employed in this report:

- The tanker circumferential seam welds (also referred to as band welds or bands) are labelled alphabetically from the front of the tanker to the rear of the tanker. The front-most weld is band A/10, where the 10 indicates that this is a ten-banded GRW tanker. Throughout this report, as only a ten-banded tanker is under consideration, the '/10' may be dropped from the reference. The rear-most weld is J/10.
- The offside of the tanker is the driver side. If one is positioned at the rear of the tanker and looking down the axis of the tanker then the offside is the right-hand side.
- The nearside of the tanker is the passenger side. If one is positioned at the rear of the tanker and looking down the axis of the tanker, then the nearside is the left-hand side.

3.4 Internal fillet weld inspection

Before any instrumentation was applied to the tanker, ultrasonic inspection of tanker J3857 was performed in order to determine the existence and location of internal fillet welds for each of the tanker band welds. The objective of this inspection was to provide information about the fillet weld geometry and location in order to prevent strain gauges being attached at positions where fillet welds were present, which could then result in inaccurate post-processing of the strain data. The inspection report is provided in Appendix A of this report.
A summary of the report is as follows:

- It was noted that a continuous fillet weld joining the toe of the extrusion profile to the tanker shell was present in bands C, D, E, F and G from positions 3 to 9 o-clock (bottom half of the tanker).
- From 9 to 3 o-clock positions (top half of the tanker), the fillet weld was 'stitched', typically alternating 100mm weld and 600mm gap.
- Bands A, B, H, I and J were noted to be stitched over their full circumference, but the stitched weld pattern was irregular and varied considerably throughout the ten bands of the tanker.
- The approximate location and toes of each internal fillet weld were marked with indelible ink on the outer face of the tanker shell to facilitate marking out of the strain gauge positions relative to the weld toes.

3.5 Tanker instrumentation

All instrumentation was applied to tanker J3857 at Wincanton's workshop in Thurrock (Wincanton Group Ltd premises at Thurrock was identified as a suitable location to perform the tanker trials by DfT). In total, 62 electrical

resistance strain gauges were attached to the outer surface of the tanker at various positions around the circumference and along the length of the tanker. Two of the gauges were attached to unstrained locations to assess the extent of electrical noise, for example from passing under overhead power lines. All gauges were single element type FLA-2-23 with a gauge length of 3mm and resistance of 120Ω. They were bonded to clean polished bare metal with cyanoacrylate cement and coated with M-COAT D for environmental protection.

The strain gauge plan was developed based upon the findings of previous work (TWI, 2013a-b) which in turn was based upon an assessment of GRW's analysis of a static model of the tanker. In this finite element model, three different loading conditions were considered: a 1g forward acceleration, 1g lateral acceleration and a 1g vertical acceleration. In each load case, the body accelerations were resisted by the king pin and/or suspension. From the results of these simulations, TWI identified regions where significant stresses acted normal to the circumferential seam welds. These regions in turn represent positions on the tanker where it is likely that fatigue damage may be most severe. Based on this review of the simulation results, the following strategy was employed for the strain gauge positions:

- Tanker bands B and G were the most densely instrumented. Along these bands, both circumferentially-and axially-oriented strain gauges were placed at multiple positions along the circumference. In particular, the regions near the cradle featured a cluster of four axial gauges and one circumferential (hoop) gauge so that local biaxial stresses could be calculated and linearly extrapolated back to the hypothetical crack plane.
- Tanker bands C and D were the next most densely instrumented. For these two bands, circumferentially-oriented gauges were not employed, but axial gauges at the same circumferential position having different longitudinal offsets from the welds were used to enable linear stress extrapolation back to the hypothetical crack plane.
- For the remaining circumferential seam welds, a single axial gauge was placed on the offside of the tanker where the cradle is attached to the tanker. This allowed for strain data to be collected from the same position from each circumferential seam weld of the tanker.
- Two 'remote' axial gauges were placed on the tanker away from the circumferential seam welds and other local stress raisers. One was placed half-way between bands E and F and one was placed between bands I and J. In both cases, the gauges were located on the offside, mid-height. The purpose of these two gauges was to provide additional model validation/calibration in regions where high strain gradients were not expected.

A detailed description including diagrams of the placement of all of the 62 strain gauges is provided in Appendix B.

Additionally, two 5g range triaxial EXAGT3 accelerometers were mounted on the tanker. The front accelerometer was mounted on the chassis behind the king pin and the rear accelerometer was mounted on the chassis at the rear of the tank at half width.

All gauges and accelerometers were wired in a three-wire quarter bridge configuration and connected to remote data acquisition equipment via long cables. 'End to end' calibration was carried out to compensate for cable losses.

Strain and acceleration data were recorded using a digital data acquisition system and were captured at a rate of 200Hz per channel. The system was interfaced with a computer on which a comprehensive suite of software was installed for processing the data. The accuracy of this system was the greater of 0.5% and 5με.

3.6 Tanker fatigue data collection

3.6.1 Route planning

A route for the tanker was chosen by Wincanton in correspondence with TWI and DfT. The route was selected as it followed a typical journey that Wincanton-operated tankers would follow (See Figure 3) and comprised significant portions of motorway and A and B class roads, including urban sections. Details of the route are provided below:

- The tanker started at Central Yard on Motherwell road (See Figure 4), and drove to Coryton (Corringham, Stanford-le-Hope, Essex SS17, see Figure 5).
- From Coryton the tanker travelled to a truck stop on the A130 Chelmsford CM3 (see Figure 6).
- From the truck stop in Chelmsford it travelled to the A120, Black Notley CM77 (see Figure 7).
- From Black Notley it then travelled to 'Street CM2 5' (see Figure 7).
- From Street CM2 5 it travelled back to Coryton (see Figure 8).
- From Coryton it travelled to the roundabout where the M25 meets the A12 (see Figure 9).
- It then travelled back to Coryton, and from Coryton, it then travelled to the starting point at Central yard on Motherwell road (see Figure 10).

3.6.2 Unladen fatigue data collection

3.6.2.1 Overview

The unladen fatigue data collection exercise was carried out on Tuesday 13 and Wednesday 14 May 2014. An initial figure-of-eight test was carried out on 14 May, and the main driving events were undertaken on 14 May. Detailed descriptions of the eleven discrete 'tests' involved in the unladen fatigue data collection exercise are provided in Appendix C.

3.6.2.2 Emergency stops

Two controlled emergency stops were performed during the unladen fatigue data collection exercise.

Based on the telematics information provided to TWI, the first stop occurred from 23mph at 11:24am (Figure 20) and the second stop occurred from 34mph at 11:26am (Figure 21). However, the tachograph data below is considered more accurate for timing.

More detailed information about these events can be obtained from the digital tachograph (recorded at a frequency of 1Hz) provided to TWI by Wincanton and shown in Figure 22. Sudden, full braking was applied via the footbrake from 11:23:17am to 11:23:21am. The vehicle slowed from 77kph (48mph) to 20kph (12mph) over 68 metres. A peak braking rate of -4.72 m/s^2 was recorded. Full braking was then applied again from 11:25:14am to 11:25:18am over 67 metres. The vehicle slowed from 83kph (52mph) to 26kph (16mph) across 67 metres. A peak braking rate of -5.27m/s^2 was recorded.

3.6.2.3 Additional recorded events

The following events/incidents were recorded during the unladen fatigue data collection exercise:

- Number of recorded speed humps: 20
- Number of recorded pot hole events: 6
- Number of roundabout encounters: 92

In addition to the strain data, the maximum and minimum peak data from the accelerometers will be used in the Phase 2 report to derive severe loading conditions that may arise from operation.

3.6.3 Filling compartments fatigue data collection

The tanker was filled with an equivalent mass of its normal petrol capacity on 13 June 2014 at PCL. The compartments were filled sequentially from compartment (pot) 1 at the rear of the tanker to compartment (pot) 6 at the front of the tanker. A detail of the time series for the filling test is provided in Appendix C.

3.6.4 Laden fatigue data collection

3.6.4.1 Overview

The laden fatigue data collection exercise was carried out on 13 June 2014. Detailed descriptions about the discrete 'tests' involved in the laden fatigue data collection exercise are provided in Appendix D.

3.6.4.2 Emergency stops

Two controlled emergency stops were performed during the laden fatigue data collection exercise. These were performed at nominally the same location as those completed for the unladen test.

A digital tachograph report was also provided by Wincanton for these events, for which the speed and acceleration are shown in
Figure 23.

Sudden, full braking was applied via the footbrake from 12:14:46pm to 12:14:49pm. The vehicle slowed from 67kph (42mph) to 22kph (14mph) over 55 metres attaining a peak braking rate of -4.16m/s^2. Full braking was then again applied from 12:17:06pm to 12:17:09pm. The vehicle slowed from 72kph (48mph) to 34kph (21mph) over 61 metres, attaining a peak braking rate of -4.44m/s^2.

3.6.4.3 Additional recorded events

The following events/incidents were recorded during the laden fatigue data collection exercise:

- Number of recorded speed humps: 6
- Number of recorded pot hole events: 5
- Number of roundabout encounters: 94

Note that any discrepancy between the figures for the laden testing and unladen testing may not be due to different routing but may arise from a lack of recording of the event.

As with the unladen data, in addition to the strain data, the maximum and minimum peak data from the accelerometers will be used in the Phase 2 report to derive severe loading conditions that may arise from operation.

3.6.5 Emptying compartments fatigue data collection

The tanker was emptied at PCL on 16 June 2014. The compartments were emptied sequentially from compartment (pot) 1 at the rear of the tanker to compartment (pot) 6 at the front of the tanker. During the emptying process, the tanker instrumentation was active and recorded the resulting strains and accelerations. A detail of the time series for the emptying test is provided in Appendix D.

3.7 Data processing

3.7.1 Strain gauges

3.7.1.1 Overview

All measured strains were converted into stresses acting normal to the circumferential seam welds (axial stresses). Depending on the number and orientation of gauges at a given location, one of four methods was used to derive stresses, as detailed below.

3.7.1.2 Single uniaxial gauge

Measured strains were converted to uniaxial stress using the relationship:

$\sigma = E\varepsilon$

Where

σ = stress, MPa
E = modulus of elasticity, 70,000MPa (70GPa) assumed
ε = measured strain (converted from microstrain, 10^{-6} mm/mm, to mm/mm)

Strictly, this relationship applies only to a uniaxial stress field where the strain gauge orientation is parallel to the direction of stress. In a biaxial stress field, the relationship ignores the Poisson effect of the stress in the direction perpendicular to the gauge direction. This would lead to the stress parallel to the gauge being underestimated by 30% in the case of equibiaxial stress distribution. In Appendix B, the legend for a single uniaxial gauge is a black rectangle.
This relationship was applied to the following gauges:

- Band A: G1;
- Band B: G12, G13;
- Band C: G24, G25, G26, G27;
- Band D: G34, G35, G36, G37;
- Band E: G38, G39 (midway between E and F);
- Band F: G40;
- Band G: G51, G52;
- Band H: G57;
- Band I: G58, G59 (midway between I and J);
- Band J: G60.

3.7.1.3 Local cluster of three uniaxial gauges

This occurs when a single axially-oriented gauge (black rectangle from the legend in Appendix B) is 20mm circumferentially offset from a set of two, aligned, axially-oriented gauges (red rectangle from the legend in Appendix B). This results in the configuration shown in Figure 24.

By way of explanation, let G1 and G2 be the pair of aligned gauges with G1 closest to the circumferential seam weld. Let G3 be the single, axially-oriented gauge 20mm circumferentially offset from the G1-G2 pair (see Figure 24). In order to obtain a local measure of the stress acting on the hypothetical crack plane, the following is performed:

$$\varepsilon_{1,3} = \frac{1}{2}(\varepsilon_1 + \varepsilon_3)$$
$$\sigma_{1,3} = E\varepsilon_{1,3}$$
$$\sigma_2 = E\varepsilon_2$$
$$\sigma_{SSE} = 1.7\sigma_{1,3} - 0.7\sigma_2$$

Where

ε_1 = measured strain at G1
ε_2 = measured strain at G2
ε_3 = measured strain at G3
$\varepsilon_{1,3}$ = average of strains ε_1 and ε_3
$\sigma_{1,3}$ = uniaxial stress calculated from the average strain $\varepsilon_{1,3}$
σ_2 = uniaxial stress calculated from strain ε_2

The term σ_{SSE} is the stress obtained from surface stress extrapolation, ie the linear extrapolation of the stresses $\sigma_{1,3}$ and σ_2 (which are 14mm and 34mm away from the hypothetical crack plane, respectively) back to the crack plane. The benefit of this approach is that by averaging the strains at G1 and G3, a more robust 'local' measure of stress can be obtained that is less sensitive to any geometric imperfections that might otherwise influence G1 and G3 separately.

This relationship was applied to the following gauges:

- Band C: G18-G20 (offside cradle) and G21-G23 (nearside cradle);
- Band D: G28-30 (offside cradle) and G31-G33 (nearside cradle).

3.7.1.4 Local cluster of two perpendicular gauges

This occurs when a single axially-oriented gauge is paired with a single circumferentially-oriented gauge. In Appendix B, this corresponds to the yellow and black hatched rectangle. Both gauges are typically 5mm offset (in the axial/longitudinal direction) from a circumferential seam weld and 20mm circumferentially separated. In this case, the local stress can be determined from the following biaxial pane stress equation:

$$\sigma = \frac{E}{(1-\nu^2)}(\varepsilon_A + \nu\varepsilon_C)$$

Where

ε_A = strain measured at axially-oriented gauge
ε_C = strain measured at circumferentially-oriented gauge

ν = Poisson's ratio, assumed to be 0.3
σ = the local stress acting normal to the circumferential seam weld

This relationship was applied to the following gauges:

- Band B: G14-G15 (offside valence) and G16-G17 (nearside valence);
- Band G: G53-54 (offside valence) and G55-G56 (nearside valence).

3.7.1.5 Local cluster of five gauges

This occurs when a pair of aligned, axially-oriented gauges (red rectangle from the legend in Appendix B) is positioned near a set of three gauges - two aligned axial gauges and one circumferentially-oriented gauge – corresponding to the red and black hatched rectangle from the legend in Appendix B. This configuration is illustrated in Figure 25, where for this example, gauges G1-G5 are labelled. In this case, the local stress is obtained as follows:

$$\varepsilon_{1,3} = \frac{1}{2}\left(\varepsilon_1 + \varepsilon_3\right)$$

$$\varepsilon_{2,4} = \frac{1}{2}\left(\varepsilon_2 + \varepsilon_4\right)$$

$$\sigma_{2,4,5} = \frac{E}{\left(1-\nu^2\right)}\left(\varepsilon_{2,4} + \nu\varepsilon_5\right)$$

$$\sigma_{1,3,5} = \frac{E}{\left(1-\nu^2\right)}\left(\varepsilon_{1,3} + \nu\varepsilon_5\right)$$

$$\sigma_{SSE} = 1.7\sigma_{2,4,5} - 0.7\sigma_{1,3,5}$$

Where

ε_1 = measured strain at G1 (axial)
ε_2 = measured strain at G2 (axial)
ε_3 = measured strain at G3 (axial)
ε_4 = measured strain at G4 (axial)
ε_5 = measured strain at G5 (hoop)
$\varepsilon_{1,3}$ = average of strains ε_1 and ε_3
$\varepsilon_{2,4}$ = average of strains ε_2 and ε_4
$\sigma_{1,3,5}$ = stress (incorporating biaxiality) from the average strain $\varepsilon_{1,3}$
$\sigma_{2,4,5}$ = stress (incorporating biaxiality) from the average strain $\varepsilon_{2,4}$

The term σ_{SSE} is again the stress obtained from surface stress extrapolation, ie the linear extrapolation of the stresses $\sigma_{1,3,5}$ and $\sigma_{2,4,5}$ (which are 14mm and 34mm away from the hypothetical crack plane, respectively) back to the crack plane. This method assumes that the hoop strain is constant over the local gauged region; however, inspection of finite element simulation results indicates that the local hoop strain variation is indeed small. This approach is considered the most accurate and robust estimate of the local stress, due to the inclusion of biaxial strains and the local averaging at G1-G3 and G2-G4 that minimises the sensitivity to local geometric imperfections.

This relationship was applied to the following gauges:

- Band B: G2-6 (offside cradle) and G7-11 (nearside cradle);
- Band G: G41-G45 (offside cradle) and G46-50 (nearside cradle).

3.7.2 Accelerometers

As previously noted, two 5g range triaxial EXAGT3 accelerometers were mounted on the tanker. The front accelerometer was mounted on the chassis behind the king pin and the rear accelerometer was mounted on the chassis at the rear of the tank at half width.

The orientation of the accelerometers was such that:

- The positive y-direction was forward in the direction of travel.
- The positive x-direction was lateral in the direction of the nearside.
- The positive z-direction was vertical upwards.

A preliminary modal-based frequency analysis of the GRW finite element model indicated that all eigenmodes involving full-body deformation (bulk excitations) had eigenfrequencies less than 10Hz. The implication of this is that excitations of the chassis where the accelerometers were positioned having frequency greater than 10Hz will not contribute to the full-body deformation, but only result in short-term, local, breathing-type (panting) deformation modes of individual sections of tanker shell. Therefore, all accelerometer time-series were passed through a 2^{nd} order, 10Hz low pass Butterworth filter with passband gain of 0dB.

The purpose of the accelerometers is to provide correlation/calibration with the finite element model of the GRW tanker as follows:

- For an instrumented position (ie where strain gauges were positioned), identify whether it is closer to the front accelerometer or the rear accelerometer. By way of example, assume the position under consideration is the offside cradle location of band B, where there is a cluster of five strain gauges. This is almost directly above the front accelerometer.
- With the finite element model of the GRW tanker, run a simulation involving three, non-interacting, load cases: a 1g acceleration in the forward direction, a 1g acceleration in the lateral (towards nearside) direction, and a 1g acceleration in the vertical-upwards direction. Assume small strains, linear elastic material behaviour and static behaviour (no inertial effects).
- For each load case, output the surface strain at the positions of the strain gauges.
- For each series of filtered accelerometer data (forward, lateral and vertical), scale the appropriate series by the strains extracted from the corresponding load case from the finite element model. Use linear superposition to obtain the total outer surface strain at each gauge position.
- Use the same methods outlined in Sections 2.7.1.2 through 2.7.1.5 to derive a local value of stress from the superposed strain versus time series. For this example, the method described in Section 2.7.1.5 (local cluster of five gauges) would be used.
- Apply the rainflow counting method to obtain the FEA stress range histogram for the position (see Section 3.8).
- Compare the experimental stress range histogram with the FEA stress range histogram.

This approach takes the pragmatic viewpoint that at any specific position and time, it is unlikely that the strain gauge measurements will exactly match the FEA predictions for the instrumented location, primarily due to

dynamic effects, geometric variability and other non-linearities that may be present in the tanker. However, the frequency of cyclic stresses over large periods of time should agree. An example at the position described above (offside cradle, band B) is shown in Figure 26. In Figure 26 it can be seen that as a result of passing the accelerometer data through the low-pass filter, the number of low stress range cycles is different from the experimental measurements, but this is expected. These low stress range cycles do not contribute to fatigue crack growth (they typically result in stress intensity range values below threshold), and therefore are not important. For a more direct comparison, a line has also been included where the experimental data has also been passed through the low-pass filter. Indications show that there is an acceptable level of agreement between the model predictions with the experimental measurements using this method.

3.8 Derivation of stress range histograms

As described above, associated with each local region (cluster of gauges) a local, normal stress has been derived from the strain data. Where appropriate, linear extrapolation was employed to estimate the normal stress acting on the hypothetical crack plane.

Based on the appropriate duty cycle construction described in Section 3.9, a rainflow counting analysis will be conducted to calculate the number of cycles per stress range at each location for each circumferential weld for the representative duty cycle. The resulting stress range histogram will then be used to perform fatigue crack growth calculations.

3.9 Construction of duty cycle

3.9.1 Distance-based approach

The approach employed by GRW (2013a) assumed that a typical high utility duty cycle in industry includes the following:

- Annual travel distance: 220,000km (ie 616km/day for 357 work days a year);
- Number of loads delivered per day: 6;
- Ratio of laden vs unladen travel distance: 50/50.

The route travelled for both the laden and unladen fatigue data collection exercises was an actual route that would be travelled by a fuel tanker and comprised 150miles (241km). Due to the repetitions included in the route planning, the responses obtained over this 150miles could be assumed to be representative of a typical UK tanker route in the Southeast of England.

To employ a distance-based duty cycle construction, first, all of the data recorded from the unladen test should be concatenated. This concatenation will not include the figure-of-eight manoeuvres or the emergency stop tests. Because the Paris-type fatigue crack growth law used in BS 7910 does not take into account periodic overload-induced crack growth retardation, the exclusion of the emergency stops may not produce a significant impact on the fatigue life. Similarly, all of the laden data should be concatenated to produce a continuous signal covering the 150miles travelled during the laden test.

Once the unladen and corresponding laden fatigue data has been concatenated, it should be further partitioned into data corresponding to

Class A roads and data corresponding to Class B roads. This can be done by employing the travel event logs and the route plan to identifying the time segments during specific tests that correspond to the separate road classes. This partitioning will create sets of fatigue data comprising X_A miles of Class A data and X_B miles of Class B data, where $X_A + X_B = 150$ miles. A rainflow counting procedure can be performed to determine the number of cycles per stress range for the Class A data and the Class B data. This will give the stress range histogram corresponding to X_A miles of Class A road and the stress range histogram corresponding to X_B miles of Class B road. These can then be normalised to provide stress range histograms per mile.

Finally, in order to generate the annual, 220,000km (136,701mlesi) duty cycle, an assumed ratio of Class A to Class B road travel should be selected. Then the appropriate linear combination of the normalised Class A and Class B histograms can be applied to obtain the annual duty cycle. In addition to the fatigue data arising from road travel, the stress range histograms arising from emptying and filling six times per day should be added.

3.9.2 Time-based approach

An alternative to a distance-based duty cycle, can be obtained from time-based considerations. Correspondence with Wincanton indicated the following:

- Most operations are 24/7 involving a driver driving for 6 hours per shift for two shifts a day, Monday to Friday and 6-7 hours a day on Saturday and Sunday, day shift only. Depending on the operator, this could alternatively be an 11 or 12 hour shift, 7 days a week.
- The time that the tanker is on the road depends on how many deliveries are undertaken in one shift, but will involve 20 minutes to load the vehicle; 45 minutes to empty the tanker; 30 minutes of vehicle checks and paperwork, and a 45 minute comfort break.
- If, as proposed in the distance-based approach, 6 loads are delivered per day, and each load involves full emptying of the tanker, then each load/unload is associated with a down time of 1hr and 35 minutes. Over the course of a day, the tanker is not being driven for 9.5hrs, or equivalently, the tanker is on-road for 14.5hrs/day.
- Ratio of laden vs unladen travel distance is also 50/50, hence 7.25hrs empty and 7.25hrs laden.

Thus, an alternative time-based approach is as follows:

- Concatenate the entire unladen (empty) test data. This includes the two emergency stops and figure-of-8 manoeuvres, which could be representative of partial manoeuvres required to enter depots, for example. The entire concatenated data comprises 4.9 hours of data.
- Assuming that this is representative of unladen travel, then the frequencies in the stress range histograms (see Section 3.8) obtained from the entire concatenated unladen data could be multiplied by (7.25/4.9) = 1.48 to obtain stress range histograms representative of one day of unladen travel.
- Concatenate the entire laden test data. Again, this will include two emergency stops and figure-of-8 manoeuvers. The entire concatenated data comprises 5.2 hours of data.
- Assuming that this is representative of laden travel, then the frequencies in the stress range histograms obtained from the entire concatenated

laden data could be multiplied by (7.25/5.2) = 1.39 to obtain stress range histograms representative of one day of laden travel.
- To create one entire day's stress range histogram, join the six copies of the emptying stress ranges to the histogram.
- Multiply the representative one-day duty cycle by 365 to obtain one-year histogram.

3.9.3 Finalising the duty cycle for fatigue calculations

Due to the ambiguities that may arise from employing the time-based duty cycle approach, it has been agreed to employ the distance-based approach. Correspondence with Wincanton recommended the 220,000km per year figure which is in exact agreement with GRW; therefore, an annual distance of 220,000km was employed in the fatigue stress spectra generation. It was determined that the dependence on Class A and Class B roads was insignificant. Therefore, the fatigue stress spectra used in this report assume 60% Class A road and 40% Class B road travel annually. This ratio is the same ratio that was tested during the fatigue data collection exercise.

For each instrumented position, the stress range histograms corresponding to the entire concatenated test data are presented in Appendix E. Note that these stress range histograms are for the concatenated unladen data (including figure-of-eight and emergency stop tests) and for the concatenated laden data (again, including the figure-of-eight and emergency stop tests).

3.10 Conclusions

In this section, the instrumentation and fatigue data collection exercise for GRW tanker J3857 has been described in detail. Post-processing of the strain gauge data to derive stresses acting on the circumferential weld seams has been discussed. The method used for converting these stresses into stress range histograms for fatigue crack growth calculations has also been provided. Additionally, the post-processing of the accelerometer data and how it is being used to calibrate and verify the finite element model predictions has been described.

The analysis of the fatigue data identified the cradle positions on bands B/10 and G/10 as susceptible to fatigue crack growth, provided an initial defect is present. On a 10-banded GRW tanker, the bands are identified alphabetically from the front-most band (A/10) to the rear-most band (J/10).

4 Engineering Critical Assessment

4.1 Overview

A detailed engineering critical assessment has been undertaken in order to assess the structural integrity of circumferential seam welds in petrol tankers manufactured by GRW that may contain crack-like defects. The objective of the ECA is to assess the acceptability of lack of fusion defects in terms of their fracture and fatigue integrity. All assessments have been performed in accordance with the methods and guidance of BS 7910:2013.

The review of previous analyses provided in Section 2 highlighted several potential shortcomings in past ECAs such as overly conservative geometric considerations and the treatment of residual stresses. In order to refine the assessment calculations, the effect of the weld cap has been analyses, the effect of a potentially more realistic welding residual stress profile, and the

fatigue data collected from UK roads have been considered. Consequently, the primary objective of the ECA detailed below was to quantify the effects of geometric variability and to refine previous fatigue and fracture assessments, considering the sensitivity of the results to changes in the input data.

4.2 Failure assessment diagram methods

The failure assessment diagram is comprised of two axes: K_r and L_r. The K_r axis quantifies the proximity of the flawed structure to fracture failure, and the L_r-axis quantifies the proximity of the flawed structure to plastic collapse. A curve called the failure assessment line separates the acceptable (or safe) region from the unacceptable (or potentially unsafe) region. Points contained within (below) the failure assessment line are considered acceptable, whereas points outside of the failure assessment line are considered unsafe.

In the context of the present report, the K_r coordinate of the failure assessment diagram is defined by

$$K_r = \frac{K_p + VK_s}{K_{mat}}$$

Where

K_p is the primary stress intensity factor arising from the primary stresses;
K_s is the secondary stress intensity factor arising from welding residual stress;
V is a plasticity interaction correction factor;
K_{mat} is the fracture toughness of the material.

The Lr coordinate is defined to be the ratio of the applied load to the collapse load of the flawed structure.

For additional information on failure assessment diagram methods, see BS 7910 (2013).

4.3 Geometry

4.3.1 Overview

Considerable attention has been paid to the geometric variability associated with the GRW tanker band joint. In particular, the review of previous analyses (Section 2) highlighted the need for careful consideration of the effect of the weld cap height, weld cap width and the presence of axial misalignment. In previous TWI and HSE studies, a 'flush ground' joint was considered, in effect, assuming no weld cap was present. This approach is conservative, and, in the absence of measurements of the weld dimensions and their statistical variance, appropriate, but the level of potential over-conservatism was not fully quantified. Therefore, to refine the previous ECA work, the effect of the presence of a weld cap/overfill and axial misalignment on the stress intensity factor solutions and plastic collapse loads was quantified.

4.3.2 Finite element model of joint geometry

A parametric finite element model generation script was developed in Python to automate the creation of local models of the GRW tanker band

joint in Abaqus/CAE version 6.13-2 (SIMULIA, 2013). The local model comprises the extrusion band profile, two lengths of tanker shell (either side of the extrusion band), and a bulkhead. The underlying geometry is an axisymmetric model of the GRW tanker band joint. The mean radius of the tanker joint model was assumed to be 2000mm, approximately equal to the average of the major and minor axes of the tanker along the length of the tanker. The nominal tanker shell wall thickness was 5.0mm. The extrusion band profile was provided to TWI by GRW as an AUTOCAD sketch that was imported into Abaqus/CAE and used to define the axisymmetric part. A bulkhead was modelled based upon the engineering drawings of various GRW tankers provided to TWI. A 'seam' was created in Abaqus to represent the unfused surface between the extrusion band beyond the positioning lip and the inner surface of the tanker shell. No contact was modelled along this interface; however, because the loads under consideration are tensile membrane and bending stresses, the deformation of the tanker shell (and the section containing the flaw) does leads to negligible inter-penetration of the surfaces, if any at all.

The axisymmetric assumption in the model implies that the flaws under consideration are fully-circumferential (or 'long' surface flaws in the terminology of BS 7910). There are primarily two reasons for basing the finite element model calculations on axisymmetric models:

- The Mistras radiographic inspection report (2014) from J3910 indicates the presence of continuous lack of fusion indications ranging in lengths from 3cm up to 1700cm. The present ECA is concerned with the association of any lack of fusion indications with the potential presence of crack-like defects. Therefore, given that the nominal tanker wall thickness is 5mm, the flaws under consideration potentially have very small aspect ratios (depth, a, divided by length, 2c) and can therefore be treated as essentially fully circumferential flaws (aspect ratio 0) without being overly conservative.
- In order to model finite length flaws, three-dimensional models would be required, thereby limiting the detail of the study on the significance of geometric variability due to the computational requirements.

However, as described below in Section 4.8.2, the assessment of finite length defects can be handled by modifying the axisymmetric finite element solutions by a finite length correction factor.

Once the base geometry had been defined, a weld cap profile was added. The weld cap was defined by two parameters: the height, h, and the width, w. The weld cap profile assumed the shape of a circular arc passing through three points: one being the apex of the circle positioned on the crack plane a distance h beyond the nominal tanker outer surface, and the other two points were positioned w/2 either side (in the axial direction) of the apex of the weld cap as shown in Figure 27. In general, the position of the 'peak' of the weld cap may or may not be directly above the crack plane, and the weld cap will not assume the idealised shape of a circular arc. However, it is not feasible to model all possible weld cap profiles, and the definition of weld cap geometry assumed in this report is sufficient to represent the typical weld cap shape and therefore capture the mechanics of the welds under consideration.

Axial misalignment was modelled by offsetting the section of tanker shell containing the defect from the axis of symmetry by a distance m (see Figure 27).

It is important to note that the flaw depth, a, is measured from the inner surface of the tanker shell and not from the tanker extrusion band. This provides a consistent definition of crack depth when misalignment is present. Thus, for a geometry case with misalignment, m, and crack depth, a, the crack tip is located m+a from the unfused surface between the extrusion band and the inner surface of the tanker shell.

It is known from engineering drawings and inspection of tankers that an internal fillet weld is typically present from the 3 o'clock position to the 9 o'clock position for most bands. Additionally, this fillet weld is continued by 'stitching' the extrusion band toe to the inner surface of the tanker shell from the 9 o'clock position back to the 3 o'clock position for some bands (though the stitching pattern is frequently irregular and the presence is not well defined). Nevertheless, the presence of the additional internal fillet weld is significant as the positions experiencing the peak stresses under design (ADR) load cases and the most damaging fatigue stress spectra are along the bottom of the tanker. Therefore, the last geometric modification considered was the presence of an additional internal fillet weld joining the toe of the extrusion band to the inner surface of the tanker shell. In order to reduce the scope of the parametric study, the leg length of the fillet weld was assumed to be 12.0mm, independent of whether or not misalignment was present. The detailed geometric representation of the fillet weld in the model is not considered to be particularly important; the primary factor is that the existence of the fillet weld provides an alternative load path that may significantly reduce the crack tip loading and thus the crack tip stress intensity.

Once the geometry had been defined, the entire model was meshed with quadrilateral, biquadratic, reduced integration, axisymmetric elements (type CAX8R in Abaqus). A spider web crack tip mesh was created with 14 rings of elements surrounding the crack tip. The innermost elements were modelled with collapsed and degenerate wedge elements. For the linear elastic simulations, the mid-side nodes of the innermost wedge elements were shifted to the quarter-point position and single-node degeneracy was employed to accurately resolve the $1/\sqrt{r}$ crack tip singularity (SIMULIA, 2013). For the elastic-plastic models, the mid-side nodes were left unshifted and duplicate node degeneracy was employed. The finite element mesh was biased so as to be dense in the proximity of the defect and coarser away from the defect. A global element seed size of 0.35mm was used to ensure a suitably fine mesh resulting in about 20k elements for each model. A typical finite element mesh is shown in Figure 28.

4.3.3 Definition of geometry cases

Tanker J3910 was laser scanned prior to topple testing by HSL and the preliminary measurements were provided to TWI in a Microsoft Excel spread sheet (HSL, 2014a). Details of the laser scanning and measurement methods are provided in the Work Package 1 reports. The measurements for weld cap height and weld cap width are shown in Table 1 for the offside and in Table 2 for the nearside. Note that TWI is not able to confirm that the measurement of misalignment in its present state is a suitable and accurate representation of the actual axial misalignment; nevertheless, the values used are indicative measurements of axial misalignment for the purposes of the geometric variability study. The average, maximum and minimum values of the measurements were computed and are listed in Table 3.

Based on the HSL preliminary measurements, ten geometric cases were defined to analyse the sensitivity of the engineering critical assessment to geometric variability. The ten cases are listed in Table 4 and were defined as follows:

- Cases 01-08 are comprised of all possible permutations of maximum and minimum values: 3 variables (cap height, cap width, and misalignment), 2 values (maximum and minimum) resulting in $2^3 = 8$ permutations. Note that because of the definition of the geometry, it is not possible to pair a value of axial misalignment, m with a value of weld cap height, h, if m > h. Therefore, when appropriate, the value of axial misalignment has been adjusted to the maximum possible for that arrangement. The Case 01 and Case 02 geometries are shown in Figure 29 and Figure 30, respectively.
- Case 09 uses the average values for the geometric dimensions. Although the measurements were taken from a single tanker, Case 09 can be seen as a representative average to compare to the more extreme cases 01-08. The Case 09 geometry is shown in Figure 31.
- Case 10 is defined as the flush-ground geometry with no misalignment as previously considered in HSE and TWI studies. This case was used as a benchmark for comparison with the other 9 cases. The Case 10 geometry is shown in Figure 32.

In Table 4, the rightmost two columns describe the minimum and maximum crack sizes modelled for each case. For example, for Case 10, the minimum crack size was 1.0mm and the maximum crack size was 4.5mm. Note that when a weld cap is present, it is possible to model cracks with depths greater than 5.0mm (the nominal tanker shell wall thickness). Typically, 15 to 21 crack sizes were modelled between the minimum and maximum specified values, resulting in approximately 200 linear elastic finite element simulations that were used to derive geometry-specific stress intensity factor solutions. For each separate set of applied primary loads, collapse solutions were also obtained from elastic-perfectly-plastic simulations with a specified yield stress of 133MPa, Young's modulus of 70GPa and Poisson's ratio of 0.3.

4.4 Material properties

4.4.1 Overview

Detailed information about the properties of the materials under consideration in an ECA allows for a reduction in conservatism by expanding the acceptable region underneath the failure assessment line. A full stress-strain curve allows for an Option 2, material-specific failure assessment line to be generated. In contrast when only single point tensile properties or information from literature is available, an Option 1 failure assessment line is used.

Additionally, the material properties obtained from mechanical testing in this phase of work has allowed for a quantitative comparison and characterisation of the variation of material properties across multiple GRW tankers to be assessed. In this section, the tensile properties and fracture toughness properties used in the detailed ECA are described.

4.4.2 Tensile properties

Tensile testing has previously been undertaken by TWI on samples from the GRW tanker J3025 and additional tensile testing was performed on samples

from J3146 during this phase of work. The details of the tensile testing for samples from J3146 are provided in Appendix H. The stress-strain curves for the parent metal samples showed only small variation between GRW tankers J3025 and J3146 (see Figure 33). The weld metal stress-strain curves, however, showed a more pronounced difference in terms of the strain hardening behaviour between the sets of samples taken from the different tankers (Figure 34). All of the stress-strain curves are shown together in Figure 35. Although the curves appear different, the single-point tensile data shown in Table 5 and Table 6, shows only small variations. As in the previous TWI assessment report, a weld metal sample from J3025 (herein labelled J3025 W02) represents the lower-bound stress-strain curve; the properties from this curve were used to define the failure assessment diagram. They are as follows:

- Young's modulus: 70GPa
- Poisson's ratio: 0.3
- Yield stress: 133MPa
- Ultimate tensile stress: 270MPa

4.4.3 Fracture toughness

TWI also performed fracture toughness testing on single edge notched bend (SENB) specimens extracted from a section taken from GRW tanker J3146. Details of the testing are also provided in Appendix H.

Six SENB specimens were machined from a section extracted from the front-most circumferential seam weld (ie band A from tanker J3146). The resulting J-R curve is shown in Figure 36. A power-law fit to the data results in the following equation:

$$J(\Delta a) = -106.8 + 159.2(\Delta a)^{0.13}$$

In the previous TWI report for DfT, six SENB specimens were also machined from a GRW tanker – tanker J3025. The resulting J-R curve is shown in Figure 37. The power-law fit to the data results in the following equation:

$$J(\Delta a) = 10.70 + 62.60(\Delta a)^{1.00}$$

Superficially, these two J-R curves seem relatively different due to their distinct pre-exponential and exponential coefficients. However, to quantitatively compare the J-R curves from GRW tankers J3025 and J3146, a power-law fit was applied to all relevant data points. The resulting J-R curve is shown in Figure 38 and the equation is as follows:

$$J(\Delta a) = 9.350 + 63.80(\Delta a)^{1.00}$$

Note that the exponent is 1.0 in the combined J-R equation is the same as in the J-R curve for J3025. Additionally, there is strong agreement for the tearing-initiation point. Therefore, from the fracture toughness tests conducted on samples taken from J3025 and J3146, there is not extensive variability in the tearing resistance of the materials.

In conclusion, the J-R curve that can be used for a tearing assessment is the combined J-R curve. The corresponding material toughness is $J_{0.2BL}$ = 23.46N/mm, or equivalently $K_{mat}(J)$=42.4MPa√m. This is slightly lower than the value of 44MPa√m previously used.

4.5 Applied stress

4.5.1 Primary stress

4.5.1.1 Overview

Two sets of distinct load cases were considered: ADR load cases and the preliminary topple test load case. The ADR load cases were considered as realistic design load cases that the tanker is likely to be subjected to (or experience) throughout the duration of its operation. In addition to the ADR load cases, two 'roll-over' load cases were considered: (1), the previously analysed case arising from the 2bar pressure-impulse simulation, and (2), the preliminary topple test load case as analysed by HSL and detailed below in Section 4.5.1.3.

4.5.1.2 ADR load cases

The 'ADR load cases' were obtained from ADR (2013). As per Section 6.8.2.1.2 of ADR:

The tanks and their fastenings shall be capable of absorbing, under maximum permissible load, the forces exerted by:

- In the direction of travel: twice the total mass (ADR Load Case 1);
- Vertically upwards: the total mass (ADR Load Case 2);
- Vertically downwards: twice the total mass (ADR Load Case 3);
- At right angle to the direction of travel: the total mass (ADR Load Case 4).

In order to obtain the primary stresses arising from the ADR load cases, TWI modified the existing proprietary GRW finite element model of a 10-banded tanker. The main objectives of the modification were to improve the quality of the finite element mesh (to facilitate more controlled stress extrapolation) and to change the geometry to match that of the specific tanker employed in the fatigue data collection exercise, tanker J3857. All details of the finite element model modification and post-processing are presented in Appendix F.

The analysis of the modified tanker model resulted in the definition of the ADR load case for the present ECA. This was done by identifying the largest tensile net section, membrane and through-wall bending stresses at each of the tanker bands for each ADR load case. The results indicated that both tanker bands B/10(-) and E/10(+) at the triple joint position, where the cradle gusset plate is joined to the tanker shell in the vicinity of the chassis rails, were the most severely stressed under ADR Load Case 3. Based on considerations of the proportion of the net section stress that was through-wall bending stress, it was determined that tanker band E/10(+) was the critical position to assess. At this location, under ADR Load Case 3, the following stresses are present:

- Net section stress: 67.45MPa
- Through-wall bending stress: 40.53MPa
- Membrane stress: 26.92MPa

The primary stresses above therefore define the 'ADR Load Case' considered in the ECA. Note that all of the most highly stressed positions under the ADR design load cases are located along the bottom of the tanker for each tanker band. From measurements and observations within the scope of this work, these positions experiencing the highest stresses are positioned along bands

where an additional internal fillet weld is present (as this weld is typically present from the 3 o'clock to the 9 o'clock position).

4.5.1.3 Roll-over load cases

Two 'roll-over' load cases were considered.

The first load case comes from the previously analysed 2bar pressure-impulse simulation. For background information about this load case, see (GRW, 2013a) and (TWI, 2013a and 2013b). Note that TWI did not perform the pressure-impulse simulation, but only post-processed the results of the output database file for the simulation that GRW provided to TWI. In summary, in order to simulate the conditions of a roll-over, GRW simulated the tanker subject to a short-term 2bar internal pressure impulse. The dynamic stress analysis was analysed to identify the time increment at which the peak tensile stress occurred. At this time increment and at the position of the peak tensile stress, the local section stresses (membrane and through-wall bending) were evaluated. Figure 39 illustrates the post-processed through-wall bending stresses at the critical time increment along each band. The thick black line shows that the peak through-wall bending stress attained was approximately 150MPa. At this location, the membrane stress was negligible. Therefore, in the present ECA, 'roll-over load case 1' is considered to be a pure, through-wall bending stress with the applied bending stress equal to 150MPa. It is important to note that the 150MPa bending stress is an elastic-plastic bending. Assuming the lower-bound stress-strain curve for the weld metal, a 150MPa is equivalent to a local, normalised bending moment of 823N.mm/mm. The equivalent elastically-calculated bending stress is approximately 200MPa.

In Section 3.4.3 of the HSE ECA report (2013), the following critical defect sizes are cited:

- Long (ie fully-circumferential) surface critical crack depth: 1.1mm
- Surface critical crack depth (with a surface length, 2c = 25mm): 1.5mm
- Through-thickness critical crack length, 2a: 13.1mm

To make a comparison between the definition of the roll-over load case provided above and the results specified in the HSE report (2013), consider the following: using these critical values and the tensile properties specified in the HSE report, it is possible to approximately back-calculate the applied primary stress that was used in the HSE ECA, if it is assumed that the applied primary stresses had zero membrane stress component. Further assuming yield magnitude tensile residual stresses in the as-welded structure (and therefore with relaxation of the residual stresses enabled due to large primary loads), the applied primary bending stress is evaluated as approximately 140MPa for both the long surface flaw and for the 25mm long surface flaw. However, for the through-thickness flaw, the applied primary bending stress is back-calculated as 123MPa. These applied stresses are different from those being considered within this report, and therefore any differences in the findings of the HSE report and the present ECA in terms of critical defect sizes may partially be attributable to the difference in applied primary stresses.

The second roll-over load case comes from the preliminary results of the HSL topple tests conducted within WP1 (HSL, 2014b). This simulation involved the tanker filled with fuel oil and an initial rotational component of

2.6rad/s. Henceforth, this load case is referred to as the 'Roll-over load case 2'. The preliminary results of the HSE modelling are as follows:

- The critical location is Band F/8(+) just above the impact zone;
- The high stress area extends circumferentially along a length of approximately 250mm;
- The local, normalised bending moment is 1460 N.mm/mm which corresponds to an elastic-plastic, through-wall bending stress of 254MPa;
- The section membrane stress is 21.5MPa;
- When the results of the finite element simulation are compared to the experimental test results, the FE predications agree with the experimental measurements to within 5% at the closest gauge locations on Band F/8.

Therefore, similar to roll-over load case 1, this load case is predominantly through-wall bending and involves stresses that generate plasticity (above yield stress).

As per clause 6.4.1 of BS 7910:2013, the methods in BS 7910 predominantly relate to stress-based assessments, ie when the nominal stress is lower than the yield strength of the flawed section. For both roll-over load cases, the stresses are well above the yield strength of the flawed section, as the yield strength of the weld metal has been taken to be 133MPa. Therefore, the methods of a stress-based assessment may not be wholly appropriate for the fracture assessment of the GRW tanker joints under roll-over load cases. Moreover, the stresses experienced during the roll-over (or topple test) are dynamic and thus occur over short time-periods. In order to assess these cases, the associated strain rates that the section under consideration experiences are required in order to ensure that a suitable fracture toughness definition is being applied. A standard, stress-based ECA assumed quasi-static fracture toughness properties.

The methods of a stress-based ECA have been applied to the roll-over load case and the preliminary HSL topple test load case. However, the applicability and accuracy of the ECA calculations should be considered in the context of the preceding discussion.

4.5.1.4 Summary of the primary stress load cases

The primary stress load cases are summarised as follows:

- ADR load case:
  - Design load case; position subject to most significant stresses amongst all ADR load cases.
  - Membrane stress: 40.53MPa
  - Through-wall bending stress: 26.92MPa

- Roll-over load case 1:
  - Derived from GRW 2bar pressure-impulse simulation.
  - Membrane stress: 0.00MPa
  - Through-wall bending stress: 150MPa

- Roll-over load case 2:
  - Derived from HSL fluid-structure interaction simulation of topple test.
  - Membrane stress: 21.50MPa

- Through-wall bending stress: 254.25MPa

4.5.2 Secondary stress

In the previous TWI ECA, due to the absence of any residual stress measurements or additional guidance, the defects under consideration were assumed to be subject to yield-magnitude, tensile residual stresses as recommended by BS 7910. This assumption was thought to be a potential source of over-conservatism.

In Section 2.8, the experimental residual stress measurements undertaken by Sheffield Hallam University on behalf of GRW were reviewed. It was concluded that the measurements could not be used in their current form because of the potential effect of cold working on the measured residual stresses and because the sub-surface measurements did not cover the region of interest where the hypothetical crack tips under consideration are positioned.

In order to improve upon the residual stress input for the engineering critical assessment, TWI was provided the tanker band joint welding procedure specification (WPS) by GRW (2010). The WPS was used to develop a detailed thermo-elastic-plastic finite element simulation of the welding process in order to predict the likely residual stress profile. The details of this activity are provided in Appendix G.

The primary result of the finite element simulation of the welding process is shown in Figure 40. In this figure, the main results are the red solid and dashed curves which represent the transverse and linearised membrane residual stress patterns acting on the hypothetical crack plane. The residual stress profiles are plotted from the root of the weld (ie at the positioner lip on the extrusion band) along a radial path out to the outer surface of the joint. At the weld root, the transverse stress is 121MPa, nearly equal to the yield stress, 125MPa. However, as the radial position increases (moves towards the outer surface), the linearised membrane residual stress, Qm, decreases to less than 50% of the yield stress.

The finite element simulation of the welding residual stresses involved the use of material properties from literature, and therefore provides only indications of the likely residual stress profile. However, when compared to the experimental measurements, the agreement is relatively good. In Figure 41, the experimentally measured transverse residual stresses from (GRW, 2013d) have been plotted on top of the simulated residual stresses. It can be seen that from the cap of the weld down to about 3mm through the joint wall thickness, the simulated residual stresses agree with the X-ray diffraction measurements (taking into account the error estimates on the XRD measurements). The calculation of critical defects that follows considers both yield magnitude tensile residual stresses (relaxed, possibly by high L_r values) as well as the welding simulation residual stresses.

4.6 Fatigue crack growth calculations

Fatigue crack growth calculations were undertaken based upon the guidance of BS 7910 Clause 8. Preliminary calculations employed the one-stage Paris law:

$$\frac{da}{dN} = A(\Delta K)^m \quad if \quad \Delta K > \Delta K_{th}$$

Where

da/dN is the fatigue crack growth rate (crack growth per stress cycle)
A and m are the Paris law coefficients
ΔK is the stress intensity range
ΔK_{th} is the threshold stress intensity factor, below which fatigue crack growth does not occur.

In BS 7910, Paris law coefficients are provided for steel, and it is recommended that for other materials with elastic modulus E_{mat}, the exponent m = 3 can still be used, but that the following equations should be used to derive the other material-specific coefficients:

$$A_{mat} = 5.21\times 10^{-13}\left(\frac{E_{steel}}{E_{mat}}\right)^3$$

and

$$\Delta K_{th,mat} = \Delta K_{th,steel}\left(\frac{E_{steel}}{E_{mat}}\right).$$

Assuming E_{steel} = 207000MPa and E_{mat} is the Young's modulus of the aluminium alloy under consideration, 70000MPa, then A_{mat} = 1.35E-11 and $\Delta K_{th,mat}$ = 21.3.

Note that the Paris law coefficients employed above are the mean plus two standard deviation coefficients specified in BS 7910. Although one could derive material-specific Paris law coefficients for the GRW tanker weld metal, this was beyond the scope of work and would require an extensive testing programme to ensure statistically relevant results. Additionally, consideration was given to the two-stage Paris law in BS 7910. However, the use of a two-stage Paris law for aluminium is not explicitly referred to in BS 7910 (ie the conversion of the two-stage law for steel in air to a two-stage law for aluminium in air), and therefore it was not employed. There exist other fatigue laws that incorporate improved accuracy in fatigue life predictions for near-threshold crack growth as well as Stage III crack growth such as NASGRO and the Collipriest laws, but these require significant fine-tuning of parameters and were not the focus of the present work programme.

BS 7910:2013 Clause 8.2.1.5 discusses variable amplitude loading. It states that, due to the complexities associated with variable amplitude loading, the use of the Paris law may overestimate fatigue life and therefore, for critical conditions, the calculated fatigue life should be halved. In the results that follow, the fatigue life directly calculated from the integration of the Paris law is reported (ie no safety factor is included). However, in the presentation of the results that follows, a lower bound fatigue life estimation curve is created. Point-wise, this curve typically incorporates a safety factor (ie an offset from the calculated curve), and therefore there is no significant inconsistency between the presentation of the findings of this work and BS 7910. A sensitivity study was undertaken to further highlight this point.

It was noted that, when the fatigue stresses were obtained from the accelerometer readings, the ratio of bending stress to membrane stress on average was typically between 0.35 and 0.6 (eg of the total section stress,

35-60% was through-wall bending and the remainder was membrane stress). It is conservative to assume that the entire fatigue stress spectrum is applied as a membrane stress. However, this may be overly conservative as the stress intensity factor associated with membrane stress is higher than the corresponding stress intensity factor for the same magnitude of through-wall bending stress. This point is highlighted in order to further ensure the conservatism of the lower bound fatigue life estimation curve without having intrinsically included the recommended safety factor from BS 7910.

4.7 Failure assessment line

A material specific (Option 2) failure assessment line was constructed based on the lower bound tensile stress-strain curve and was produced in accordance with BS 7910:2013. The lower bound stress-strain curve was used based upon Clause 7.1.3.1 (BS 7910, 2013): '… safe assessments can be made of flaws located in welded regions (weld metal and HAZ) if the tensile properties assumed are the lower of the parent metal, weld metal or HAZ'.

4.8 Results

4.8.1 Stress intensity factor solutions

For each geometry case (01 – 10), with and without the additional internal fillet weld, linear elastic finite element simulations were performed in order to evaluate the stress intensity factors. For each axisymmetric model, sharp cracks were modelled ranging in size from 0.75mm deep flaws to 7.0mm deep flaws, depending on the height and presence of the weld cap. Typically, 15-20 different cracks were modelled for each geometry, allowing for a smooth parameterisation of the geometry-specific stress intensity factor solution. Each simulation comprised three distinct static steps: a 1MPa membrane stress, 1MPa through-wall bending stress, and 1MPa crack flank pressure.

Due to the principle of linear superposition, the resulting stress intensity factors arising from these unit loads can be scaled and combined to obtain the stress intensity factor for any combination of applied membrane, bending and crack flank pressure. For a defect of height a, the secondary stress intensity factor was calculated as Qm(a) times the stress intensity factor for a 1MPa crack flank pressure.

Examples of the stress intensity factor solutions for membrane stress are shown in Figure 42 and Figure 43 for the geometry cases without and with fillet welds, respectively. For the through-wall bending stress cases without fillet weld, the results are shown in Figure 44. Note that when the additional internal fillet weld is present and the loading is pure through-wall bending, the crack tip is under compression in almost all cases.

In the evaluation of critical defect sizes and fatigue crack growth calculations, a piecewise linear interpolation method was employed to evaluate the stress intensity factors. For flaws marginally larger than those modelled, a polynomial extrapolation method was employed. This typically involved an even ordered polynomial fit (order 4-8). As polynomial interpolation is typically poor near the ends of the interval of interpolation, a check was made to ensure that the extrapolation followed the appropriate trend.

4.8.2 Considerations for finite length defects

The discussion of results thus far has considered only fully circumferential flaws, based upon the results of the axisymmetric finite element simulations. However, it is reasonable to consider finite length surface flaws, and therefore this section considers how to approximate the stress intensity factor solutions for finite length flaws from the existing fully circumferential solutions.

In BS 7910:2013, the stress intensity factor solution most similar to the GRW tanker band joint is the curved shell with a fully circumferential or finite length internal surface flaw (Solution M.6). As can be seen in Figure 45 for membrane stress and Figure 46 for through-wall bending stress, the long (fully circumferential) flaw solution is the upper bound of finite length flaw solutions. As the length, 2c, of a finite length inner surface flaw increases, the stress intensity factor solution converges to the long surface flaw solution. Therefore, the effect of the finite length can be quantified by defining a parameter ψ as follows:

$$\psi(a,2c)\cdot K_{long}(a) \;=\; K_{2c}(a)$$

Where

$K_{long}(a)$ = the stress intensity factor solution for a long flaw with depth a;
$K_{2c}(a)$ = the stress intensity factor solution for a finite length flaw with depth a and length 2c.

Based on this definition of ψ, once the stress intensity factor solution is known for a long flaw, the stress intensity factor for a finite length flaw for the same geometry can be approximated. Given that the geometry of the GRW tanker joint is geometrically similar to an inner surface defect in a curved shell, the geometry-specific stress intensity factor solutions derived for fully-circumferential flaws from the different geometry cases can be combined with ψ to approximate the geometry-specific stress intensity factor for a finite length flaw in a GRW tanker joint by:

$$\psi(a,2c)\cdot K^{FEA}_{long}(a) \;\approx\; K^{FEA}_{2c}(a)$$

Where

ψ(a, 2c) = finite length correction factor obtained for inner surface flaws in curved shells;
$K^{FEA}_{long}(a)$ = the geometry-specific stress intensity factor for a long flaw with depth a;
$K^{FEA}_{2c}(a)$ = the geometry-specific stress intensity factor for an a x 2c finite length flaw.

Concerning plastic collapse, it is conservative to use the FEA-based, geometry-specific, long surface flaw solution, because for long flaws (with aspect ratio a/2c < 100) collapse is primarily dominated by the size of the ligament immediately below the deepest point of the flaw.

4.8.3 Plastic collapse solutions

The definition of the load ratio in an ECA is given by:

$$L_r \;=\; \frac{P_a}{P_c}$$

Where

Lr is the load ratio;
P_a is the applied load (or applied stress);
P_c is the collapse load (or collapse stress).

The plastic collapse load is evaluated using finite element analysis by assuming an elastic-perfectly-plastic material behaviour and incrementally and proportionally applying the loads until the plastic zone at the crack tip spreads through the remaining ligament ahead of the crack tip. The level of applied loads when this criterion is met is considered to be the collapse load. This definition of the collapse load is more specifically the net section collapse load, as it refers to the collapse of the local section containing the flaw. For the various GRW geometry cases, when flaws are shallow or more frequently, when the additional internal fillet weld is present, collapse of the joint occurs away from the section containing the flaw. In Clause 7.3.7, BS 7910:2013 notes that such a remote (or global) collapse can be used as the plastic collapse load in an assessment, but it might be overly conservative. An alternative approach to employing a global collapse solution is to use a J-based approach as employed in (TWI, 2013a-b). When appropriate, or the global solution was deemed too conservative, the J-based method was used.

The load ratios for the ADR load case are shown in Figure 47 and Figure 48 for the geometries without and with the additional internal fillet weld, respectively. Additionally, in Figure 49, a limited selection of the load cases are compared with and without the additional fillet weld. The presence of a 'flat line' in the load ratio plots indicates that the global collapse solution is being employed. For this load case, it can be seen from Figure 48 that for all geometries considered, the global collapse solution is dominant for flaws up to approximately 2.5mm deep.

Two other load cases were considered: roll-over load case 1 and roll-over load case 2. Both cases were assumed to be pure bending. The self-similarity of the load ratio (and reference stress) can be illustrated as follows:

$$L_r = \frac{P_a}{P_c} = \frac{\sigma_{ref}}{\sigma_Y}$$

Where

σ_{ref} is the reference stress;
σ_Y is the yield stress.

Based on this definition, suppose that two sets of loads, P_1 and P_2, are under consideration with P_1 a constant multiple of P_2, $P_1 = \lambda P_2$. Then, once the load ratio has been determined for P_2, the load ratio can be determined for P_1 without the need for an additional simulation.

Load ratios were evaluated for geometry cases 09 and 10 with and without the additional internal fillet weld.

4.8.4 ADR load case assessment

4.8.4.1 Critical defect sizes

The critical defect sizes were determined by changing the crack size until the assessment point intersected the failure assessment line. Critical defect sizes for the geometry without the additional internal fillet weld and with assumed tensile, yield magnitude residual stresses (with relaxation enabled) are shown in Table 7. Similarly, in Table 8, the critical defect sizes are shown for the geometry without the additional internal fillet weld and with the through-thickness residual stress profile obtained from the welding simulation. In these tables, the calculations have been performed for the axisymmetric case (a long surface flaw) as well as for the finite length flaw cases. Additionally, for comparison, the BS 7910:2013 curved shell solutions are shown with the Option 1 and Option 2 failure assessment lines. It can be seen that the smallest critical defect amongst all geometry cases is 2.10mm. This occurs in a geometry in which significant misalignment is present. The critical defect size for a long surface flaw in the 'average' geometry (Case 09) is 2.56mm whereas it is 2.48mm for the flush ground joint (Case 10). Note that a comparison between the results in Table 7 and Table 8 indicates that, on average, when the through-thickness residual stress profile obtained from the welding simulation is used, the critical defect heights are only 7% larger. The methods used to calculate the critical defect sizes are shown in Figure 50 and a chart of the results is shown in Figure 51.

When the additional internal fillet weld is present, the critical defect size was almost always larger than the deepest flaw modelled. Although some extrapolation of the results was attempted, the critical defect sizes listed in Table 9 indicate the critical defect height as '>a' when this occurred and 'a' was the deepest flaw modelled. For this reason, it may be assumed that surface flaws under the ADR load case when the additional fillet weld is present are acceptable.

As a consequence of the potential for large critical defect heights for the inner surface flaws analysed, consideration was given to leak-before-break and through-thickness flaws. Calculations were performed using the BS 7910:2013 solutions for through-thickness flaws in curved shells (solutions M.6 and P.10.1). Under the ADR load case, the critical defect length, 2a, for a through-thickness flaw is 21.4mm. In light of other calculations in this report, it is expected that this may be a conservative approximation of the critical through-thickness flaw length for the actual GRW joint geometry. Consider, for example, the 'average' geometry with a 50mm long surface flaw. The critical defect height is 4.09mm as shown in Table 7. The flaw re-characterisation rules in Annex E of BS 7910 allow for this flaw to be re-characterised as a through-thickness defect with length, $2a = 50 + B$, where B is the remaining ligament. In this specific example, $B = 2.25$mm, taking into account the weld cap height. Therefore, the re-characterised through-thickness flaw would have total length $2a = 52.25$mm. This is more than twice the critical through-thickness length (21.4mm). Although calculations have not been performed for surface flaws with length 25mm, it would be expected that the critical defect height for a surface flaw with 25mm length would be larger than the critical defect height for a surface flaw with 50mm length and hence B would be closer to 0.0mm. Nevertheless, the re-characterised flaw would still have a total length greater than 21.4mm.

Consequently, although the critical defect length for a through-thickness flaw in the GRW joint is most likely larger than the BS 7910 solution of 21.4mm, it is not likely that any leak-before-break type consideration will lead to significant changes in the acceptable flaw sizes or fatigue life calculations. This conclusion is similar to that reached by HSE (2013).

4.8.4.2 Fatigue life calculations

The most highly stressed location under the ADR load case is positioned on tanker band E/10(+) with a nearly equivalently stressed position also on tanker band B/10(-). All positions that are highly stressed under the ADR load cases are located along the bottom half of the tanker. Measurements and observations of tankers within the project have indicated that at these locations, additional internal fillet welds may be present. However, it was found that a continuous fillet weld was not always present and was either absent or stitched. The gap between welded lengths and un-welded lengths (when the fillet weld was stitched) may prevent the strengthening of the joint by the fillet weld. Additionally, the quality of the fillet weld will have an effect on how well it may reduce the stresses acting on flaws in the circumferential seam welds. Therefore, the fatigue life calculations performed for the ADR load cases (and therefore the lower bound fatigue life estimation curve) do not consider the presence of an internal fillet weld.

Fatigue life calculations were performed based on an assumed, initial 2x100mm surface-breaking defect. The reasons for choosing this initial defect size are as follows:

- GRW have reported findings of a continuous crack-like defect, at the location of a radiographic lack of fusion indication, that is 80mm long and has a maximum height of 2mm. Based on the principles of BS 7910, this flaw would be characterised as a 2x80mm initial defect.
- In the HSE report, an initial defect size of 2x100mm was used in the fatigue calculations based on their measurements of sectioned GRW joints.
- TWI has undertaken metallographic examination of multiple sections from multiple GRW tankers and has observed both 2.19mm and 2.04mm deep surface-breaking defects with length less than 200mm.

It is therefore realistic to expect that a 2x100mm initial, crack-like defect could be present.

The modelling of the crack-like defects has followed established modelling best practice and the guidelines in BS 7910. Thus, measured defects are characterised by their maximum depth and total (continuous) length. Using these two dimensions, the flaw is assumed to have a semi-elliptic shape (if a finite length flaw is assumed). One could model the exact defect morphology (ie the true geometric shape of the crack front) if detailed information about the shape was available. However, the conclusions obtained from modelling a specific crack front morphology would not be scalable, as the present non-destructive inspection methods are not capable of characterising the defects present in GRW joints to a suitable of accuracy. Thus, by analysing one or more specific crack front shapes, the results obtained could not be applied to the entire GRW tanker fleet because it is not possible to conclude that other, more severe defects are not present. Only destructive examination of GRW joints would enable exact analysis of specific defects but this would require a significant sampling (and hence significant sectioning of tankers).

This is not believed to be a valuable exercise and does not follow standard practice and application of engineering critical assessment methods.

Due to the use of assumed material properties for the welding simulation of residual stresses, and due to the aforementioned small influence (on average) that the through-thickness residual stress profile has on the critical defect height, yield magnitude residual stresses with relaxation enabled were used to calculate the fatigue life.

Finally, in the results that follow, the fatigue life is presented in terms of 'years'. Note that, by definition, this is a 220,000km year and may not refer to an actual one-year time period, as this will depend on the tanker operator.

The results of the fatigue life calculations are as follows:

When an additional internal fillet weld is present and continuous, the fatigue life of each of the joint geometries is greater than 20 years.

When an additional internal fillet weld is not present, for a 100mm long surface flaw with an initial defect height of 2.0mm, assuming the one-stage Paris law for aluminium, tensile, yield magnitude residual stresses (with relaxation enabled), and when the fatigue stress ranges are assumed to be pure membrane stress:

- Case 01 has a fatigue life of 3.9 years. Note that Case 01 considers a weld cap of 2.84mm and misalignment of 2.84mm.
- Case 02 has a fatigue life of 39.3 years. This geometry has no misalignment and a 2.84mm weld cap height; hence, the weld cap plays a significant role in increasing the fatigue life.
- Case 03 has a fatigue life of 3.8 years. This case is the same as Case 01 but with a slightly smaller weld cap width. There is only a marginal difference between the fatigue life for Case 03 and Case 01 and therefore the weld cap width does not seem to be a significant factor.
- Case 04 has a fatigue life of 37.3 years. This case is the same as Case 02 but with a slightly smaller weld cap width. As in Case 02, the weld cap height is the dominant parameter for this geometry and consequently, the fatigue life is high.
- Case 05 has a fatigue life of 4.1 years. Geometry Case 05 has a 0.55mm weld cap height and misalignment equal to 0.55mm. The weld cap height of 0.55mm was the minimum measured value; however, the mean weld cap height was 1.96mm and 0.55mm is less than the mean minus 1 standard deviation.
- Case 06 has a fatigue life of 7.4 years. Geometry Case 06 does not have any misalignment present, but has only a 0.55mm weld cap height.
- Case 07 has a fatigue life of 4.1 years. This case is the same as Case 05 but with a slightly smaller weld cap width. As previously noted, the weld cap width seems to have had only a minor influence.
- Case 08 has a fatigue life of 7.3 years. This case is the same as Case 06 but with a slightly smaller weld cap width.
- Case 09 has a fatigue life of 14.8 years. This geometry incorporates the average weld cap height, weld cap width and misalignment values from the HSL laser scan measurements.
- Case 10 has a fatigue life of 4.46 years. This is the flush ground joint geometry.

The calculated fatigue lives shown above need to be interpreted with respect to the following: in order to analyse a potential relationship between the geometry of the joint and the calculated fatigue life, a parametric study was undertaken. The geometries considered **do not necessarily represent geometric configurations that have been measured from actual GRW tanker joints**. Consequently, TWI is not suggesting that measurements of actual GRW joints to-date indicate that there is the potential for a fatigue failure after 3.8 years as the result from Case 03 indicates. Instead, the parametric study was used to understand the relationship between geometry and fatigue life as described in more detail in Section 4.9.

4.8.5 Roll over load case assessments

4.8.5.1 Critical defect sizes

Critical defect sizes have been calculated for roll-over load case 1 and roll-over load case 2 for the geometry cases 09 and 10 without the additional internal fillet weld. Two methods were employed, depending on the requirements of the simulations. First, the traditional FAD-based determination of critical size was employed. However, when global collapse was occurring before local collapse (under the assumed elastic-perfectly-plastic material behaviour), it was not always possible to evaluated the critical defect size. In order to take account of the possibility for some stable ductile tearing to occur, alternative simulations, employing the full stress-strain curve in the finite element simulation were performed. The objective is to evaluate the J-integral under the applied loads for a series of defect heights. This generates a curve of J-integral (applied J-integral) as a function of crack depth. The point of tearing instability (ie the position where stable tearing transitions to unstable tearing) occurs when there is a tangency between the applied J-integral curve and the material tearing resistance curve. This is illustrated in Figure 52 where the applied J-integral curve is shown with solid lines; the material tearing resistance curve is shown with dashed lines, and the critical defect height is the location of the vertical portion of the tearing resistance curve.

For roll-over load case 1 which was derived from the 2bar pressure-impulse scenario:

- The 'average' geometry', Case 09 without an additional internal fillet weld and making allowance for some stable ductile tearing to occur has a critical defect height of 2.5mm.
- The flush ground joint geometry, Case 10, without an additional internal fillet weld has a critical defect height of 1.5mm for a long surface flaw based on the Option 2 failure assessment line.
- For comparison with Case 09, the BS 7910 curved shell solution with a long internal surface flaw and nominal wall thickness of 7.0mm (with the stresses adjusted appropriately) has a critical defect height of 2.2mm for the Option 2 failure assessment line, and a critical defect height of 2.1mm for the Option 1 failure assessment line.
- For comparison with Case 10, the BS 7910 curved shell solution with a long internal surface flaw and nominal wall thickness of 5.0mm (with the stresses adjusted appropriately) has a critical defect height of 1.0mm for the Option 2 failure assessment line, and a critical defect height of 0.8mm for the Option 1 failure assessment line.

For roll-over load case 2, which was derived from the HSL fuel oil, 2.6rad/s impact velocity simulation:

- The 'average' geometry', Case 09 without an additional internal fillet weld has a critical defect height of 1.1mm for a long surface flaw based when allowance is made for some stable ductile tearing.
- The flush ground joint geometry, Case 10, without an additional internal fillet weld has a critical defect height of 0.9mm for a long surface flaw when allowance is made for some stable ductile tearing.
- For comparison with Case 09, the BS 7910 curved shell solution with a long internal surface flaw and nominal wall thickness of 7.0mm (with the stresses adjusted appropriately) has a critical defect height of 1.35mm for the Option 2 failure assessment line, and a critical defect height of 1.2mm for the Option 1 failure assessment line.
- For comparison with Case 10, the BS 7910 curved shell solution with a long internal surface flaw and nominal wall thickness of 5.0mm (with the stresses adjusted appropriately) has a critical defect height of 0.13mm for the Option 2 failure assessment line, and a critical defect height of 0.1mm for the Option 1 failure assessment line.

For both cases, the critical depth will increase when finite length flaws are considered, but this has not been quantified in the report.

The results of the critical defect calculations for roll-over case 2 should be interpreted in the context of the previous discussion: the applied stresses are significantly higher than the yield stress (in fact, the applied elastic-plastic bending stress 254MPa, nearly equal to the ultimate tensile strength of the material, 270MPa). For this reason, a stress-based ECA may not be the most appropriate assessment method to characterise the integrity of the joint in the presence of defects.

For the cases when an internal fillet weld is present, the collapse is dominated by global collapse (ie collapse of the tanker shell and *not* the section containing the flaw). This can be explained as follows:

- The presence of the internal fillet weld significantly reduces the stress intensity factor for bending stress. In particular, for most cases considered, when an additional internal fillet weld is present, the crack tip is under compression. Therefore, when the crack height changes, the primary stress intensity factor value does not change significantly, and therefore, Kr is primarily influenced by the secondary stress intensity factor.
- The load ratio is independent of the crack height because global collapse is occurring before local collapse. Consequently, the Lr value does not change as the crack height is increased.

Consequently, the results indicate that for geometry cases 09 and 10, both roll-over load cases are insensitive to the presence of a crack-like defect and are primarily dominated by gross yielding of the tanker shell when the additional internal fillet weld is present.

4.9 Proposal for fatigue life assessment under normal operating conditions

4.9.1 Overview

The effect of geometry on the stress intensity factors, collapse load and critical defect sizes for a GRW joint with a known defect has been extensively studied. However, it is likely that field measurements of existing tankers will produce measurements of weld cap height, weld cap width and misalignment outside the scope of the parametric study undertaken in this

report. Therefore, the objective of this section is to derive and propose a lower bound fatigue life estimation equation that takes into account the results calculated thus far, but can also be applied to any weld geometry that may be encountered. This will allow a finite set of measurements, taken from the critical bands of a GRW tanker, to be used to arrive at a conservative estimate of the safe operating life of the tanker under normal operating conditions.

In the present study, normal operating conditions are defined in terms of primary stresses and fatigue stresses as follows:

- The primary stresses that a tanker circumferential seam weld is likely to experience at any point in its operating life are the severe stresses arising from the ADR design load cases as previously described.
- The fatigue stresses that a tanker circumferential seam weld will experience annually are derived from the 220,000km fatigue stress range histogram from the most highly stressed bands (bands E and B for a 10-banded tanker).

To determine the fatigue life of a component using failure assessment diagram methods, four pieces of information are required: the initial defect size; the critical defect size; the fatigue stresses; and the primary stresses.

In the context of the present study the initial defect size has been selected to be a 2x100mm flaw. There are multiple justifications for this flaw size selection. Firstly, during the metallographic examination exercise, a 2.19mm height defect was found (see Appendix I). It was not possible to characterise the length, other than to conclude it was less than 200mm. Secondly, consideration of a 2x100mm provides consistency and direct comparison with the findings of the previous HSE report (2013). In the HSE fatigue life assessment report, a 2x100mm surface flaw was chosen to be the initial defect size. The HSE justification for selecting the height of 2mm is that the lack of fusion, arising from the presence of the positioner lip on the extrusion profile (when unfused), results in a 2mm lack of fusion defect. The HSE justification for selecting the length of 100mm was that there was relatively little change in the critical defect height for flaws longer than 100mm. Finally, GRW have also identified and reported on a 2 x 80mm defect. Therefore, the 2 x 100mm initial flaw size is consistent with TWI, HSE and GRW experimental measurements.

For each geometry case analysed, the critical defect size was calculated (see Table 7). Therefore, the fatigue life is determined to be the time (in 220,000km years) that is required to grow an initial 2x100mm flaw by fatigue to the critical defect size.

4.9.2 Development of lower bound fatigue life estimation curve

From the presentation of the fatigue life calculations in Section 4.8.4.2, a relationship between the local geometric dimensions and the fatigue life is not immediately clear. It is apparent that the joint geometry significantly influences the fatigue life. Most importantly, misalignment and weld cap reinforcement appear to compete against each other:

- Increasing the weld cap height (reinforcement) increases the fatigue life of the joint.
- Increasing the misalignment decreases the fatigue life of the joint.

To determine a relationship between the weld cap size, misalignment and fatigue life, consider a non-dimensional geometry factor, β, that effectively represents the amount of weld reinforcement, where:

β = (h – m) / 5mm
h = weld cap height (mm)
m = misalignment (mm)

If β is small (approaching 0.0), then misalignment dominates, and the joint will have a low fatigue life.

If β is large (approaching 1.0), then the weld cap height dominates, and the joint will have a high fatigue life.

Note that the definition of β does not include the weld width, w. It was found that w had only a minor influence on the fatigue life, and measurements indicated that the weld width was relatively consistent. Therefore, it is reasonable to exclude the weld width from the non-dimensional geometry parameter.

For each of the ten geometry cases analysed, the non-dimensional geometry parameter β was determined, and the calculated fatigue life was plotted against β. This is shown in Figure 53. In this figure, the solid black circles are the results of the ten geometry cases. The thin black line (labelled 'Poly' in the legend) is the best-fit quadratic curve (second order polynomial) for the data. The fit is extremely good, with an R^2 score (coefficient of determination) equal to 0.9987. When R^2 equals 1, the curve passes exactly through all of the data points; hence, scores very near 1 indicate a strong approximation of the data by a quadratic curve. It was noted that eight of the ten geometry cases that were analysed represented 'extreme' cases where either the misalignment was present with no weld cap height, or the weld cap was present without misalignment. Therefore to verify the accuracy of the curve fit, three additional geometry cases were defined: two cases with β equal to 0.2 and one case with β equal to 0.4. These are plotted in Figure 53 as blue triangles. It can be seen that these follow very much the same quadratic relationship as the original ten geometry cases.

In order to take account of the spread in the data and also to incorporate a margin of safety, a lower-bound, offset quadratic curve is also shown in Figure 53 as a solid red line. This curve is given by the equation:

$$F = \begin{cases} 3.75 & \text{if} \quad \beta < 0.05 \\ 60(\beta - 0.05)^2 + 25(\beta - 0.05) + 3.75 & \text{if} \quad \beta \geq 0.05 \end{cases}$$

Where

F = fatigue life in 220,000km years.

Using this quadratic equation, it is possible to estimate the fatigue life of a joint based on the non-dimensional geometry parameter β. Alternatively, if a specific fatigue life (F) is required, then the corresponding value of β can be calculated. Since β depends on both h and m, this allows for the specification of a range of acceptable weld cap height and misalignment combinations that would achieve the target fatigue life. Tables 10 and 11

provide examples of look-up tables that could be used to assess the fatigue life based on measurements of the weld joint geometry.

Note that the presentation and development of the fatigue life estimation curve is only provided as an **informative example**. That is, it is clear from the results that it is possible to obtain a way of estimating the fatigue life of the GRW joints based upon measurements. The fatigue life estimation look-up tables have been provided as a way to demonstrate a method that would enable field measurements to be easily converted into an estimated fatigue life. However, the final presentation of the table will necessitate agreement on the assumptions used to derive the results, ie the initial defect height, defect length and fatigue stresses (see Section 4.9.3 for more information). Additionally, the feasibility and validity of implementing such a method depends on the ability to measure accurately the weld cap height and misalignment from the external surface of the tanker.

4.9.3 Fatigue life calculation sensitivity study

The main assumptions in the fatigue life calculations and in the development of the lower bound fatigue life estimation curve are the initial defect size and the use of pure membrane stresses. There are several factors that can result in different fatigue life calculations. For example:

- Initial defect height. Starting with a smaller initial defect height (ie the variable 'a') will increase the calculated fatigue life, as it will take longer to grow a smaller defect to the critical defect size. Alternatively, increasing the initial defect height will significantly decrease the calculated fatigue life, for the opposite reason. TWI has observed a 2.19mm defect, whereas HSE have reported evidence of a 2.4mm deep defect, and therefore, it is feasible to take a conservative approach and assume that all fatigue life calculations should start with the maximum observed crack height, ie an initial defect height of 2.4mm. However, TWI has also observed a defect with height 1.00mm. Therefore, potentially the initial crack height could be considered to be less than 2.0mm.
- Initial defect length. The fatigue life calculations are less sensitive to the initial defect length than they are to the initial defect height. However, if the initial length is increased, then the fatigue life will decrease, and if the initial length is decreased, then the fatigue life will increase. GRW have reported on a defect that is 80mm long, and HSE have reported on defects of much longer lengths, but potentially the maximum depth is not 2.0mm for these defects. Therefore, TWI has chosen a 2x100mm defect as the initial defect size as it is not unexpected that such a defect is present and HSE have also chosen this as the initial defect size for their fatigue life calculations for similar reasons and based upon destructive examination of sections from GRW tankers.
- Degree of bending. The 'degree of bending' is defined as the ratio of the bending stress (Pb) to the total stress (Pb + Pm) where Pm is the membrane stress. A degree of bending of 0 would indicate pure membrane stress, and a degree of bending of 1 would indicate pure bending stress. It is recognised that the degree of bending varies from band-to-band and that it has been observed that a degree of bending of up to 0.6 can be achieved in a few, short length, fatigue-sensitive locations. It a standard conservative assumption to assume pure membrane fatigue stresses as TWI has employed for the fatigue life calculations presented in this report. However, including a suitable, conservative level of degree of bending can increase the fatigue life.

- Variable amplitude loading assumption. As noted, BS 7910 recommends that for variable amplitude loading a safety factor of 2 is applied; ie if the fatigue life calculated by integrating the Paris law is F, then the reported value should be F/2. This is due to the complexities that variable amplitude loading has on fatigue crack growth rates. TWI has not applied this safety factor of 2, based on consideration of the fact that pure membrane stresses have been assumed and the fatigue life estimation curve has been deliberately 'offset' to give lower-bound estimates.

In order to assess the TWI fatigue life calculations based on the assumptions previously described, a small sensitivity study has been performed in order to assess the effect of the initial defect height, initial defect length and the degree of bending. The results are presented in Table 12. In Table 12, the results in parentheses include the safety factor of 2. In the results that follow, the fatigue life is presented in terms of 'years'. Note that, by definition, this is a 220,000km year and may not refer to an actual one-year time period, as this will depend on the tanker operator. The main conclusions from the sensitivity study are that:

- When the initial **defect height** is **decreased** to 1.5mm, and the safety factor of 2 is included, then the fatigue life for the average joint geometry (Case 09) is 18.54 years, which is about 25% larger than the fatigue life for Case 09 with an initial defect height of 2.0mm and no safety factor of 2.
- When the initial **defect height** is **increased** to 2.25, and the safety factor of 2 is included, the fatigue life for Case 09 is 4.84 years, which is about 70% reduction in the fatigue life for Case 09 with an initial defect height of 2.0mm and no safety factor of 2.
- When the initial **defect length** is **decreased** to 75mm from 100mm, and the safety factor of 2 is included, the fatigue life is 11.6 years which is about 80% of the calculated fatigue life for Case 09 with an initial defect size of 2.0 x 100mm and no safety factor of 2.
- Because the stress intensity factor associated with bending stress is much lower for the GRW joint than the corresponding stress intensity factor for membrane stress, when the **degree of bending** is varied, the fatigue life **increases**, as expected. When the safety factor of 2 is included and the degree of bending is between 0.25 and 0.5, the fatigue life is between 17.2 years and 53 years. Therefore, it would be possible to adjust the lower bound fatigue life estimation curve by a factor to incorporate expected levels of degree of bending.

4.10 Macro- and microscopic examination of sections from GRW tankers

Part of WP2 is concerned with the examination of actual samples removed from GRW tankers to confirm the existence of crack-like, lack of fusion defects; to measure the flaws when present; to observe any evidence of fatigue crack growth; and to provide post-mortem examination of sections taken following the topple testing carried out by HSL. In particular, the metallographic examination of sections taken from GRW tankers provides experimental evidence of the defect sizes used in the engineering critical assessment.

Part of WP2 is concerned with the examination of actual samples removed from GRW tankers to confirm the existence of crack-like, lack of fusion defects; to measure the flaws when present; to observe any evidence of fatigue crack growth; and to provide post-mortem examination of sections

taken following the topple testing carried out by HSL. In particular, the metallographic examination of sections taken from GRW tankers provides experimental evidence of the defect sizes used in the engineering critical assessment.

The full details of the macro- and microscopic examination of samples taken from GRW tankers are presented in Appendix I.

The first finding concerns a section taken from the rearmost band of tanker J2580 from the impacted side. In this sample, the circumferential weld ruptured during the rollover test as a result of a lack-of-fusion defect arising from the positioner lip on the extrusion band. That is, an initial surface-breaking defect tore, in a ductile manner, through-wall thickness, resulting in a through-wall flaw with length 320mm. Metallographic examination of the sample revealed the presence of a lack of fusion defect that was approximately 1.0mm deep. In order to undertake a fractographic assessment of the specimen only half of the through-wall flaw was broken open. The fracture surface revealed lack of fusion along the entire length, 230mm, of the specimen. The other half was not broken open but radiography confirmed lack of fusion was present. Without measuring the actual crack length from the other side of the through-wall defect, it can only be conclusively stated that the initial defect was at least 230mm long.

Placing this section in the context of the finite element analysis critical defect size calculations:

- The section from J2580 that ruptured through-wall had an initial axial misalignment of approximately 0.5mm, a local weld cap height slightly larger than 1.0mm, an initial defect height of 1.0mm, and a length in excess of 230mm (ie essentially a "long" surface flaw).
- The calculations for the 'average' joint geometry (Case 09), assumed a local weld cap height of 2.0mm and axial misalignment of 0.66mm. For this geometry, under the topple test conditions provided to TWI by HSL as a result of their fluid-structure interaction modelling, the FEA performed by TWI predicted a critical defect height of 1.1mm when allowance for stable ductile tearing is made.

Therefore, taking into consideration that the Case 09 geometry had a larger weld cap height than the section from J2580 that failed, it is expected that the critical defect height for the section that failed should be slightly less than 1.1mm. In this section, a 1.0mm lack of fusion defect has resulted in failure. This case therefore provides strong support for the accuracy and validity of the critical defect height calculations performed by TWI for the topple test conditions.

A macro image of the cross section of the failed joint is shown in Figure 54.

The second finding concerns a section removed from tanker J3564. This section is shown in Figure 55. In this section a 2.19mm lack of fusion defect was found (additional information about a 2.04mm defect found in the same section but in a different circumferential weld is provided in Appendix I). This lack of fusion defect is not located directly at the positioner lip but is instead slightly offset. The length of both defects was between 40mm and 50mm. Correspondence with GRW has confirmed that the location of these defects corresponds to the position of an external tack weld and machining that during manufacture of the tankers is typically at most 50mm long. These measurements agree with this explanation.

In the context of the previous critical defect calculations, consider the following:

- The critical defect height for the topple test loading and average joint geometry **assuming a fully-circumferential flaw** was 1.1mm.
- The loading in the topple test is essentially pure bending.

Based on the FEA it is not possible to conclusively state much about the criticality of the finite length defects. However, comparison to the BS7910 solutions can be made. As has been previously described, the BS7910 solutions provide conservative estimations of the critical defect size because they do not take into account all of the joint geometry. However, the FEA solutions and BS7910 solutions qualitatively follow the same trends. Figure 57 plots the critical defect height for a long surface flaw and a finite length, 2c = 50mm, surface flaw in a curved shell. To calculate the critical defect height, yield magnitude residual stresses have been assumed with relaxation enabled and the Option 2, material specific, failure assessment line has been employed. The critical defect height is plotted against the applied primary stress, assumed to be pure bending under the topple test/rollover conditions. The left vertical axis shows the critical defect height and the right vertical axis shows the percentage increase in critical defect height from the long flaw to the finite length flaw. Note that the topple test typically involves pure bending stresses greater than 150MPa. In this case, a 20% increase in the critical defect height is expected. Considering the 1.1mm calculated critical defect height from the finite element analysis for a long surface flaw under the topple test conditions and average joint geometry, it may be expected that the critical defect height for the corresponding finite length flaw would be 20% greater than this, ie 1.32mm. This is less than the 2.04mm and 2.19mm defect heights that were found for 50mm long flaws in the sample of J3564. Consequently, it is possible that the finite length defects observed in the J3564 sample could be critical under rollover. However, it is recommended that further analysis is performed to conclusively determine this.

The third finding concerns evidence of fatigue crack growth. No evidence of fatigue crack growth was found in any of the sections prepared.

Finally, independent of the assumptions made about the degree of bending of fatigue stresses, the measurements of the joint geometry made during the post-mortem examination can be used to provide indicative information about where typical field measurements of GRW joints may be located in the look up table. For each section from J3564 and J3910, the weld cap height and misalignment were measured. These values were used to calculate the non-dimensional geometry parameter β for each joint. A histogram of the β-values is shown in Figure 56. In this histogram, 60% of the values reside in the bins with β value at least 0.35. Note that in the look up table, diagonals from top-left to bottom-right correspond to constant β-values (hence the constant fatigue life along diagonals). Assuming pure membrane stresses in the current fatigue life look up table, a β value of 0.35 would correspond to a 16.65 year life and a value of 0.4 would correspond to a 19.85 year life. Thus, taking into consideration the fatigue calculation sensitivity study where introducing a degree of bending can increase the expected fatigue life significantly, the fatigue life calculations agree with the observation of no fatigue crack growth: since the tankers sectioned and analysed had been on the road for less than 6 years and the anticipated fatigue life could, on average, be greater than 20 years (potentially much greater depending on the degree of bending), then it would not be expected

that significant, observable fatigue crack growth would have occurred in the sections analysed.

4.11 Conclusions

The conclusions from the ECA related to the safe operating life of the circumferential welds found that:

1 Provided an initial defect is present, the fatigue data (for a ten-banded tanker) identified the cradle positions above the fifth wheel coupling and above the front of the rear longitudinal support members as most susceptible to fatigue crack growth.
2 Under normal operating conditions, the minimum critical defect height is greater than 2.0mm and may be as large as 4.0mm or more. Variation in this defect height will depend on three factors: the presence of an internal fillet weld between the toe of the extrusion band and the inner surface of the tanker shell; the magnitude of the misalignment between the shell and extrusion band; and the size of the weld cap.
3 Assuming an initial defect size of 2x100mm (ie a 2mm deep by 100mm long surface-breaking flaw) based on observations from the post-mortem examination of sections from GRW tankers that such a flaw would not be unexpected, the fatigue life of the joint (ie the time required to grow the 2x100mm defect to a critical size) is greater than 20 years when an internal fillet weld is present and continuous.
4 When a continuous (or potentially intermittent) internal fillet weld is not present, the fatigue life of the joint is influenced significantly by the misalignment and weld cap geometry. For this case, a parametric study involving over 300 simulations was used to derive a quadratic relationship between the fatigue life (assuming an initial 2x100mm flaw) and a geometry parameter that incorporates the weld cap height and misalignment. This allows a conservative estimate of the fatigue life of a joint (without the internal fillet weld) to be easily determined from a look-up table (derived from the quadratic relationship) using measurements of misalignment and weld cap height, which can be taken relatively quickly with a profile/laser gauge. A sensitivity study was undertaken to highlight the influence of bending stresses in the fatigue spectrum and initial flaw size assumptions on the calculated fatigue life.

The ECA of the circumferential welds related to the rollover conditions found that:

1 For the rollover case derived from the topple test, and from associated FE modelling with fuel oil undertaken by HSL, and allowing for some ductile tearing to occur, the critical defect height in an ‘average’ weld geometry is 1.1mm when no internal fillet weld is present. Here the ‘average’ weld geometry relates to measurements from GRW tanker J3910 and may, therefore, not be truly representative of all non-compliant tanker joints.
2 Taking into account geometric differences (ie smaller weld cap height in the test than in the average joint simulation), the predicted critical defect height of 1.1mm agrees well with the experimental observation of the through-wall rupture of a circumferential weld resulting from a 1.0mm deep lack of fusion defect that was over 230mm long in a section of the impacted side of GRW tanker J2580. Although the contained fluid and the impact velocity in the HSL topple test simulation were different to those in the actual J2580 test that involved water and a lower impact velocity, the moment acting on the joint was similar.

3 Considering the rollover load case derived from the pressure-impulse simulation, and allowing for some ductile tearing to occur, the critical defect height in the 'average' weld geometry is 2.5mm when no internal fillet weld is present.
4 When a well-made and suitable internal fillet weld is present, the integrity of the tank in a rollover is not governed by the quality of the circumferential weld, but by the strength of the parent metal of the tank shell or other factors such as the bulkhead to extrusion band joint(s), which were seen to fail in topple tests.

The metallographic examination of multiple sections removed from three GRW tankers found that:

1 A 320mm long, through-wall rupture of a circumferential weld was observed in a section of the impacted side from J2580. The rupture was due to an initial lack of fusion defect at the positioner lip on the extrusion band. The height of the initial defect was approximately 1.0mm and over 230mm long.
2 Examination of a section from J3910 revealed only relatively small (total height less than 1.0mm) lack of side wall fusion, embedded-type defects. This class of defect is not of as significant concern as the surface-breaking flaws analysed in the report.
3 Examination of sections from J3564 revealed both a 2.19mm and a 2.04mm deep surface-breaking defect. These defects were not located directly at the positioner lip but at a small distance offset. The length of these defects was between 40mm and 50mm. Such defects could be critical under rollover conditions if an additional internal fillet weld was not present, however further analysis is required to conclusively determine the criticality of these defects.
4 No evidence of fatigue crack growth was observed. The samples taken from J2580 and J3910 were removed from the sides of the tanker and therefore the samples were not in locations particularly susceptible to fatigue damage. The samples taken from J3564 were located along the cradle welds where fatigue crack growth may be expected. Most samples prepared had additional internal fillet welds present and therefore, fatigue crack growth was not expected. However, even for samples without additional internal fillet welds, no fatigue crack growth was observed.

5 References

ADR (2013): 'European Agreement Concerning the International Carriage of Dangerous Goods by Road', Economic Commission for Europe Committee on Inland Transport, Volume II, ECE/TRANS/225.

BS 7608:2014: 'Fatigue design and assessment of steel structures', British Standards Institution, 1993.

BS 7910:2005: 'Guide to methods for assessing the acceptability of flaws in metallic structures', British Standard Institute, 2005.

BS 7910:2013: 'Guide to methods for assessing the acceptability of flaws in metallic structures', British Standard Institute, 2013.

DfT (2013a): 'Computed Radiography of Aluminium Banded Tanker Welds. Analysis of Tanks J3861 and J2297', DfT Report 131021 – Aluminium Banded Tanker Analysis – Short Version'.

DfT (2013b): 'Technical assessment of the circumferential weld seams on GRW manufactured road tank vehicles', DfT Report 131022 – Rev 3, 23 October 2013.

EDF Energy, 2001: R6 Revision 4 and amendments, 'Assessment of the integrity of structures containing defects', EDF Energy Ltd., Gloucester, UK. (Amendments issued in subsequent years).

GRW (2008): '085-44-500-01 Tank Asm Complete 09-07-2010'. Engineering drawing of GRW Tanker J3857.

GRW (2010): 'Welding Procedure Specification (WPS)', GRW Engineering, 08/02/2010.

GRW (2013a): 'Critical crack size & Crack growth estimate – an extended study', GRW Report No. PVVR20121101, Revision 3. Report Date 30 September 2013. Received from DfT via memory stick on Friday, 25/04/2014.

GRW (2013b): 'Letter report by Prof.Dr-Ing Lothar Issler'. Date of report 21 November 2013. Received by email entitled 'DfT research on petroleum tankers – WP2 2.2 – review of GRW finite element model and analyses' from Steve Gillingham (DfT) to Tyler London (TWI) on Thursday, 17/04/2014 11:35. Document file name 'SKMBT_C28013112112291.pdf'.

GRW (2013c): 'Comments on TWI and DfT technical reports regarding UK fuel tank circumferential weld strength', GRW Report No. PVVR20131031. Date of report 19 November 2013. Received by email entitled 'DfT research on petroleum tankers – WP2 2.2 – review of GRW finite element model and analyses' from Steve Gillingham (DfT) to Tyler London (TWI) on Thursday, 17/04/2014 11:35.

GRW (2013d): 'Stress measurement of an aluminium weld using the XRD-$\sin^2\psi$ technique'. Report No: 11-13-458 (stress measurement) prepared by Dr Quanshun Luo of Materials and Engineering Research Institute, Sheffield Hallam University, 12 November 2013.

GRW (2014a): 'UK fuel tanker J2297 circumferential weld investigation'. GRW Report No. PVVR20140003. Report date 3 April 2014. Received by email entitled 'DfT research on petroleum tankers – WP2 2.2 – review of GRW finite element model and analyses' from Steve Gillingham (DfT) to Tyler London (TWI) on Thursday, 10/04/2014 11:26. Document file name 'UK fuel tanker J2297 circumferential weld investigation_3Apr2014.pdf'.

GRW (2014b): 'J2297_cut out Xrays'. Received by email entitled 'DfT research on petroleum tankers – WP2 2.2 – review of GRW finite element model and analyses' from Steve Gillingham (DfT) to Tyler London (TWI) on Thursday, 10/04/2014 11:26. Document file name 'J2297_cut out Xrays_5.pdf'.

GRW (2014c): 'Safe long flaw depth calculation for UK fuel tanker'. GRW Report No. PVVR20140001. Report date 7 April 2014. Received by email entitled 'DfT research on petroleum tankers – WP2 2.2 – review of GRW finite element model and analyses' from Steve Gillingham (DfT) to Tyler London (TWI) on Thursday, 10/04/2014 11:26. Document file name 'Safe long flaw depth calculation for UK fuel tanker_7Apr2014.pdf'.

GRW (2014d): 'Bend Test Sheet – GRW 019'. Received by email entitled 'DfT research on petroleum tankers – WP2 2.2 – review of GRW finite element model and analyses' from Steve Gillingham (DfT) to Tyler London (TWI) on Thursday, 10/04/2014 11:26. Document file name 'Bend Test 1.pdf'.

GRW (2014e): 'Bend Test Sheet – GRW 019'. Received by email entitled 'DfT research on petroleum tankers – WP2 2.2 – review of GRW finite element model and analyses' from Steve Gillingham (DfT) to Tyler London (TWI) on Thursday, 10/04/2014 11:26. Document file name 'Bend Test 2.pdf'.

GRW (2014f): 'Safety aspects of fuel tankers manufactured by GRW, SA' Report by Prof.Dr-Ing Lothar Issler. Date of report 7 April 2014. Received by email entitled 'DfT research on petroleum tankers – WP2 2.2 – review of GRW finite element model and analyses' from Steve Gillingham (DfT) to Tyler London (TWI) on Thursday, 17/04/2014 11:35. Document file name 'Prof. Issler Report 7.04.14.pdf'.

HSE (2013): 'Development of HSE's opinion on the immediate and short term safety of road going fuel tankers manufactured by GRW (Pty) Limited South Africa', Document ID 'Trim 2013/443978'. Received by email entitled 'DfT research on petroleum tankers – WP2 2.2 – review of GRW finite element model and analyses' from Steve Gillingham (DfT) to Tyler London (TWI) on Tuesday, 22/04/2014 16:16. Document file name 'CEMHD – Mechanical Engineering – development of Opinion on safe Operation of GRW Tankers – December 2013'.

HSL (2014a): 'PE05832 J3910 weld cap data – offside and nearside 19aug14.xlsx'. Received by email from Duncan Webb to Tyler London on 19 August 2014.

HSL (2014b): 'Membrane and bending for ECAS.xlsx'. Received by email from James Hobbs to Tyler London on Friday, 29 August 2014.

Kim ST, Tadjiev D and Yang HT (2006): 'Fatigue life prediction under random loading conditions in 7475-T7351 aluminium alloy using the RMS model', International Journal of Damage Mechanics, Vol 5.

Mistras (2014): 'Radiography Examination Report', Report Ref: 14/34488. Customer HSL for Tanker J3910.

NPL (2005): 'A national measurement good practice guide No. 52: Determination of residual stresses by X-ray diffraction – Issue 2. DTI, 2005.
Pearson (1975): 'Initiation of fatigue cracks in commercial aluminium alloys and the subsequent propagation of very short cracks', Engineering Fracture Mechanics, Vol 7, pp 235-247.

Rozumek, D (2005): 'Fatigue crack growth rate in aluminium alloy including mixed mode I and III', Journal of Theoretical and Applied Mechanics, Vol 43, pp 731-743.

SIMULIA (2013): 'Abaqus Analysis User's Guide', SIMULIA.

Tadjiev DR and Kim ST (2011): 'Fatigue crack growth prediction in 7475-T7351 aluminium alloy under random loading using modified root mean square model', ICF 2011.

TWI (2013a): 'Short-term Fitness for Service Assessment of GRW Road Tankers, TWI (Draft) Report 23437/1/13, September 2013.

TWI (2013b): 'Project 23437 Contract Amendment: Additional FEA for assessment of GRW road tankers, TWI (Draft) Report 23437/2/13, October 2013.

TWI (2014): 'Tanker Testing and Analysis: Work package 2 Ref: PPRO 04/30/7', TWI Proposal PR23024-2, January 2014.

Table 1 HSL laser scan measurements of the offside of Tanker J3910

Position	Tanker band	Weld 1 cap height (mm)	Weld 2 cap height (mm)	Weld 1 cap width (mm)	Weld 2 cap width (mm)
	A/8	1.62	N/A	18.79	N/A
	B/8	1.83	2.04	19.42	18.74
	C/8	2.11	2.16	19.19	17.37
	D/8	2.52	1.8	19.83	19.6
	E/8	2.59	2.02	21.35	20.48
	F/8	2.21	1.93	19.1	18.97
	G/8	2.37	1.56	19.36	21.38
Upper	H/8	1.71	N/A	19.38	N/A
	A/8	2.18	N/A	19.28	N/A
	B/8	2.11	2.22	19.11	18.41
	C/8	1.97	2.25	19.09	18.59
	D/8	2.32	1.67	19.18	19.8
	E/8	2.26	1.83	20.61	19.34
	F/8	2.18	2.1	20.56	19.6
	G/8	1.9	2.1	22.1	20.5
Middle	H/8	1.84	N/A	20.23	N/A
	A/8	1.74	N/A	17.67	N/A
	B/8	2.18	2.04	20.27	20.83
	C/8	2.03	1.86	18.96	17.53
	D/8	2.12	1.95	19.1	17.85
	E/8	1.85	1.81	18.8	19.36
	F/8	1.97	1.95	19.85	19.43
	G/8	1.62	2	18.74	19.03
Lower	H/8	1.46	N/A	19.52	N/A

Table 2 HSL laser scan measurements of the nearside of Tanker J3910

Position	Tanker band	Weld 1 cap height (mm)	Weld 2 cap height (mm)	Weld 1 cap width (mm)	Weld 2 cap width (mm)
	A/8	2.33	N/A	21.36	N/A
	B/8	1.19	2.02	20.47	19.14
	C/8	0.55	1.58	19.24	20.3
	D/8	N/A	1.83	N/A	19.91
	E/8	2.15	2.04	21.19	17.66
	F/8	1.85	2.12	20.8	17.11
	G/8	1.6	1.66	19.61	19.03
Upper	H/8	1.79	N/A	19.5	N/A
	A/8	1.52	N/A	18.59	N/A
	B/8	1.81	2.13	18.71	17.9
	C/8	1.52	1.95	19.51	19.21
	D/8	2.84	2.12	20.39	17.88
	E/8	2.32	1.96	19.6	17.37
	F/8	2.31	1.76	19.91	17.39
	G/8	2.1	2.28	18.49	18.57
Middle	H/8	1.84	N/A	20.23	N/A
	A/8	2.47	1.98	19.52	18.24
	B/8	2.06	2.39	18.72	19.96
	C/8	1.07	2.04	17.68	19.06
	D/8	2.21	2.22	20.67	19.04
Lower	E/8	2.4	2.23	20.23	18.02

	F/8	2.11	2.08	20.3	20.65
	G/8	1.71	N/A	19.94	N/A
	H/8	2.47	1.98	19.52	18.24

Table 3 Details of the representative values used to define the geometry cases

Statistic	Weld cap height (mm)	Weld cap width (mm)	Misalignment (mm)
Average	1.97	19.35	0.63
Maximum	2.84	22.10	3.14
Minimum	0.55	17.11	0.00

Table 4 Description of the geometry cases considered. Maximum crack height is indicative

Case ID	Weld cap height, h (mm)	Weld cap width, w (mm)	Axial misalignment, m (mm)	Minimum crack height, a (mm)	Maximum crack height, a (mm)
Case 01	2.84	22.10	2.84	1.00	4.75
Case 02	2.84	22.10	0.00	1.00	7.50
Case 03	2.84	17.11	2.84	1.00	4.75
Case 04	2.84	17.11	2.84	1.00	7.50
Case 05	0.55	22.10	0.55	1.00	4.75
Case 06	0.55	22.10	0.00	1.00	5.25
Case 07	0.55	17.11	0.55	1.00	4.75
Case 08	0.55	17.11	0.00	1.00	5.25
Case 09	1.97	19.33	0.63	1.00	6.00
Case 10	0.00	0.00	0.00	1.00	4.75

Table 5 Tensile data for the parent metal samples from J3146 and J3025

Specimen identification	Material	Yield stress, Rp0.2% (MPa)	Ultimate tensile strength (MPa)
J3146 M01	Tanker shell	150.9	304.5
J3146 M02	Tanker shell	154.5	308.0
J3025 M01	Tanker shell	134.9	303.2
J3025 M02	Tanker shell	136.0	304.5
J3025 M03	Tanker shell	134.8	303.5
Average value		142.2	304.7
Minimum value		134.8	303.2

Table 6 Tensile data for the weld metal samples form J3146 and J3025

Specimen identification	Material	Yield stress, Rp0.2% (MPa)	Ultimate tensile strength (MPa)
J3146 W01	Weld metal	166.6	284.3
J3146 W02	Weld metal	185.2	283.7
J3025 W01	Weld metal	139.9	270.8
J3025 W02	Weld metal	133.1	270.3
J3025 W03	Weld metal	132.9	278.1
Average value		151.5	277.5
Minimum value		132.9	270.3

Table 7 Critical defect heights for surface flaws without internal fillet weld under ADR load case. Yield magnitude residual stresses assumed with relaxation enabled

Crack length, 2c (mm)	50	100	250	500	1000	Long
Case 01	2.48	2.42	2.31	2.17	2.14	2.10
Case 02	4.53	4.39	3.79	3.53	3.47	3.43
Case 03	2.48	2.41	2.31	2.17	2.14	2.10
Case 04	4.53	4.39	3.78	3.52	3.45	3.41
Case 05	2.49	2.43	2.32	2.18	2.14	2.11
Case 06	3.12	3.04	2.94	2.75	2.68	2.64
Case 07	2.49	2.43	2.32	2.18	2.14	2.11
Case 08	3.12	3.03	2.93	2.74	2.67	2.64
Case 09	3.38	3.28	2.86	2.64	2.59	2.56
Case 10	2.91	2.83	2.72	2.53	2.50	2.48
BS 7910 M.6 Option 1	2.75	2.39	2.19	2.12	2.08	1.97
BS 7910 M.6 Option 2	3.08	2.50	2.27	2.19	2.15	2.14

Table 8 Critical defect heights for surface flaws without internal fillet weld under ADR load case. Through-thickness residual stresses from welding simulation

Crack length, 2c (mm)	50	100	250	500	1000	Long
Case 01	2.51	2.44	2.38	2.33	2.32	2.30
Case 02	4.74	4.60	4.48	4.38	4.34	4.30
Case 03	2.51	2.44	2.37	2.33	2.31	2.30
Case 04	4.75	4.60	4.49	4.38	4.34	4.30
Case 05	2.53	2.46	2.39	2.34	2.32	2.31
Case 06	3.20	3.09	3.01	2.94	2.92	2.90
Case 07	2.53	2.46	2.39	2.34	2.32	2.31
Case 08	3.21	3.08	2.99	2.93	2.91	2.90
Case 09	3.48	3.36	3.25	3.13	3.08	3.04
Case 10	2.99	2.87	2.79	2.74	2.72	2.70

Table 9 Critical defect heights for surface flaws with internal fillet weld under ADR load case. Yield magnitude residual stresses assumed with relaxation enabled

Crack length, 2c (mm)	50	100	250	500	1000	Long
Case 01	>4.50	>4.50	>4.50	4.47	4.29	4.26
Case 02	>6.00	>6.00	>6.00	>6.00	>6.00	>6.00
Case 03	>4.50	>4.50	4.48	4.43	4.41	4.25
Case 04	>6.00	>6.00	>6.00	>6.00	>6.00	>6.00
Case 05	>4.50	>4.50	>4.50	>4.50	>4.50	>4.50
Case 06	>4.50	>4.50	>4.50	>4.50	>4.50	>4.50
Case 07	>4.50	>4.50	>4.50	>4.50	>4.50	>4.50
Case 08	>4.50	>4.50	>4.50	>4.50	>4.50	>4.50
Case 09	>5.00	>5.00	>5.00	>5.00	>5.00	>5.00
Case 10	>4.50	>4.50	>4.50	>4.50	>4.50	>4.50

Table 10 Example of fatigue life calculations using the lower-bound fatigue life curve

Fatigue life (years)	9	12
Misalignment, m (mm)	Weld cap height, h (mm)	Weld cap height, h (mm)
0.00	1.02	1.33
0.25	1.27	1.58
0.50	1.52	1.83
0.75	1.77	2.08
1.00	2.02	2.33
1.25	2.27	2.58
1.50	2.52	2.83
1.75	2.77	3.08
0.00	1.02	1.33
0.25	1.27	1.58
0.50	1.52	1.83
0.75	1.77	2.08

Table 11 Fatigue life calculation look up table based on the lower bound fatigue life estimation curve. "NV" = Not Valid due to m > h.

		Misalignment, m (mm)												
		0.000	0.125	0.250	0.375	0.500	0.625	0.750	0.875	1.000	1.125	1.250	1.375	1.500
Weld cap height, h (mm)	0.375	4.41	3.75	3.75	3.75	NV	NV	NV	NV	NV	NV	NV	NV	NV
	0.500	5.15	4.41	3.75	3.75	3.75	NV	NV	NV	NV	NV	NV	NV	NV
	0.625	5.96	5.15	4.41	3.75	3.75	3.75	NV	NV	NV	NV	NV	NV	NV
	0.750	6.85	5.96	5.15	4.41	3.75	3.75	3.75	NV	NV	NV	NV	NV	NV
	0.875	7.81	6.85	5.96	5.15	4.41	3.75	3.75	3.75	NV	NV	NV	NV	NV
	1.000	8.85	7.81	6.85	5.96	5.15	4.41	3.75	3.75	3.75	NV	NV	NV	NV
	1.125	9.96	8.85	7.81	6.85	5.96	5.15	4.41	3.75	3.75	3.75	NV	NV	NV
	1.250	11.15	9.96	8.85	7.81	6.85	5.96	5.15	4.41	3.75	3.75	3.75	NV	NV
	1.375	12.41	11.15	9.96	8.85	7.81	6.85	5.96	5.15	4.41	3.75	3.75	3.75	NV
	1.500	13.75	12.41	11.15	9.96	8.85	7.81	6.85	5.96	5.15	4.41	3.75	3.75	3.75
	1.625	15.16	13.75	12.41	11.15	9.96	8.85	7.81	6.85	5.96	5.15	4.41	3.75	3.75
	1.750	16.65	15.16	13.75	12.41	11.15	9.96	8.85	7.81	6.85	5.96	5.15	4.41	3.75
	1.875	18.21	16.65	15.16	13.75	12.41	11.15	9.96	8.85	7.81	6.85	5.96	5.15	4.41
	2.000	19.85	18.21	16.65	15.16	13.75	12.41	11.15	9.96	8.85	7.81	6.85	5.96	5.15
	2.125	21.56	19.85	18.21	16.65	15.16	13.75	12.41	11.15	9.96	8.85	7.81	6.85	5.96
	2.250	23.35	21.56	19.85	18.21	16.65	15.16	13.75	12.41	11.15	9.96	8.85	7.81	6.85
	2.375	25.21	23.35	21.56	19.85	18.21	16.65	15.16	13.75	12.41	11.15	9.96	8.85	7.81
	2.500	27.15	25.21	23.35	21.56	19.85	18.21	16.65	15.16	13.75	12.41	11.15	9.96	8.85
	2.625	29.16	27.15	25.21	23.35	21.56	19.85	18.21	16.65	15.16	13.75	12.41	11.15	9.96
	2.750	31.25	29.16	27.15	25.21	23.35	21.56	19.85	18.21	16.65	15.16	13.75	12.41	11.15
	2.875	33.41	31.25	29.16	27.15	25.21	23.35	21.56	19.85	18.21	16.65	15.16	13.75	12.41
	3.000	35.65	33.41	31.25	29.16	27.15	25.21	23.35	21.56	19.85	18.21	16.65	15.16	13.75

Table 12 Fatigue life calculation sensitivity study

Initial crack depth, a_0 (mm)	Initial crack length, 2c (mm)	Degree of bending	Case 09 fatigue life, 220,000km years	Case 10 fatigue life, 220,000km years
Variation on degree of bending				
2.00	100.0	0.00	14.84 (7.42)	4.46 (2.23)
2.00	100.0	0.25	34.40 (17.2)	9.20 (4.60)
2.00	100.0	0.50	106.6 (53.3)	23.1 (11.55)
2.00	100.0	0.75	>300 (>150)	83 (41.5)
Variation on initial crack depth				
1.5	100.0	0.0	37.1 (18.55)	18.0 (9.0)
2.25	100.0	0.0	9.68 (4.84)	2.18 (1.09)
Variation on initial crack length				
2.00	75.00	0.0	23.2 (11.6)	6.48 (3.24)

Figure 1 Cut-out locations for tanker J2297. Reproduced from Figure 5 of GRW report (2014a).

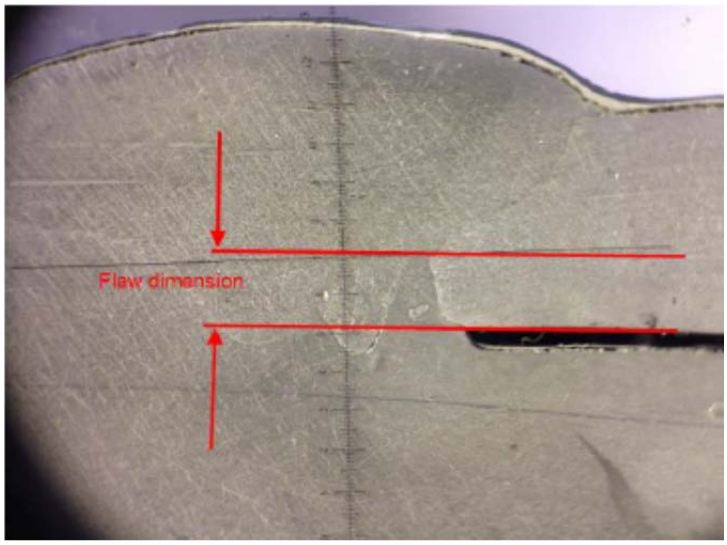

Figure 2 Typical cross section and flaw depth. Reproduced from Figure 9 of GRW report (2014a).

Figure 3 Extrusion profile showing the 2mm positioning lips (arrows) that leads to lack of fusion defects. Image taken from Figure 12 of (GRW, 2014a).

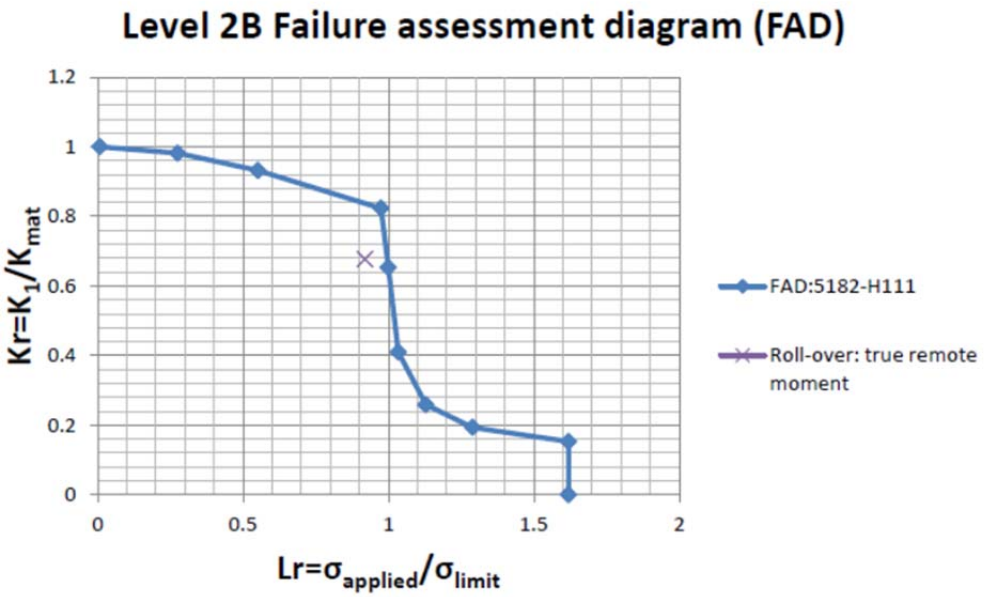

Figure 4 Failure assessment diagram for a 2mm deep long flaw under roll-over conditions. Reproduced from Figure 7 of GRW report (2014c).

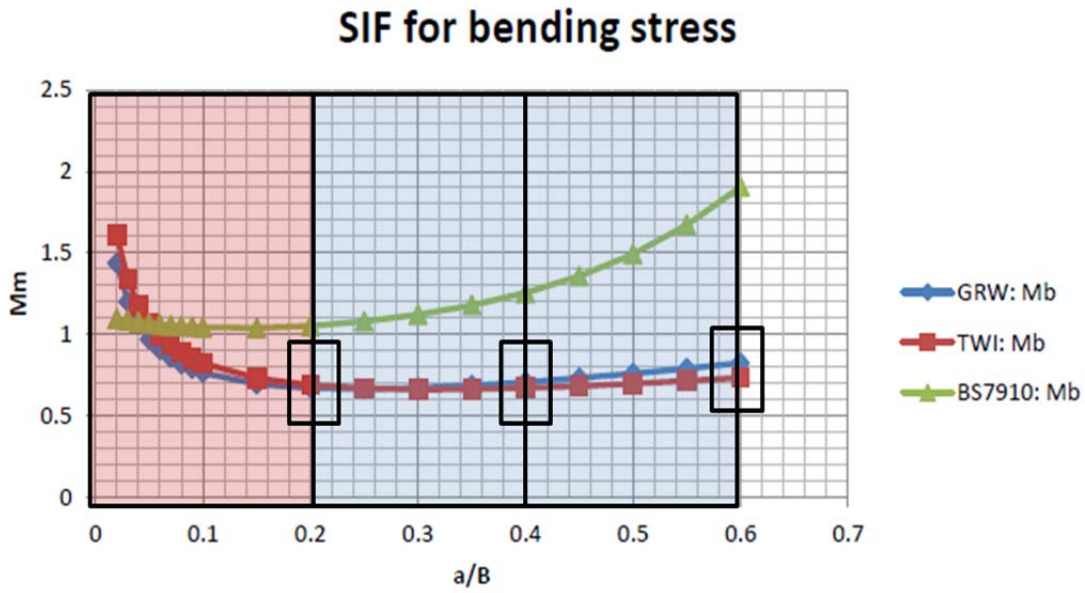

Figure 5 Stress intensity factors for remote bending stress. Reproduced from Figure 4 of GRW report (2014c). Note the y-axis label should read '$M_{b'}$. The figure has been annotated to show the calculated values form TWI (2013a) in small black boxes. All other values of the red 'TWI: Mb' curve have been constructed by GRW. The red shaded region shows an extrapolation that they have used.

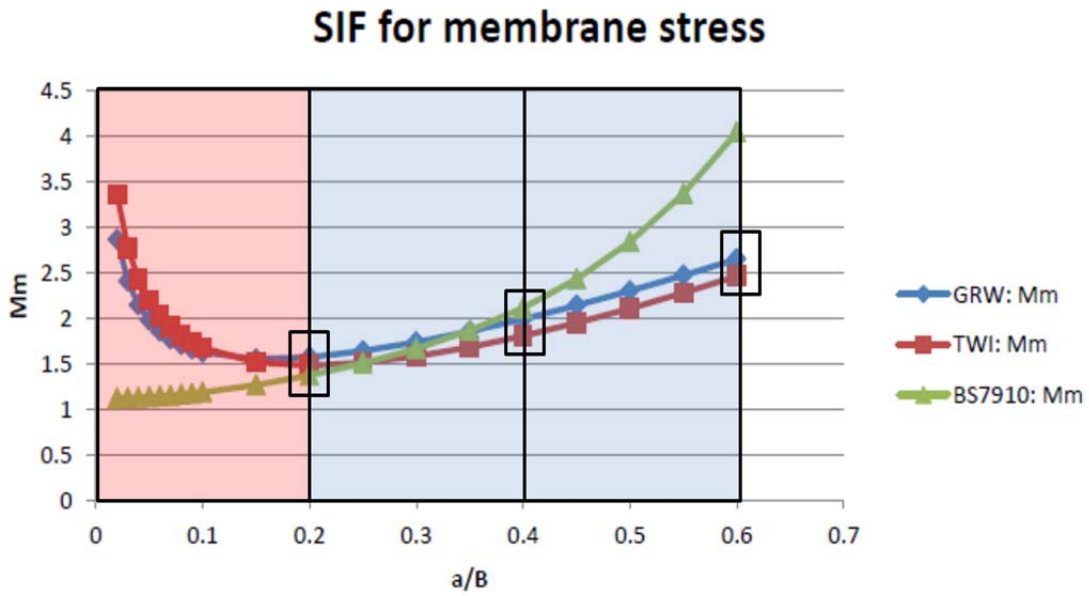

Figure 6 Stress intensity factors for remote bending stress. Reproduced from Figure 4 of GRW report (2014c). The figure has been annotated to show the calculated values from TWI (2013a) in small black boxes. All other values of the red 'TWI: Mm' curve have been constructed by GRW. The red shaded region shows an extrapolation that they have used.

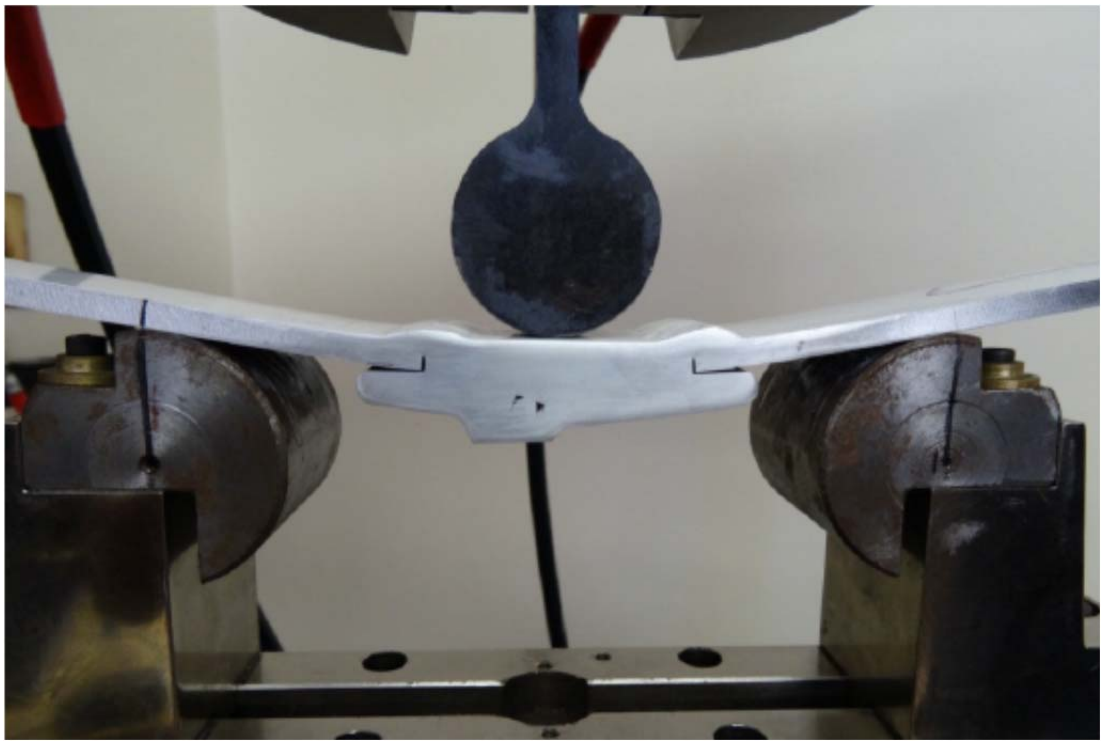

Figure 7 GRW set up for the three-point bending experiments. (Figure 3 from GRW 2013d).

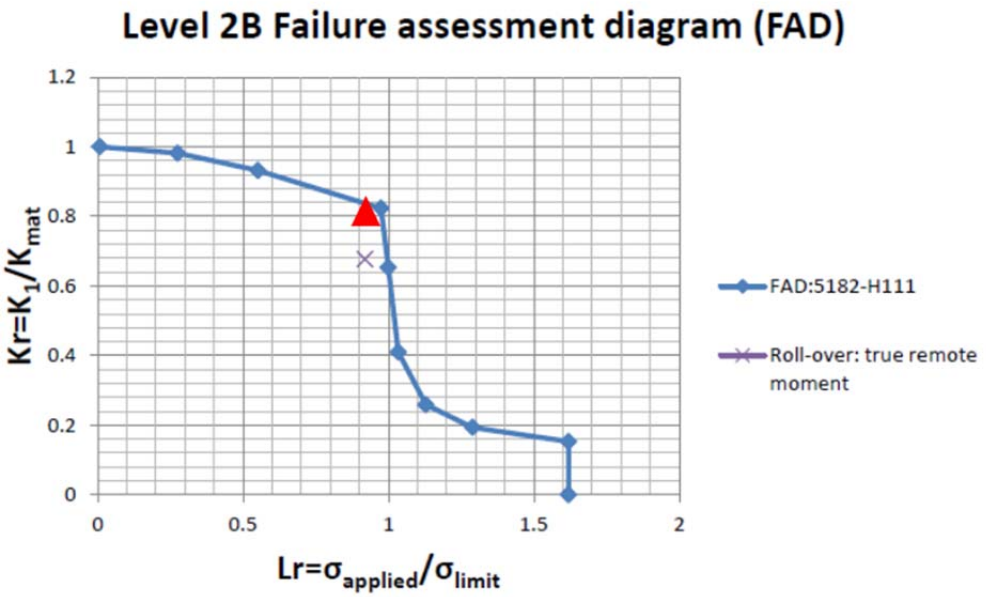

Figure 8 Failure assessment diagram with approximate assessment point for a 2.4mm deep flaw.

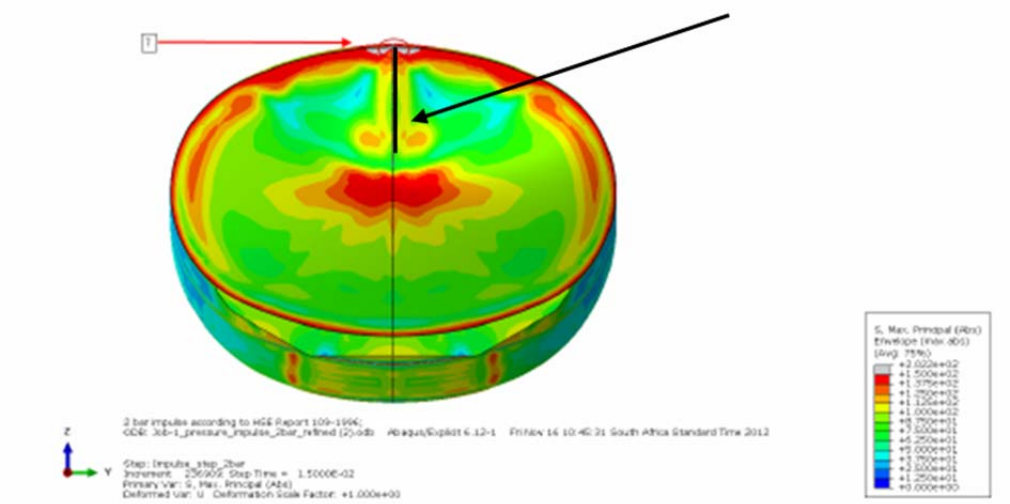

Figure 9 Image of the maximum principal stress contour during the pressure-impulse simulation by GRW. Reproduced from Figure 7 of GRW ECA report (2013a). The black vertical line and black arrow have been added in this report to highlight the incorrect boundary condition.

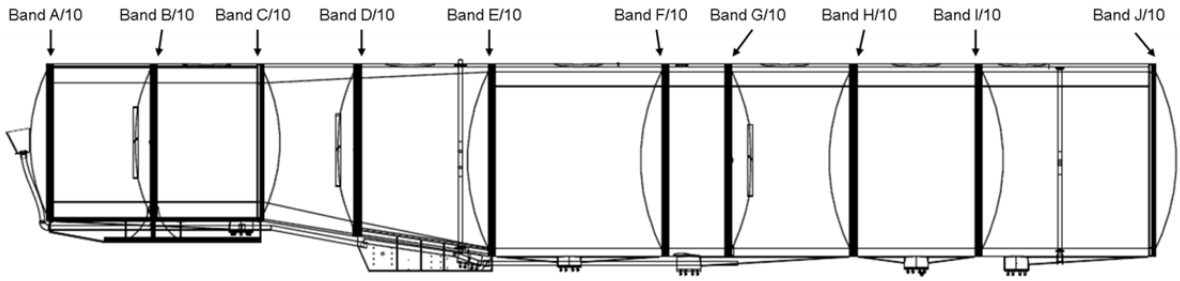

Figure 10 Planar view of Tanker J3857 reproduced from GRW engineering drawing (2008). This view shows the nearside and the naming convention for the circumferential seam welds.

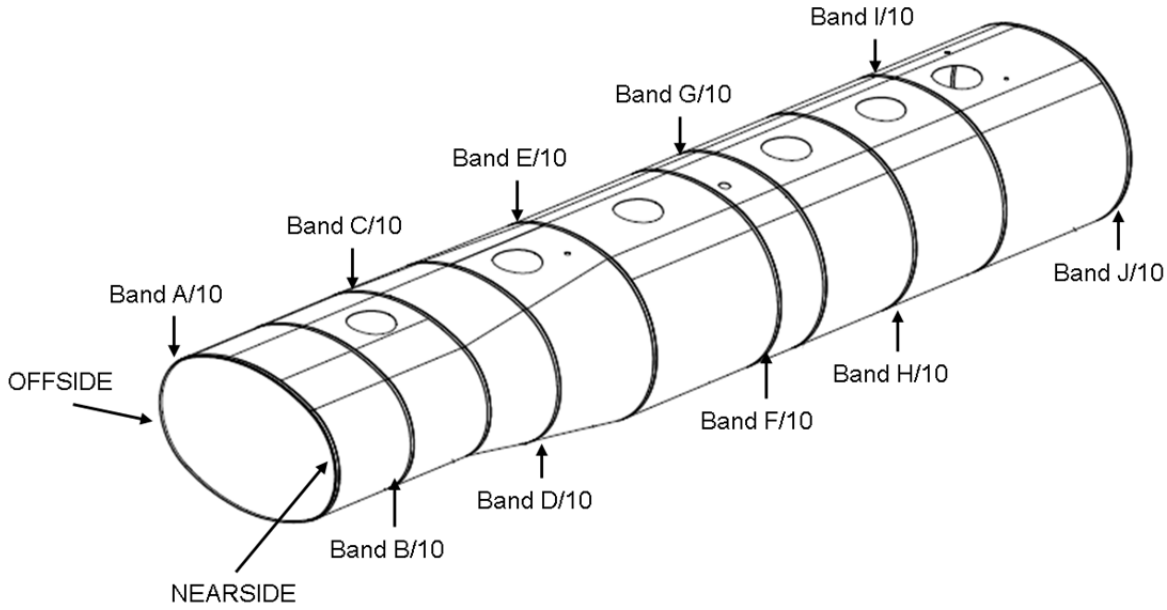

Figure 11 Isometric view of Tanker J3857 reproduced from GRW engineering drawing (2008). This view shows the offside (driver's side) and nearside.

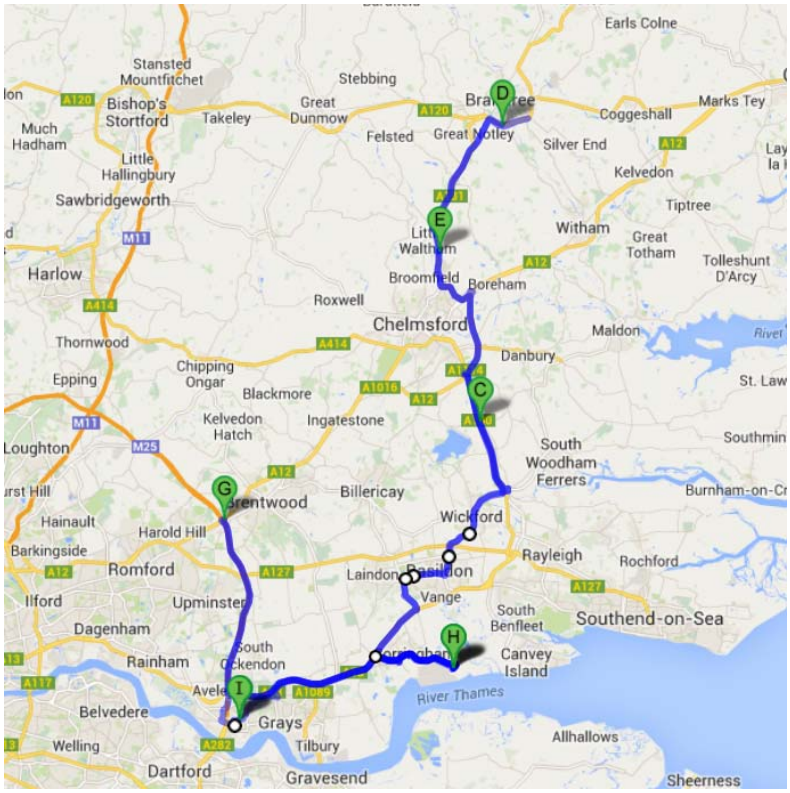

Figure 12 Overall test route.

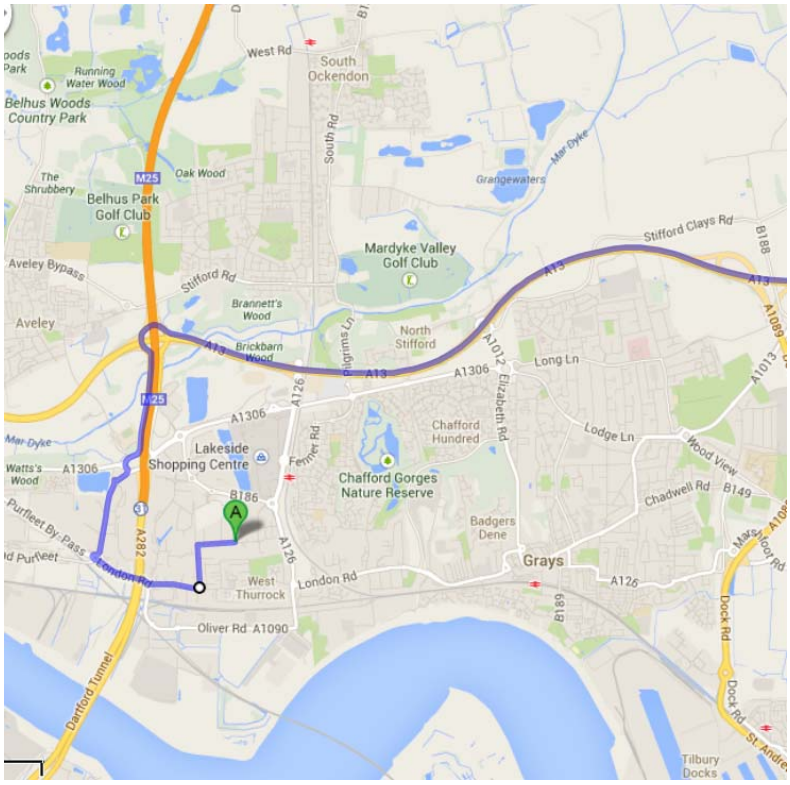

Figure 13 Starting point at Central Yard on Motherwell road (Point A).

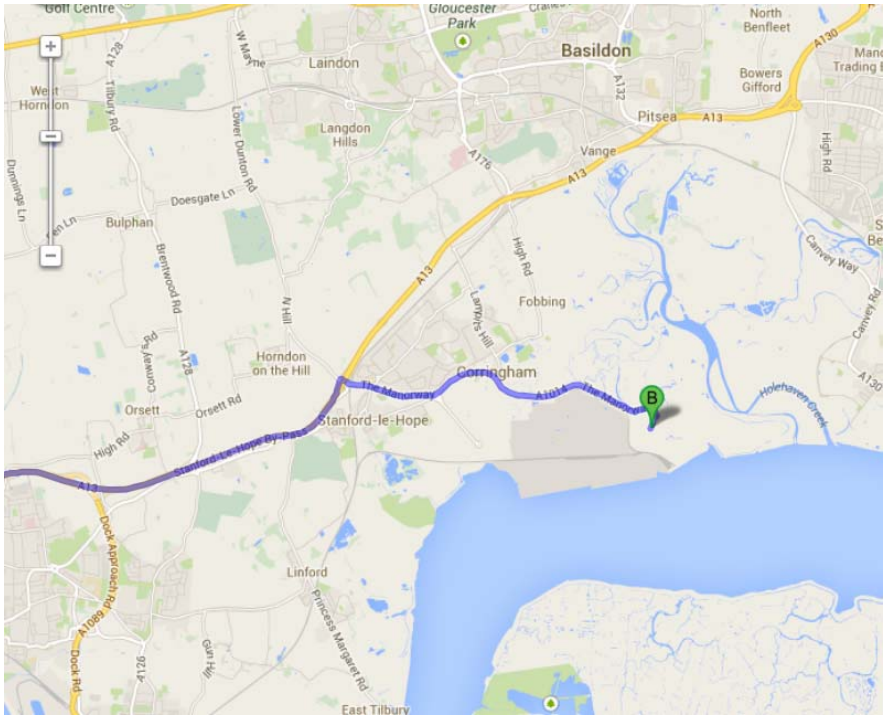

Figure 14 Stopping point at Corringham (Point B).

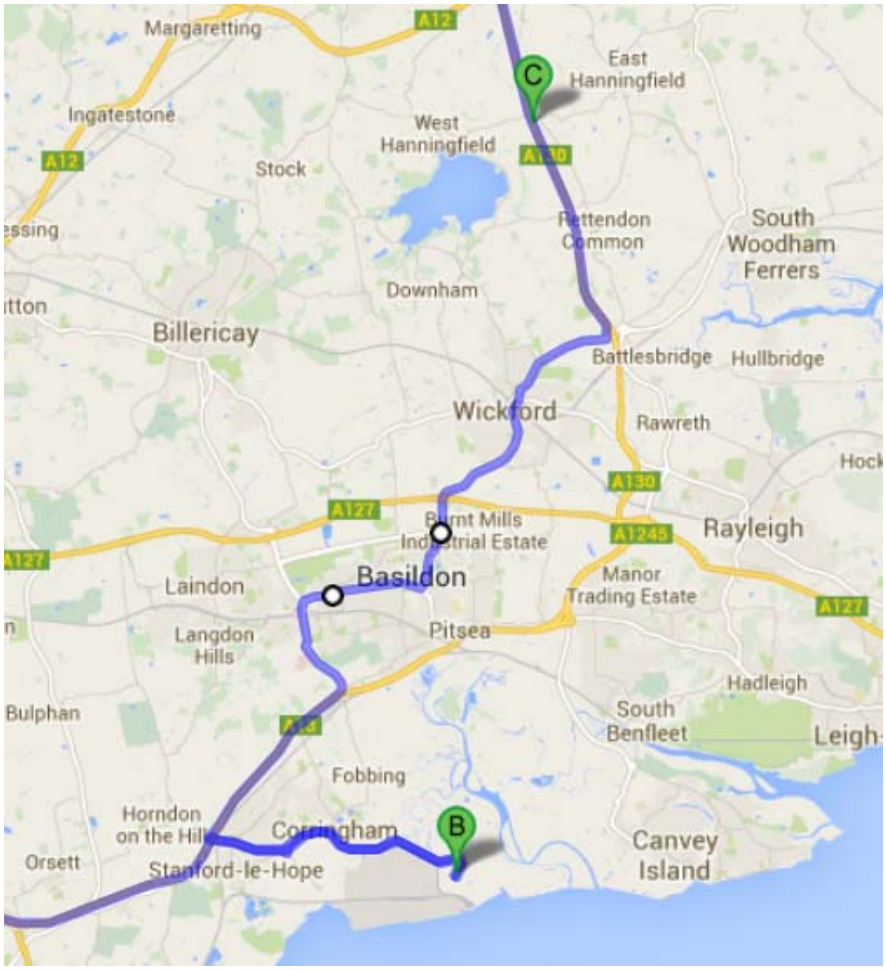

Figure 15 Stopping point at A130 Chelmsford CM3 (Point C).

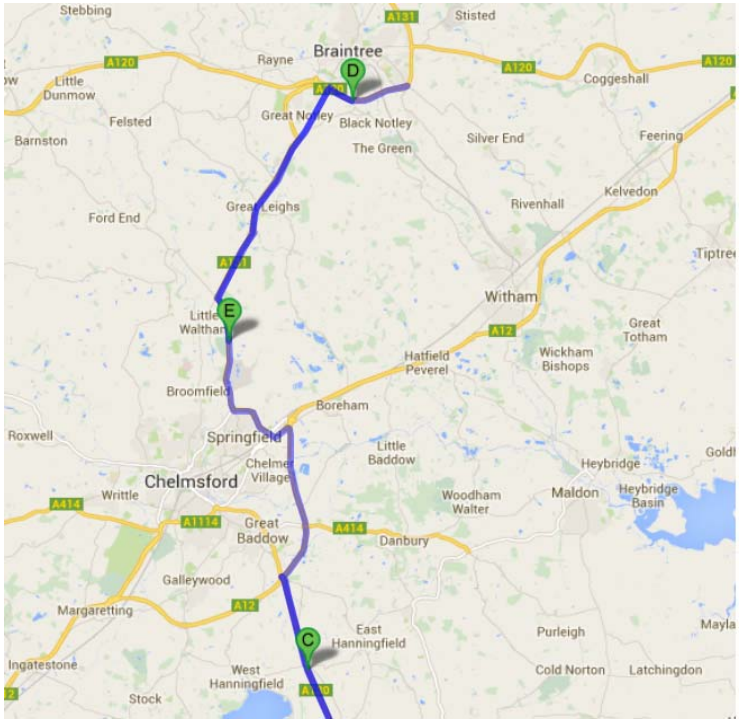

Figure 16 Travelled to A120 and back to Street CM2 5.

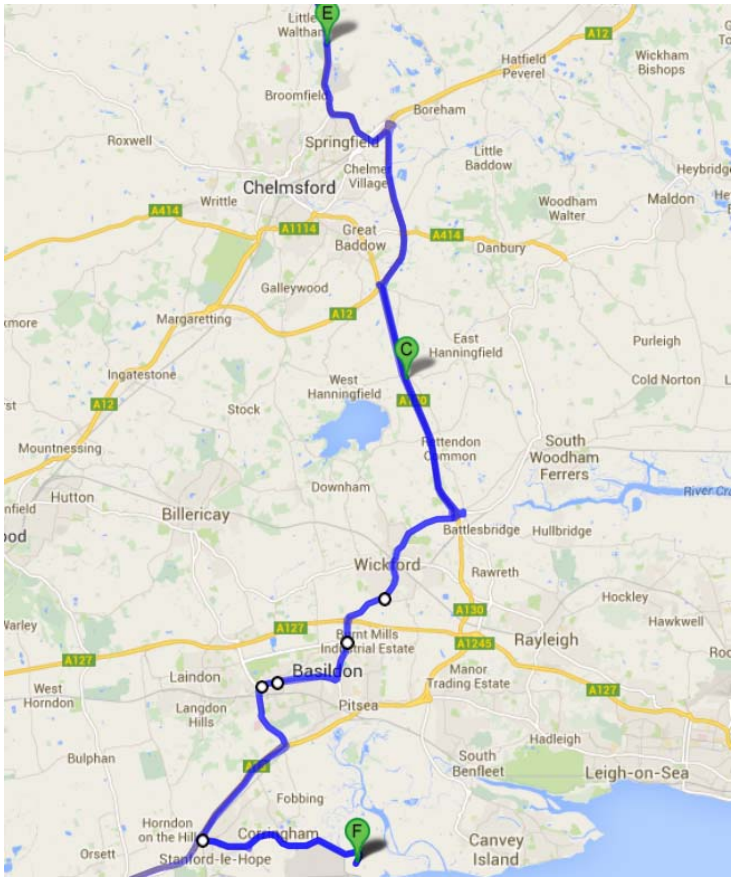

Figure 17 Travelled from Street CM2 5 back to Coryton (Point F).

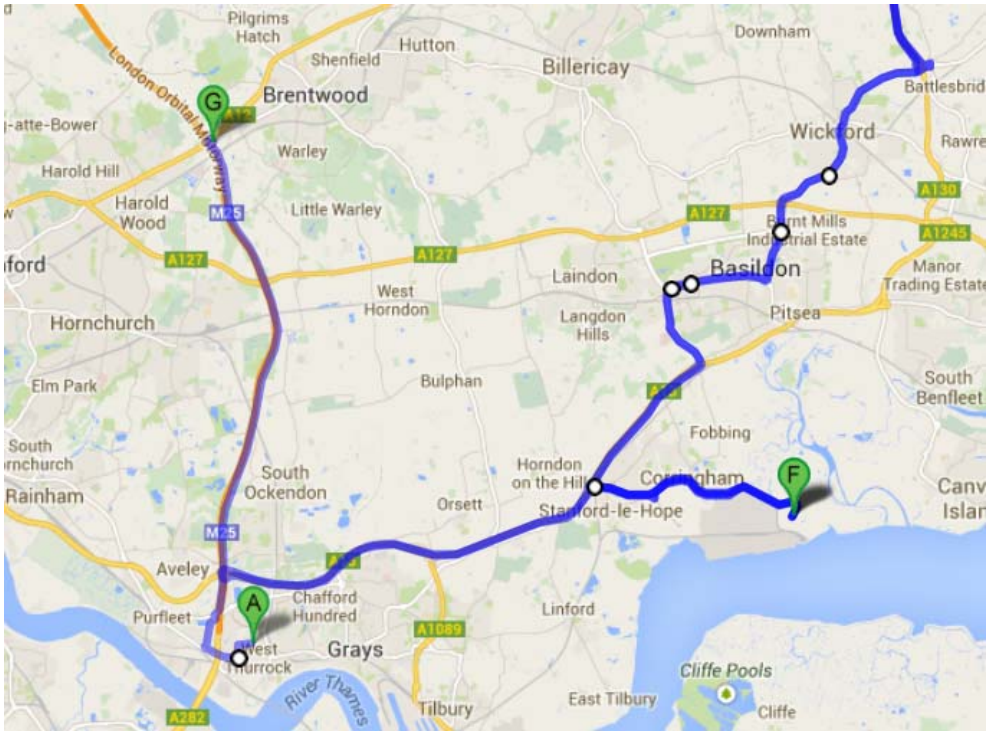

Figure 18 Travelled from Coryton to the roundabout where M25 meets A12 (Point G).

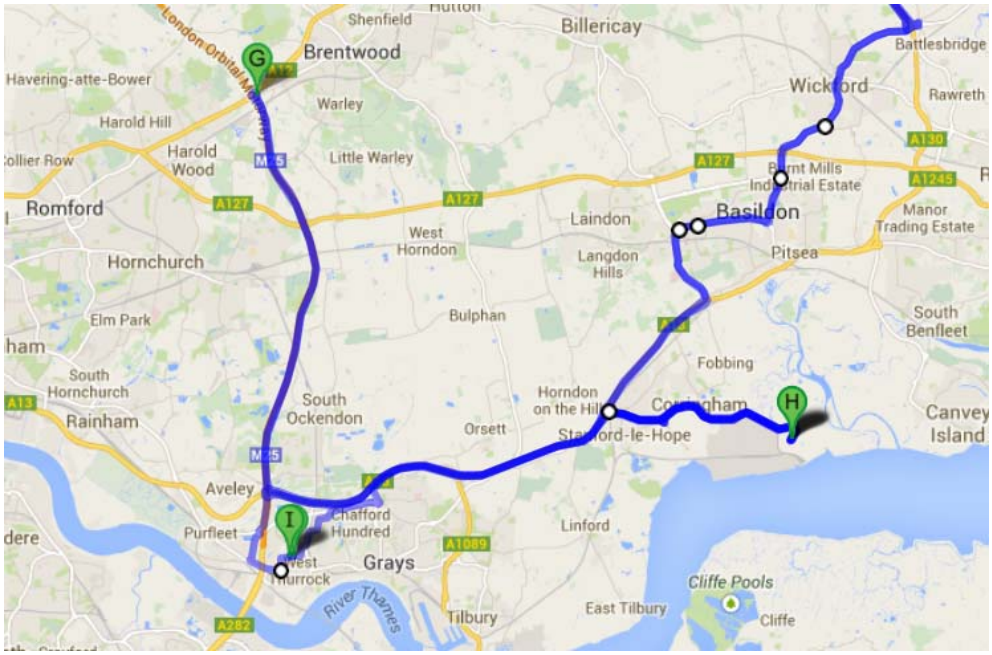

Figure 19 Travelled back to Coryton (Point H), and then travelled to the starting point at Centra yard on Motherwell road (Point I).

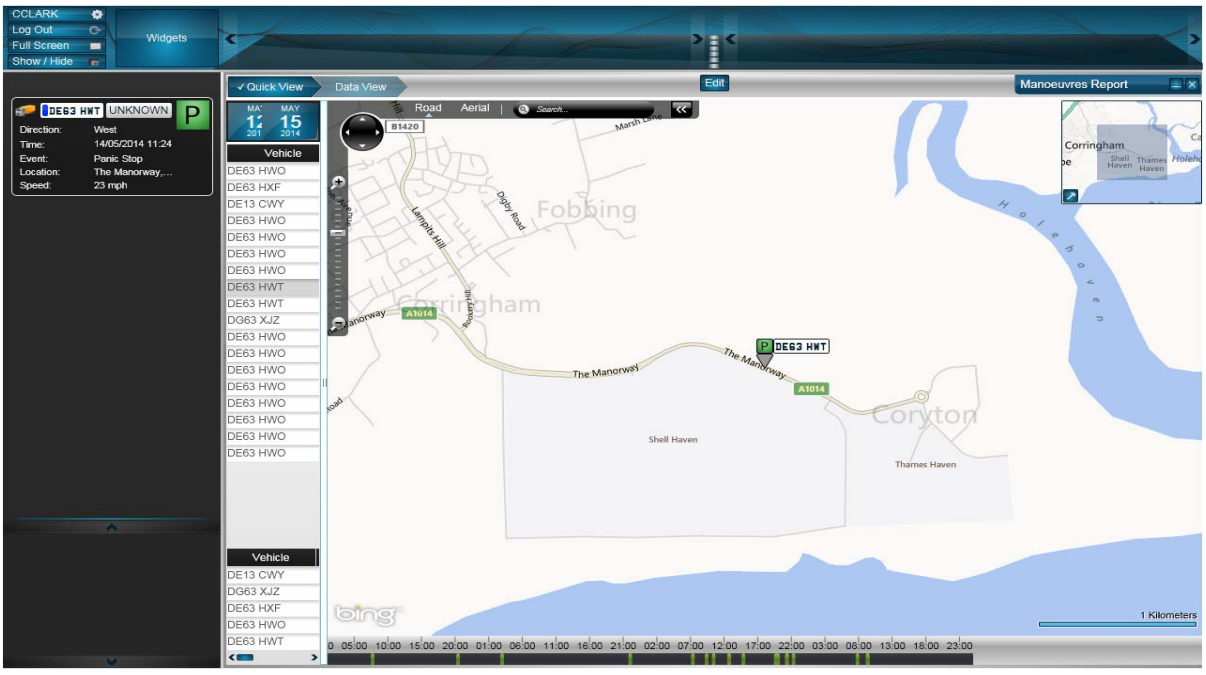

Figure 20 Telematics report for the first emergency stop performed during the unladen fatigue data collection.

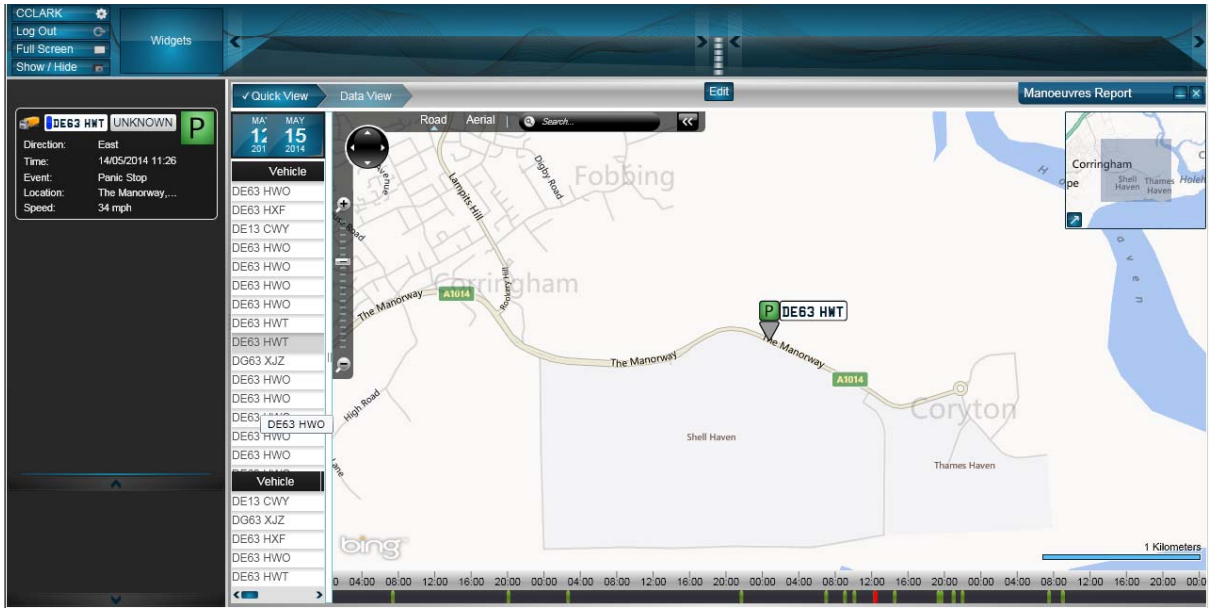

Figure 21 Telematics report for the second emergency stop performed during the unladen fatigue data collection.

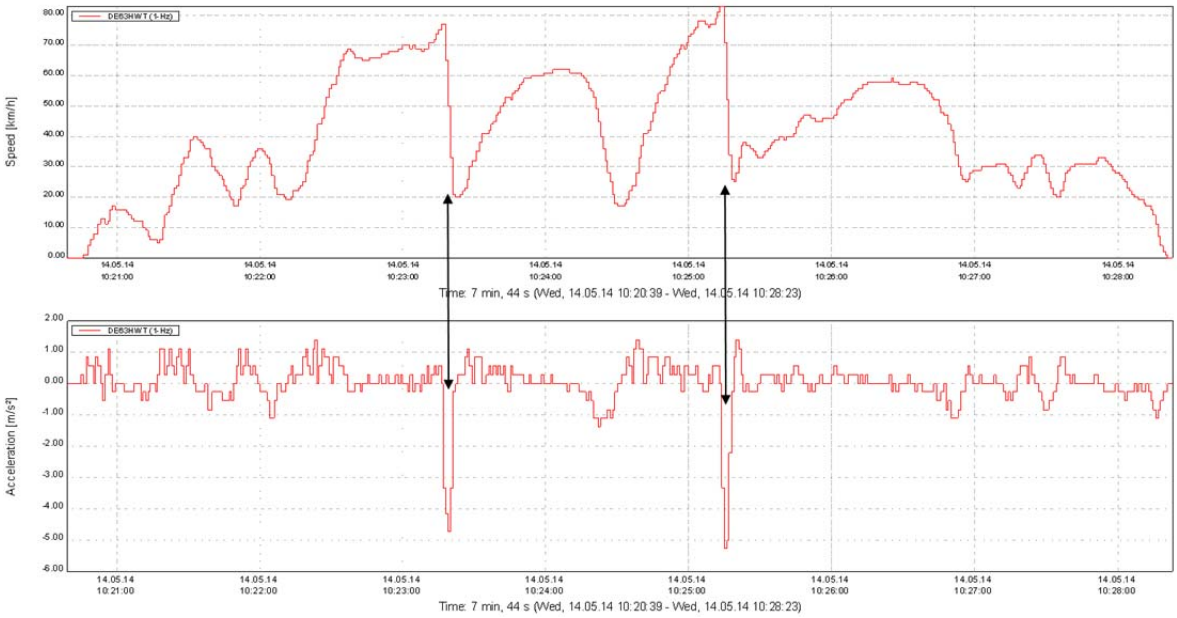

Figure 22 Digital tachograph report for the two emergency stops performed during the unladen fatigue data collection.

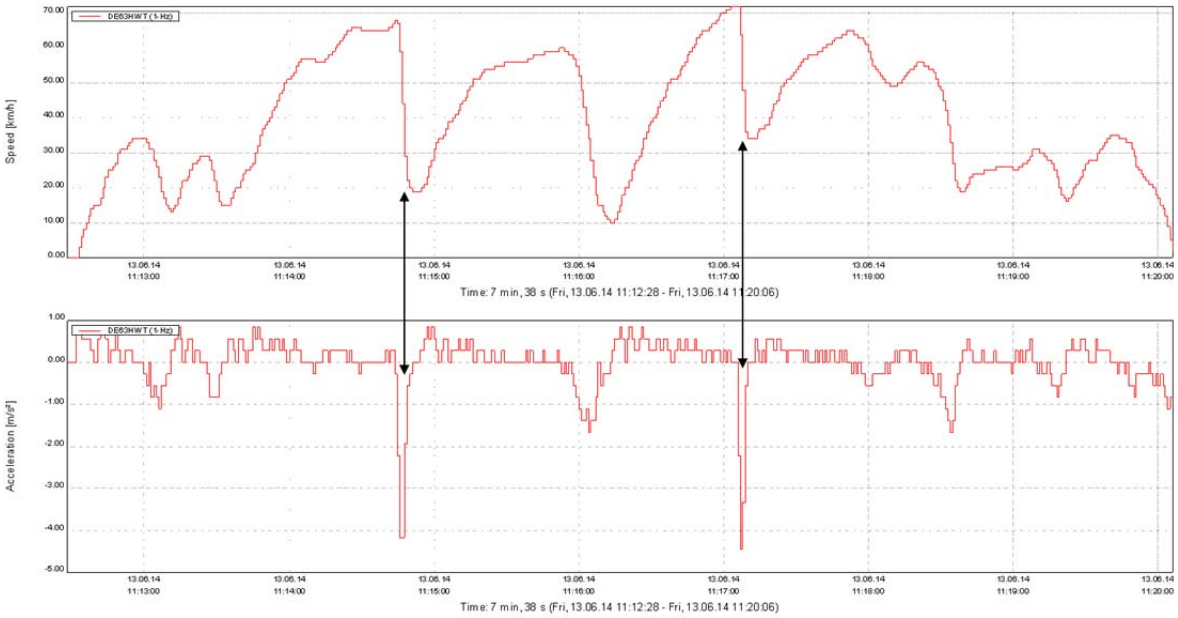

Figure 23 Digital tachograph report for the two emergency stops performed during the laden fatigue data collection.

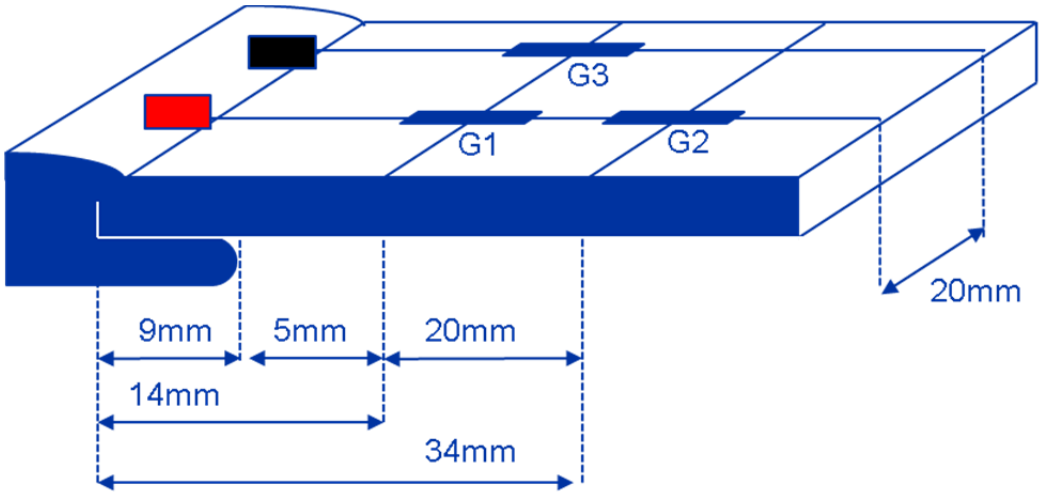

Figure 24 Illustration of the local cluster of three, axially-oriented gauges with the corresponding spacing from the hypothetical crack plane.

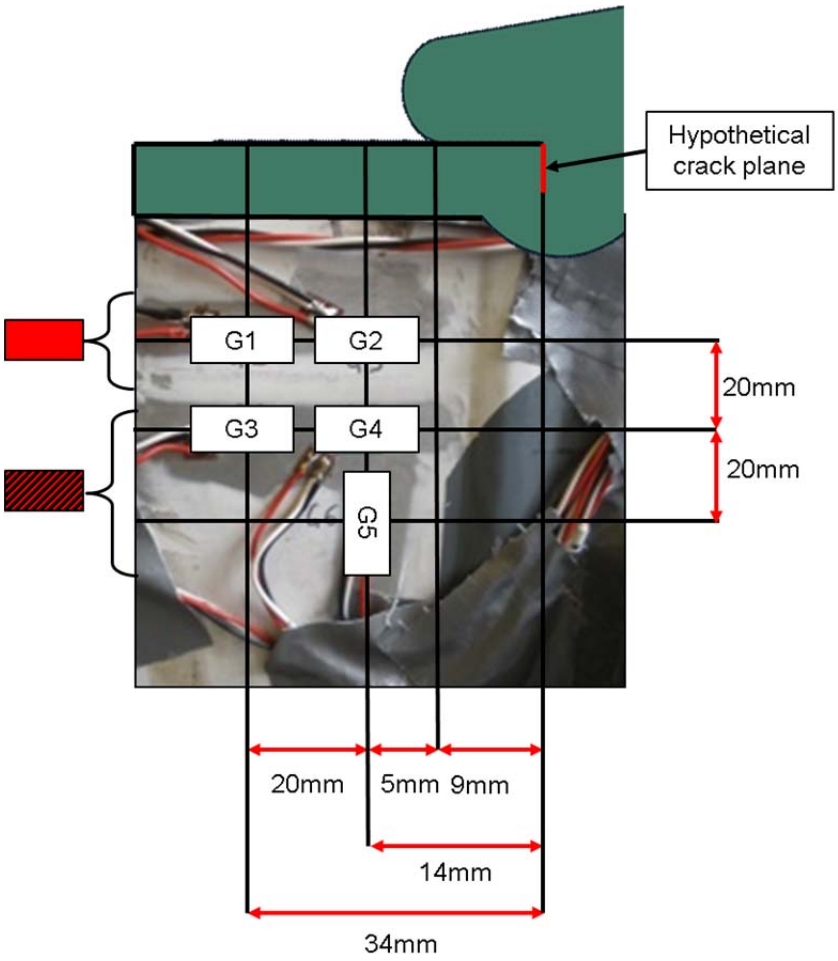

Figure 25 Illustration of the cluster of five strain gauges.

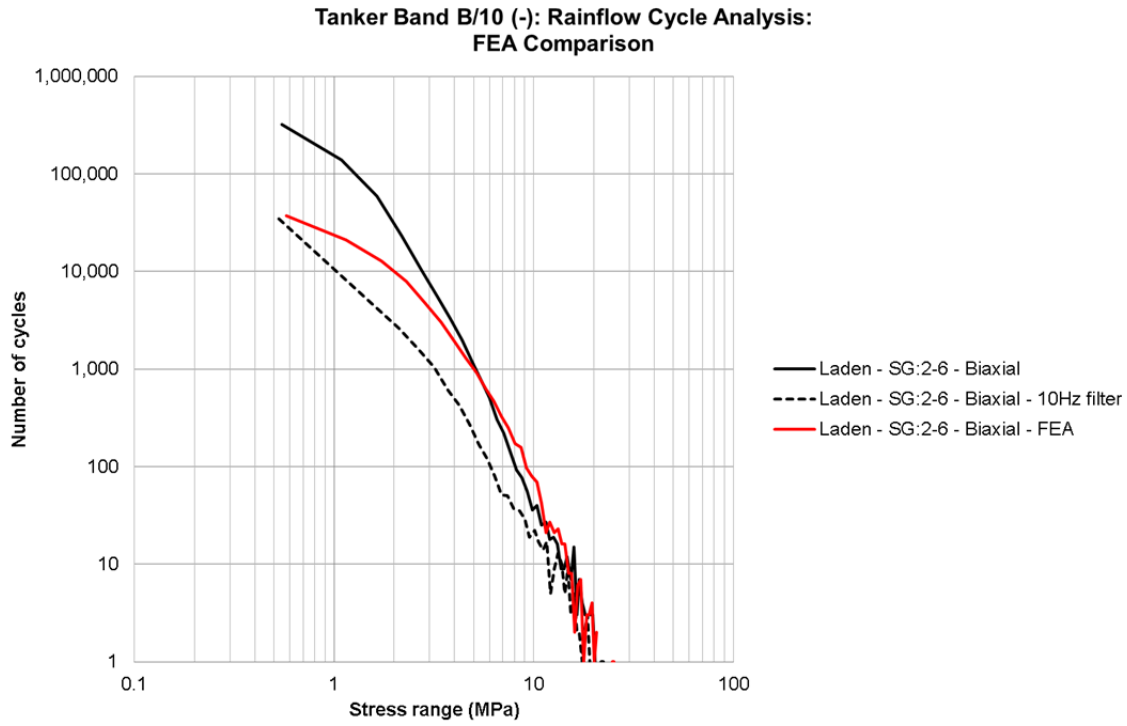

Figure 26 Comparison of FEA calibration/correlation with experimental measurements.

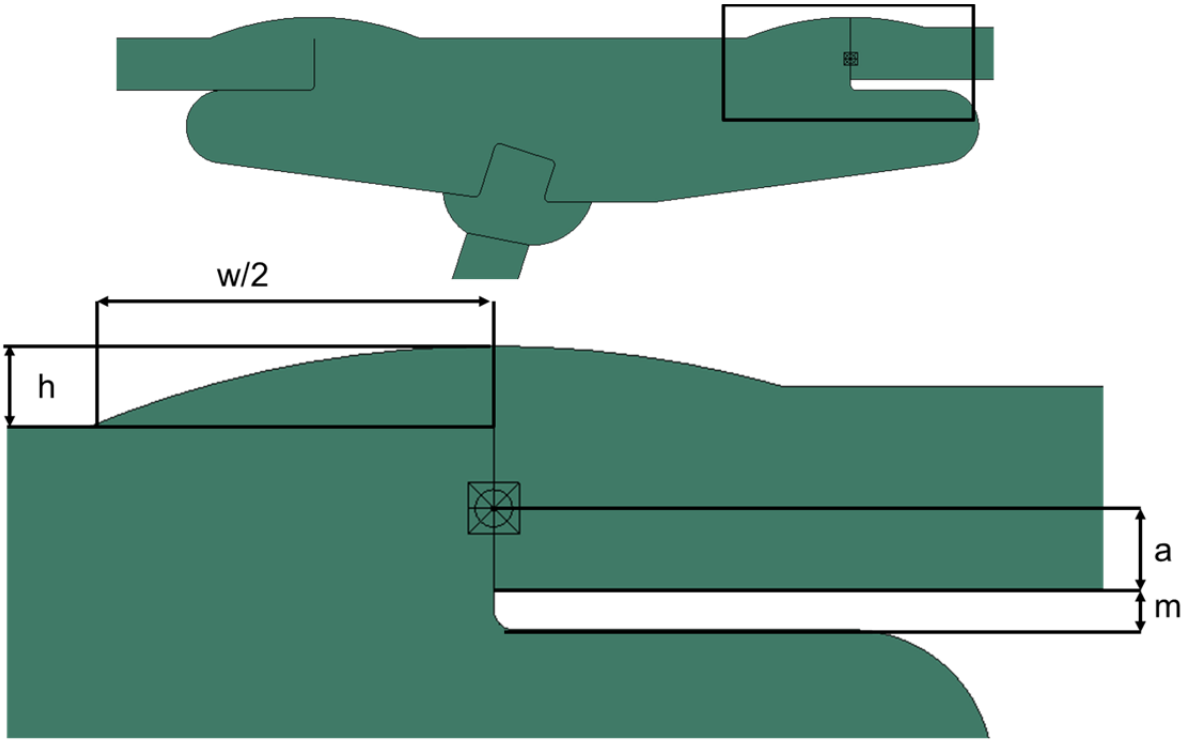

Figure 27 Definition of the geometry dimensions. Weld cap height is h; weld cap width is w; crack height is a and misalignment is m.

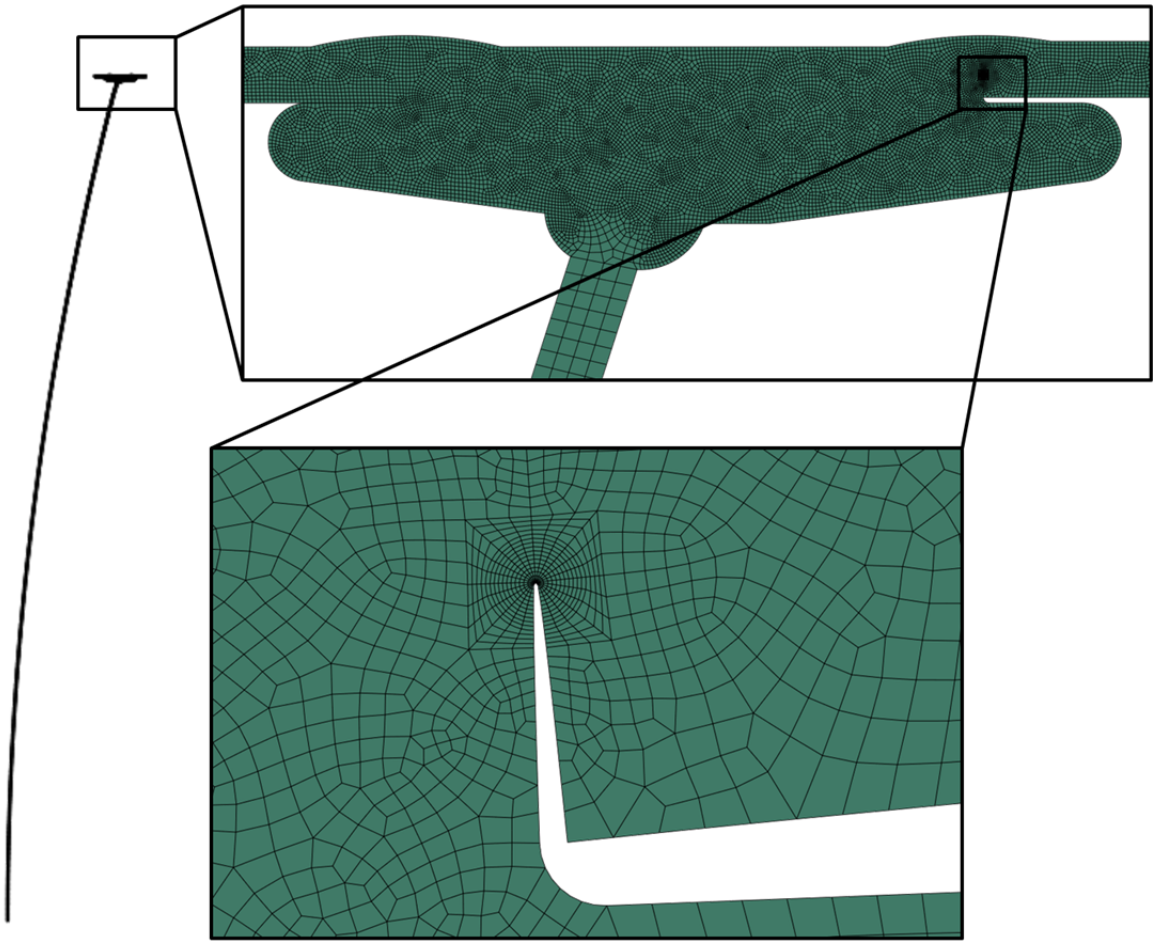

Figure 28 Typical finite element mesh for the geometries under consideration.

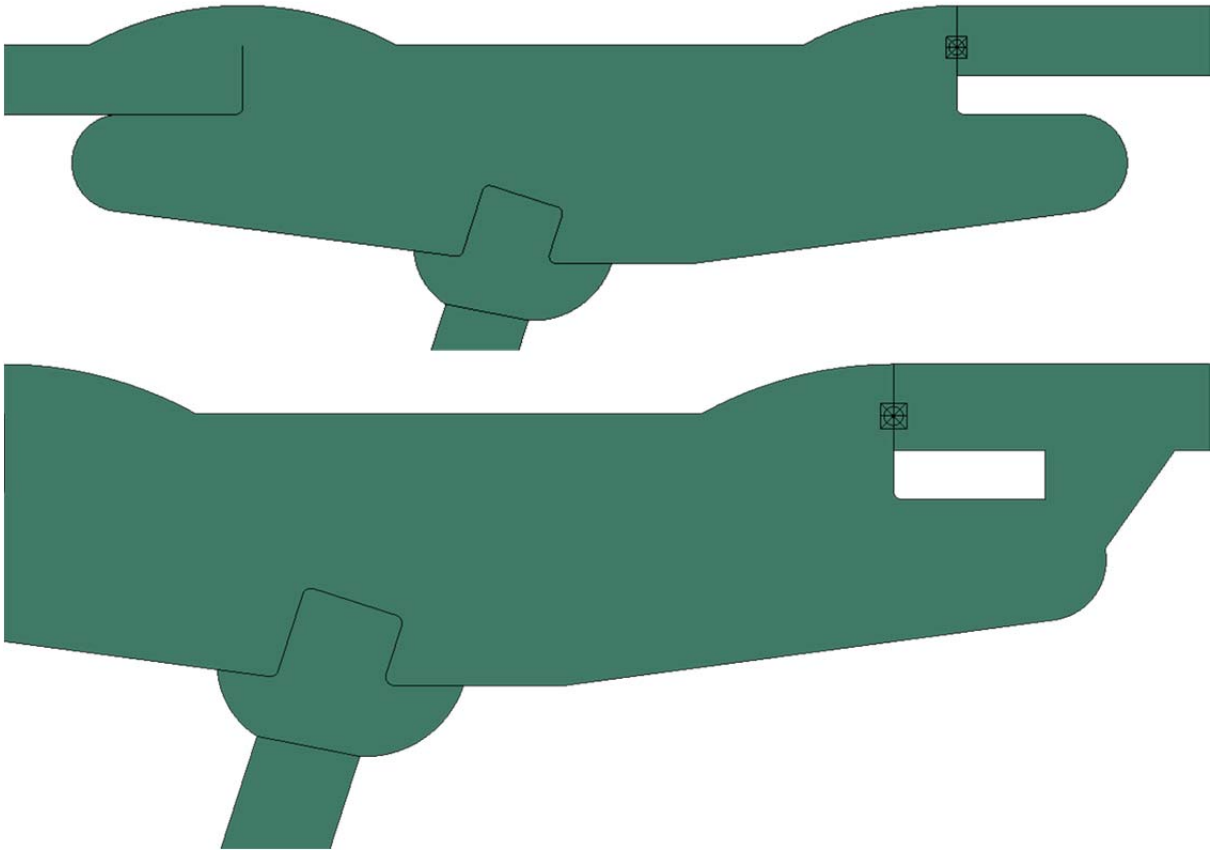

Figure 29 Illustration of the geometry for Case 01 with and without the additional internal fillet weld.

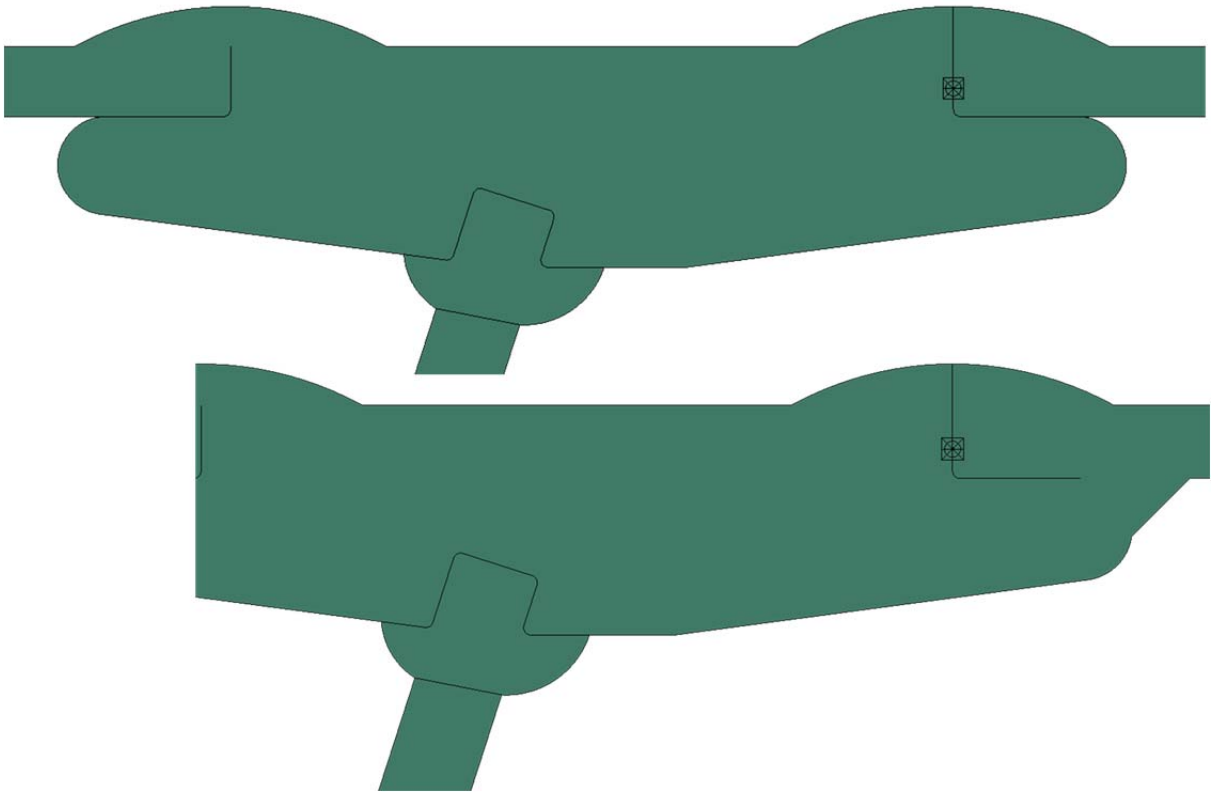

Figure 30 Illustration of the geometry for Case 02 with and without the additional internal fillet weld.

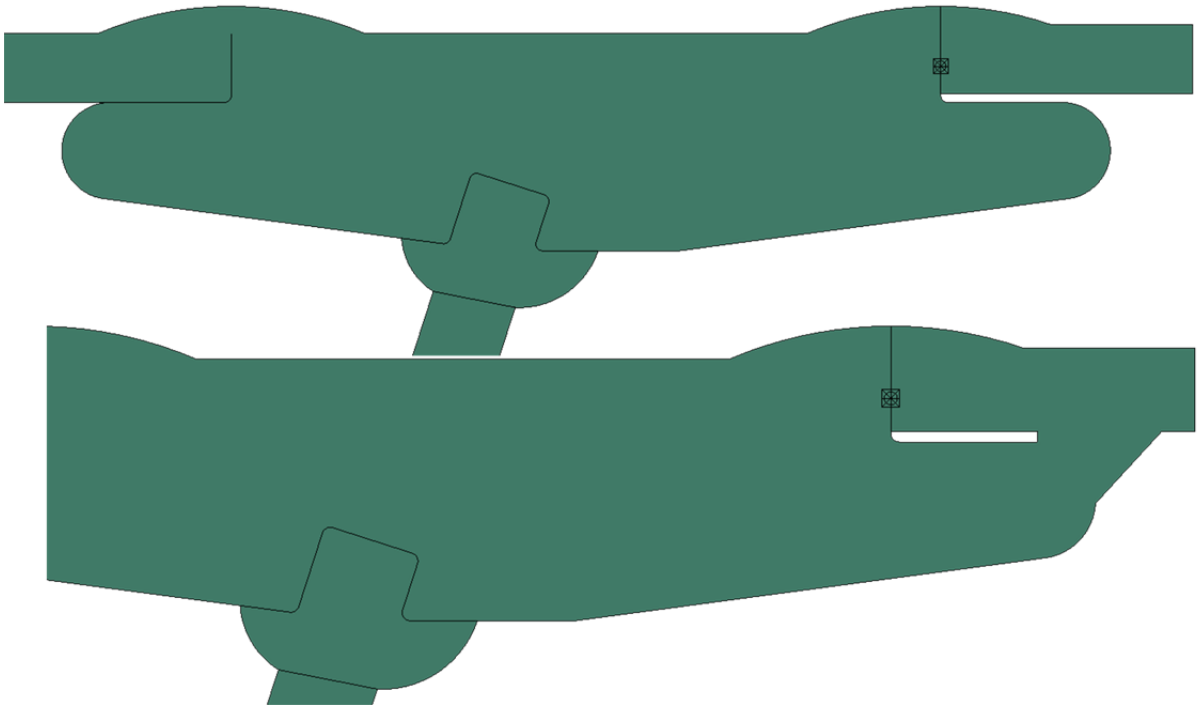

Figure 31 Illustration of the geometry for Case 09 (the average dimension model) with and without the additional internal fillet weld.

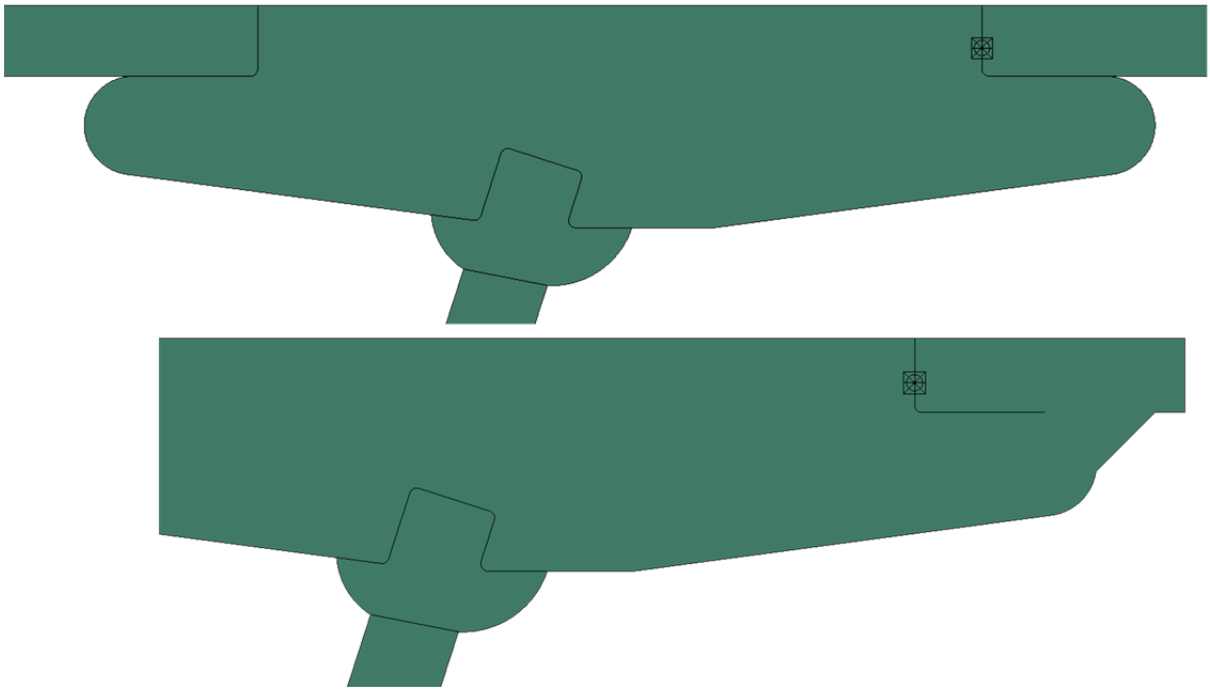

Figure 32 Illustration of the geometry for Case 10 (the flush-ground joint) with and without the additional internal fillet weld.

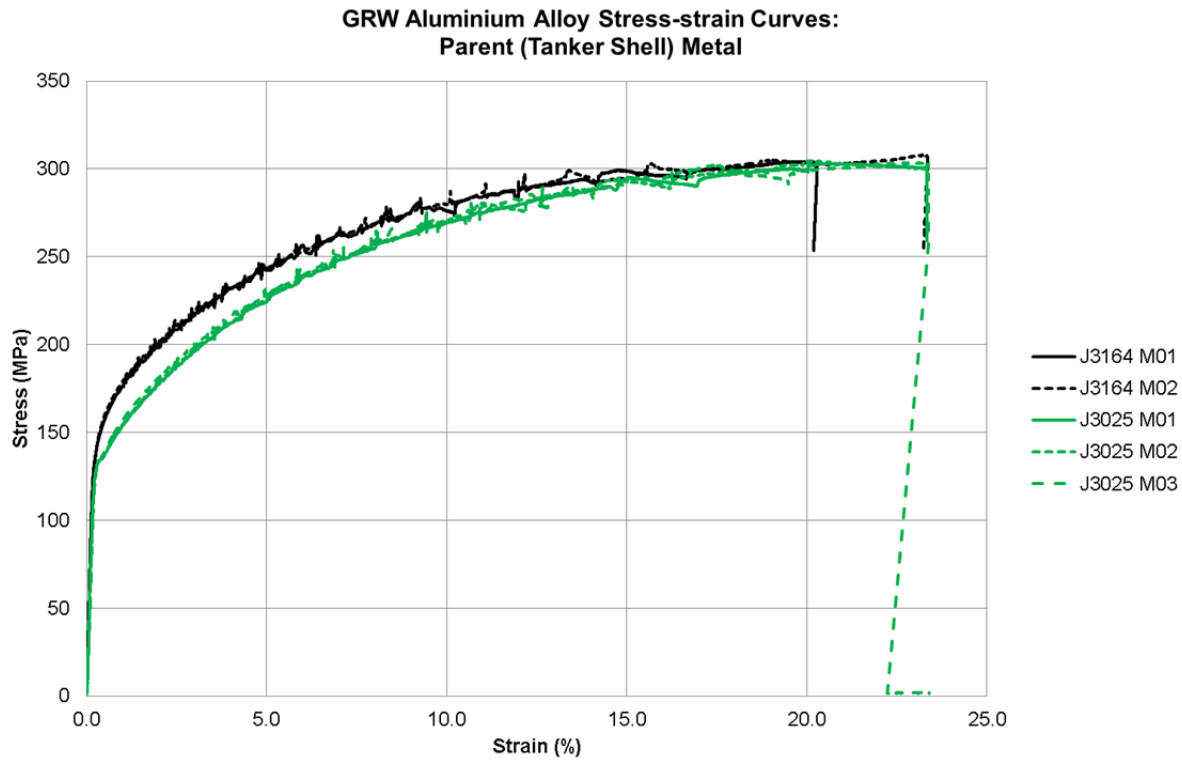

Figure 33 Parent metal stress-strain curves.

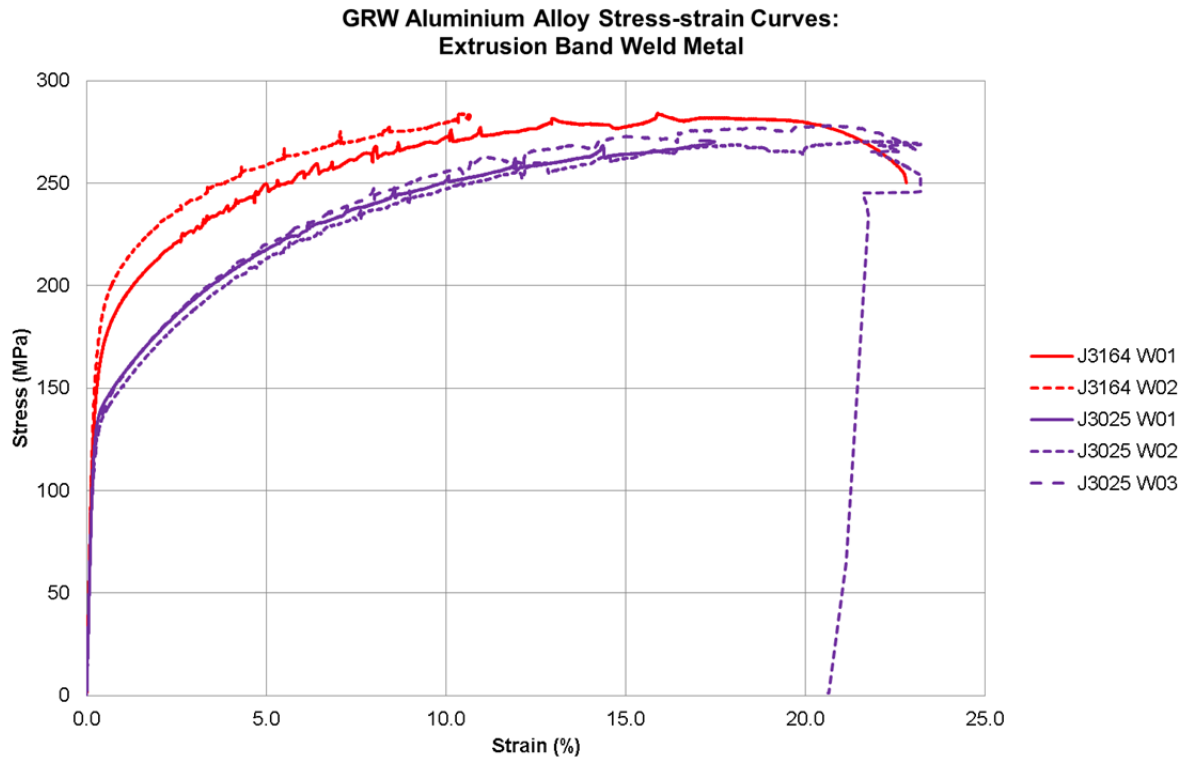

Figure 34 Weld metal stress-strain curves.

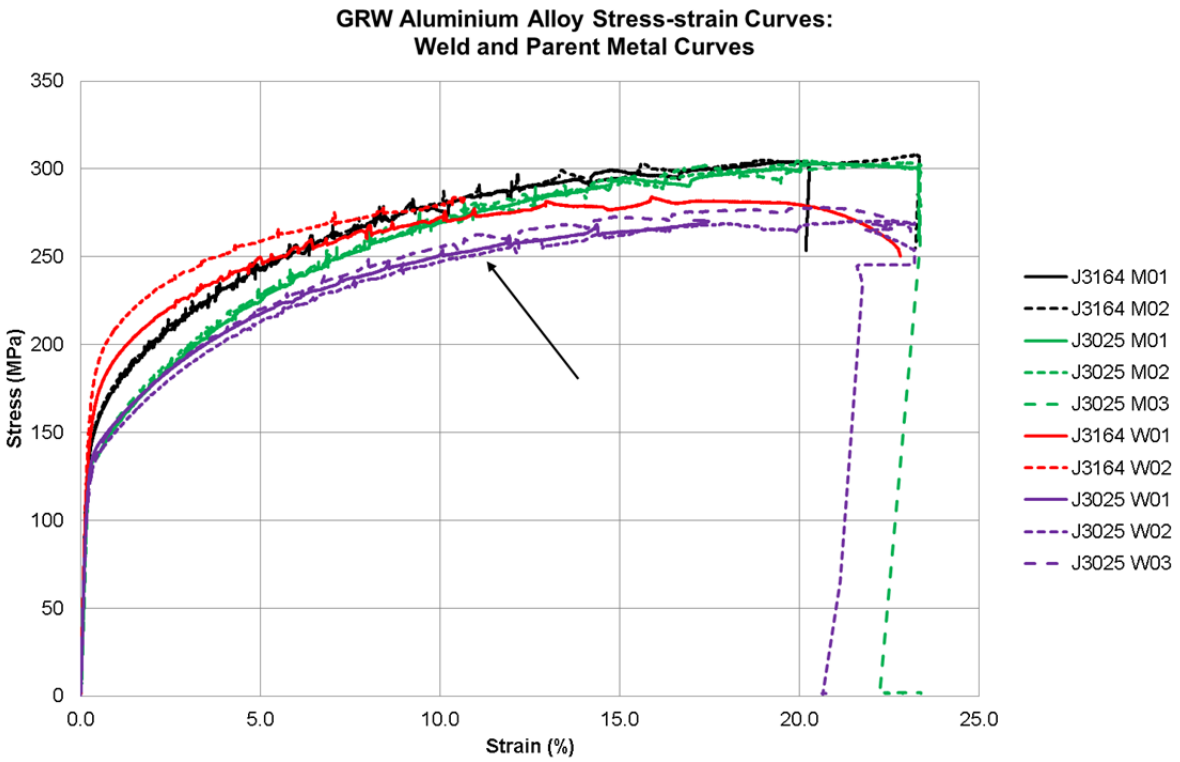

Figure 35 Parent and weld metal stress-strain curves. Arrow indicates lower bound used for failure assessment line.

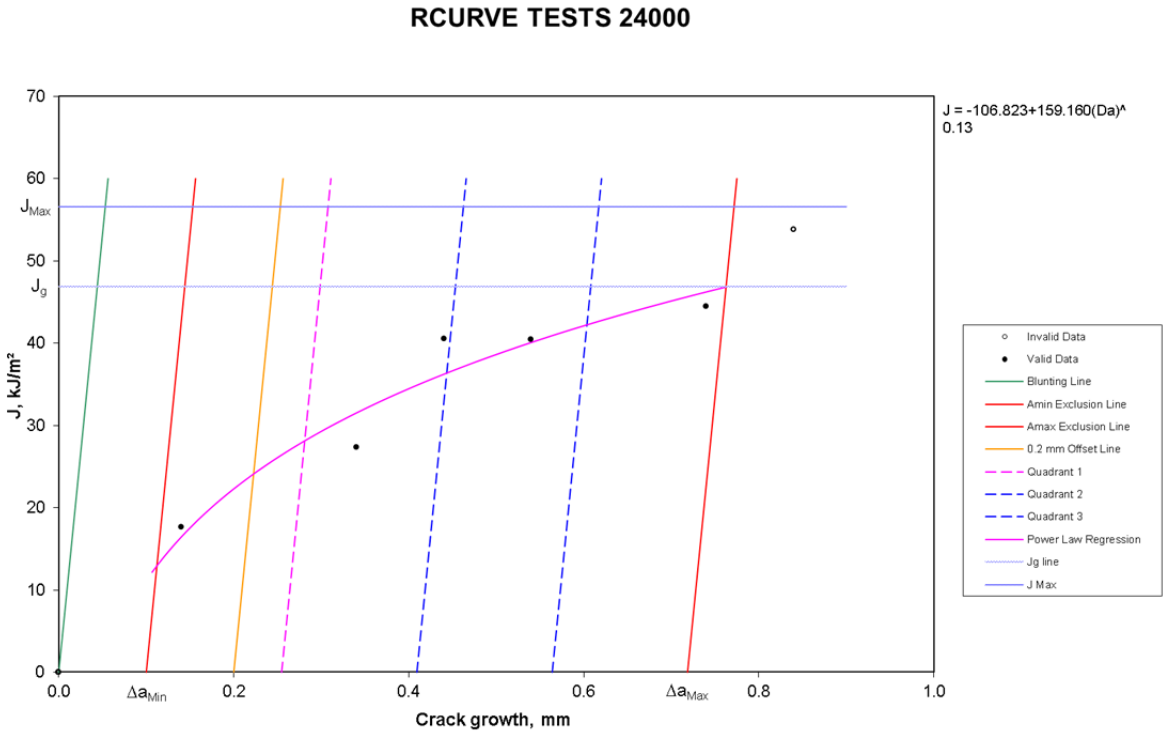

Figure 36 J-R tearing resistance curve test result for SENB samples from J3146.

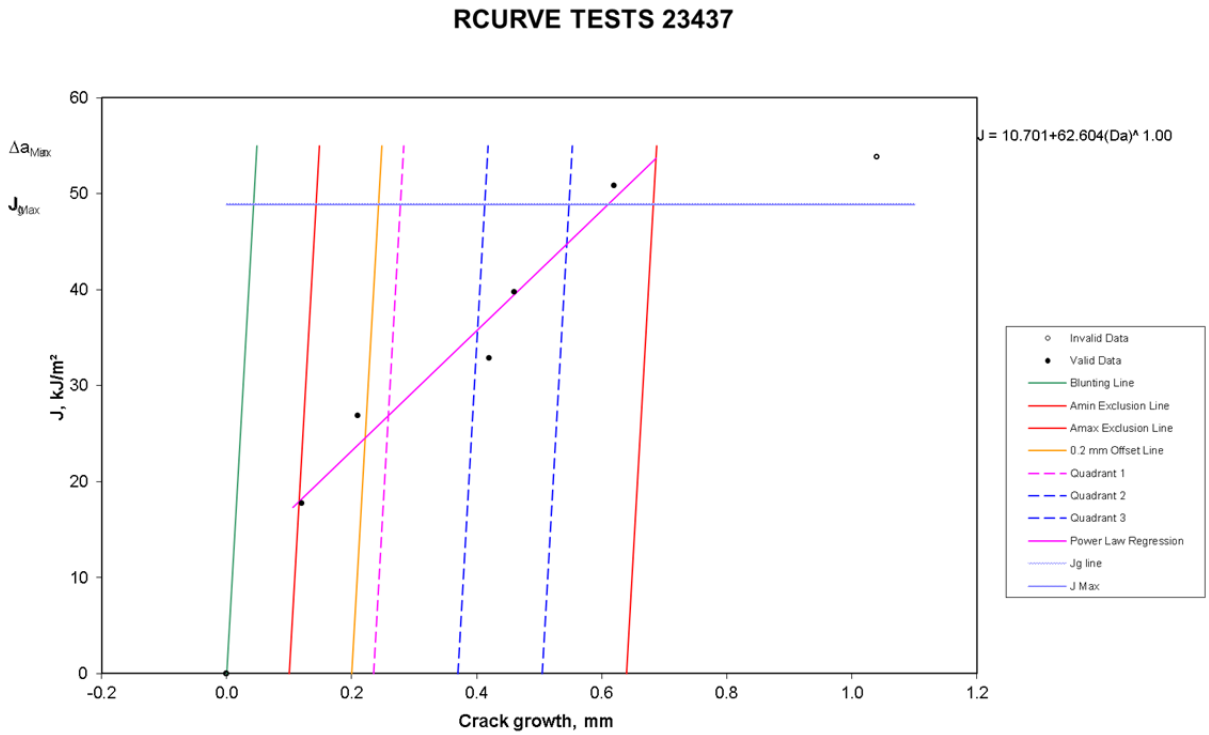

Figure 37 J-R tearing resistance curve test result for SENB samples from J3025.

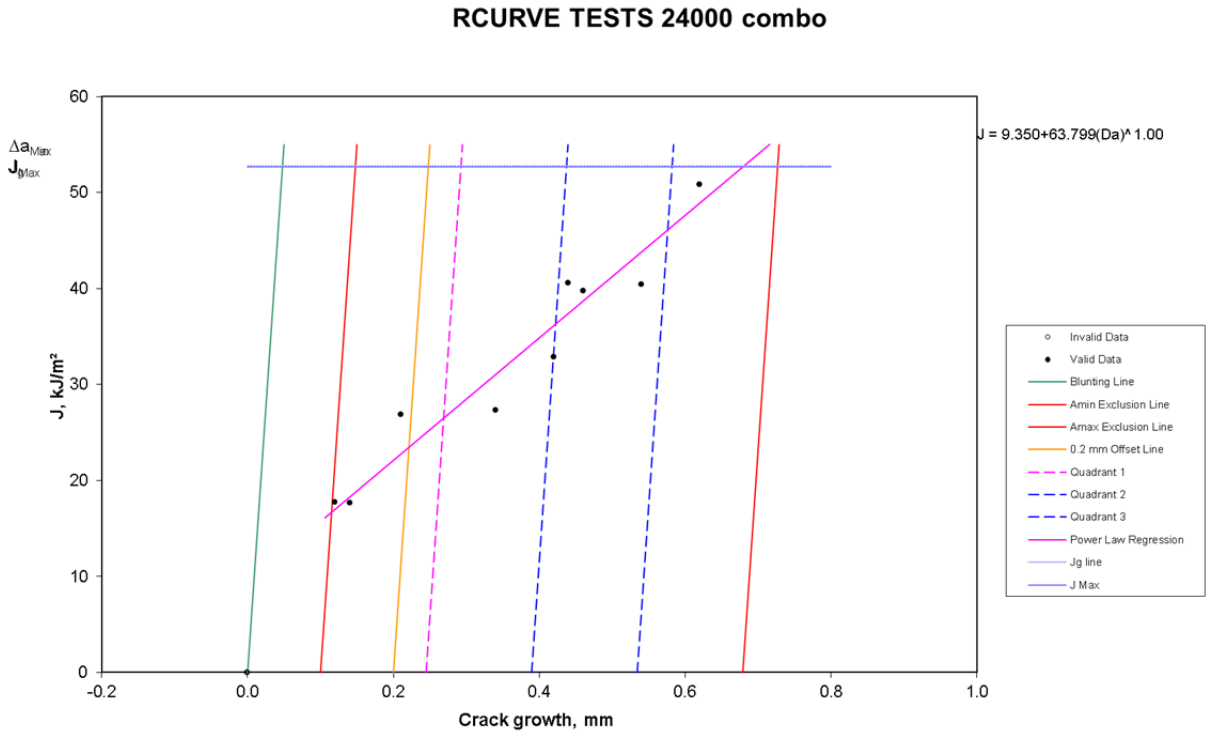

Figure 38 J-R tearing resistance curve test result for SENB samples from J3025 and J3146.

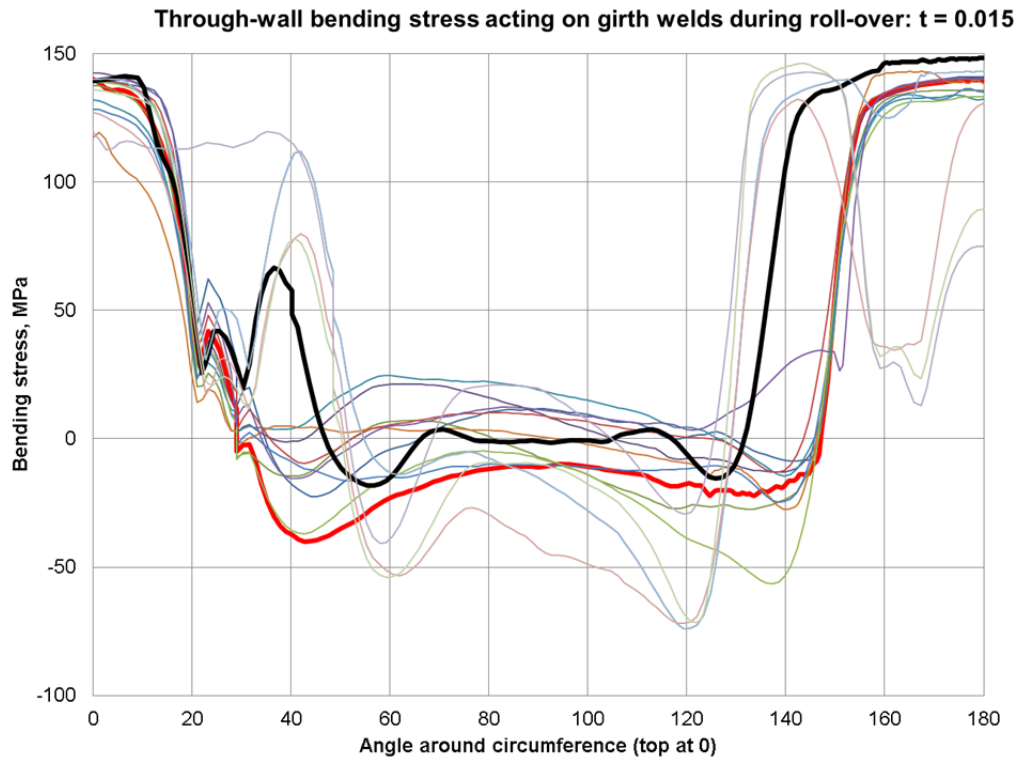

Figure 39 Post-processed through-wall bending stresses from the original GRW pressure-impulse simulation. The lines correspond to different bands and the black band indicates the tanker band exhibiting the largest tensile through-wall bending stress, approximately equal to 150MPa. Reproduced from (TWI, 2013a).

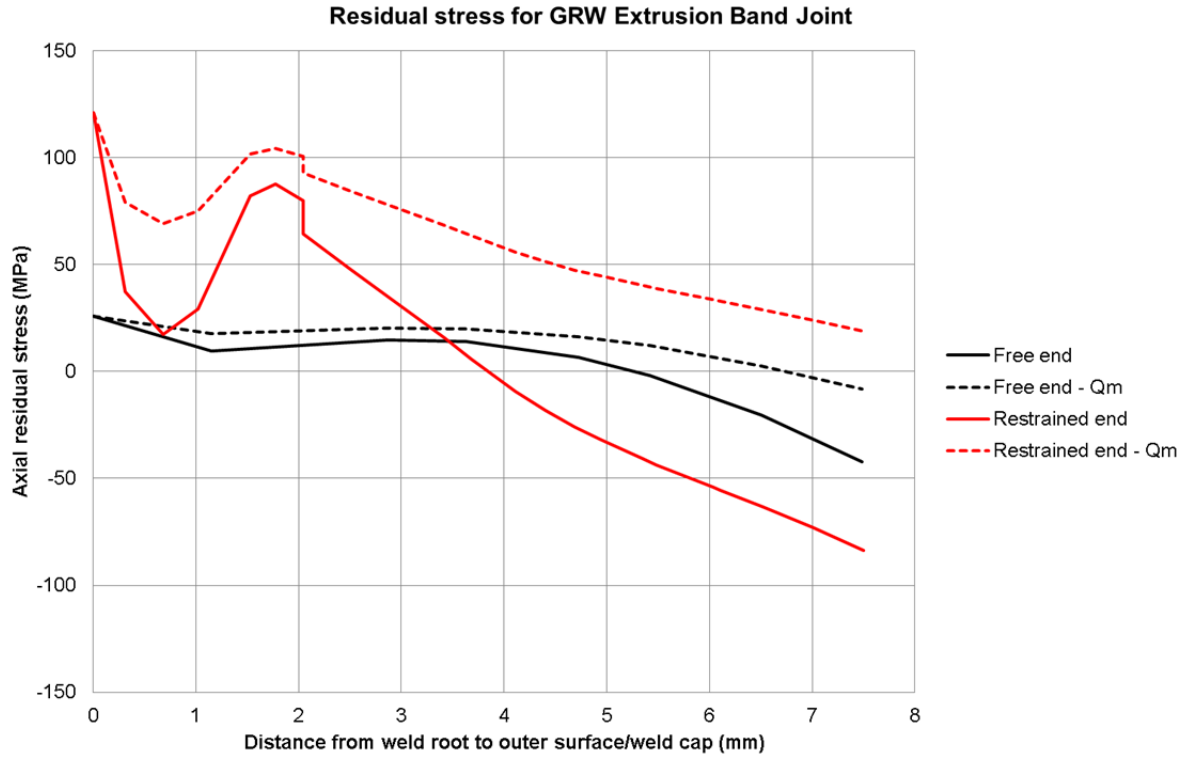

Figure 40 Transverse residual stress profiles (solid lines) and linearised membrane residual stress profiles (dashed lines) from Appendix G.

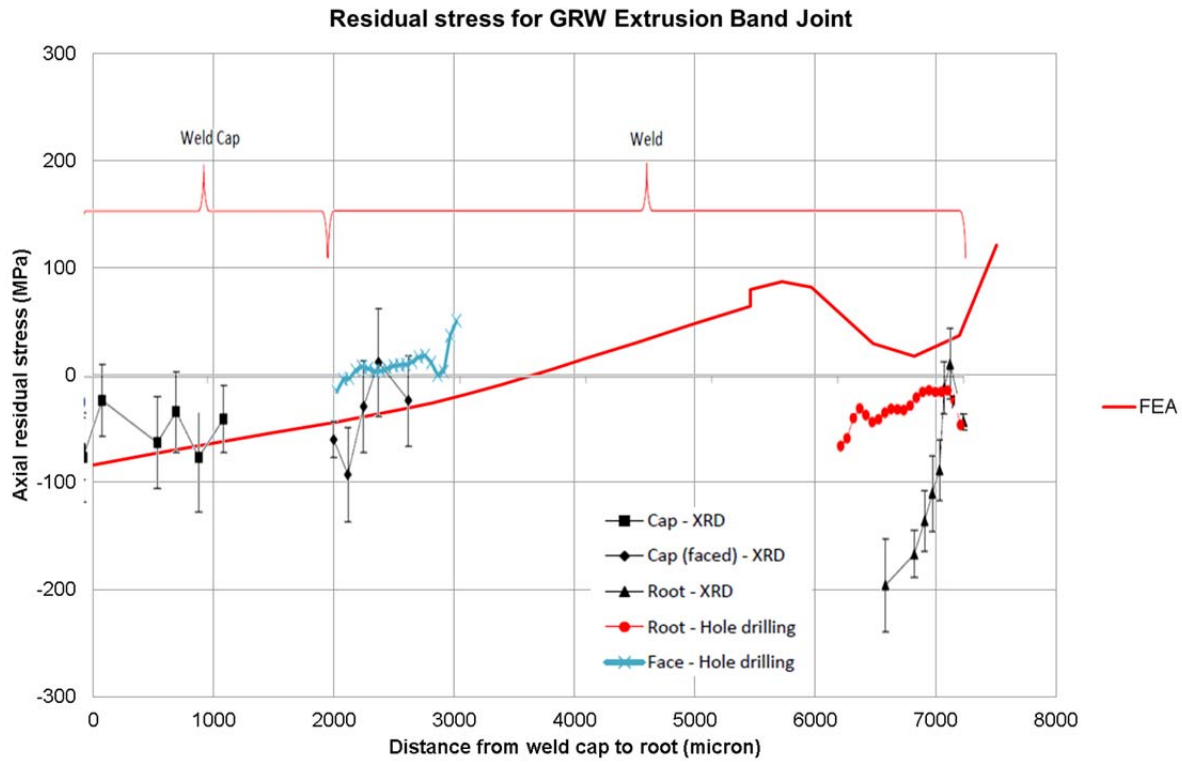

Figure 41 Comparison of the simulated welding residual stress pattern (solid red line) and the experimental measurements from (GRW, 2013d).

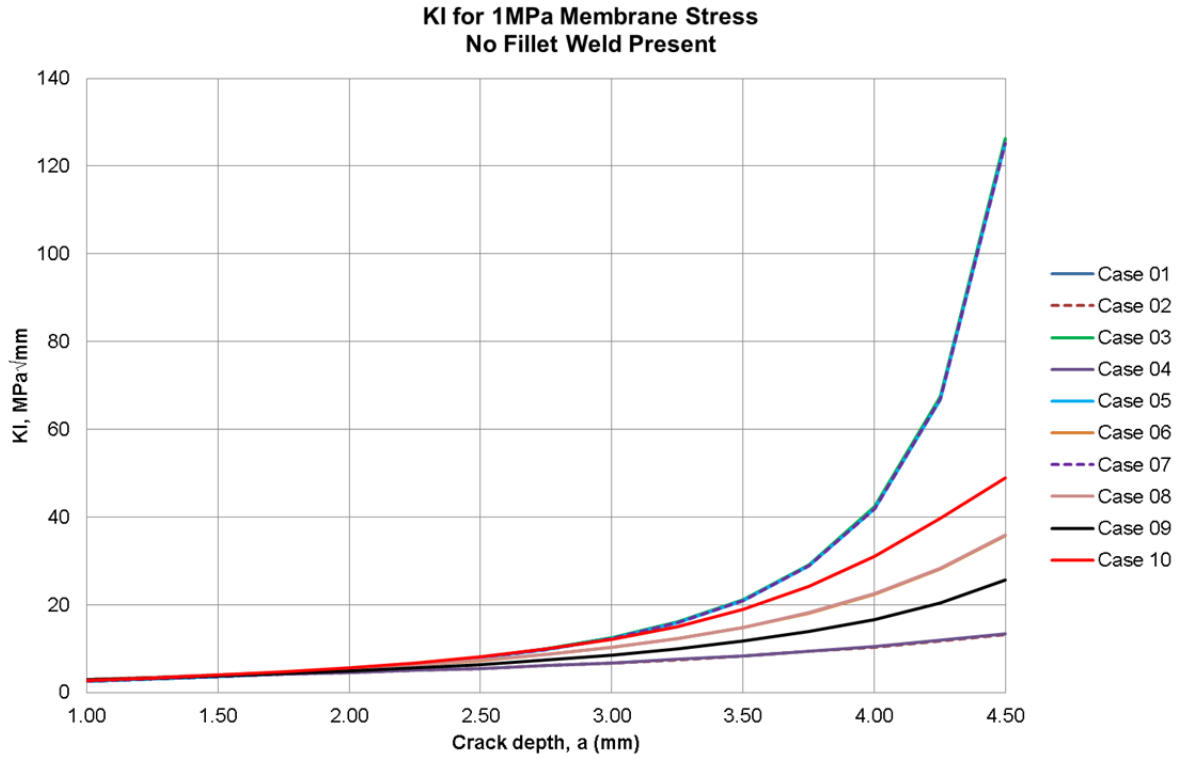

Figure 42 Comparison of stress intensity factors under 1MPa membrane stress without fillet weld.

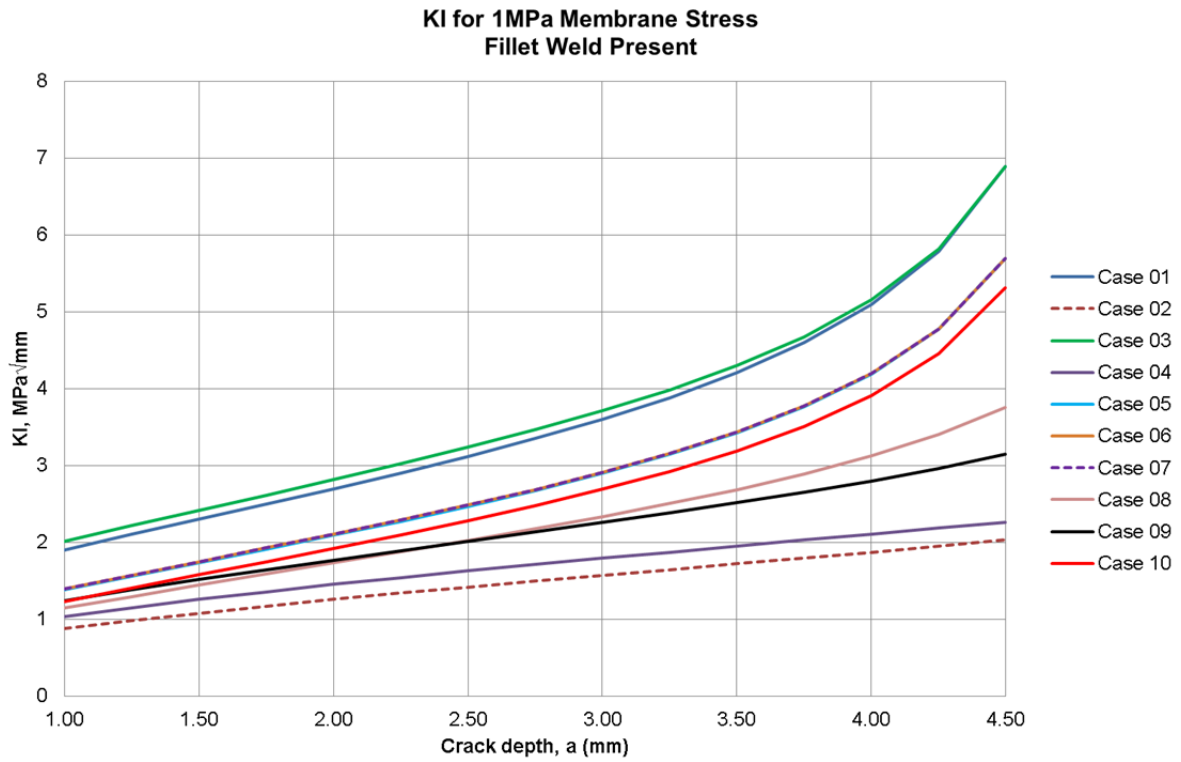

Figure 43 Comparison of stress intensity factors under 1MPa membrane stress with additional internal fillet weld.

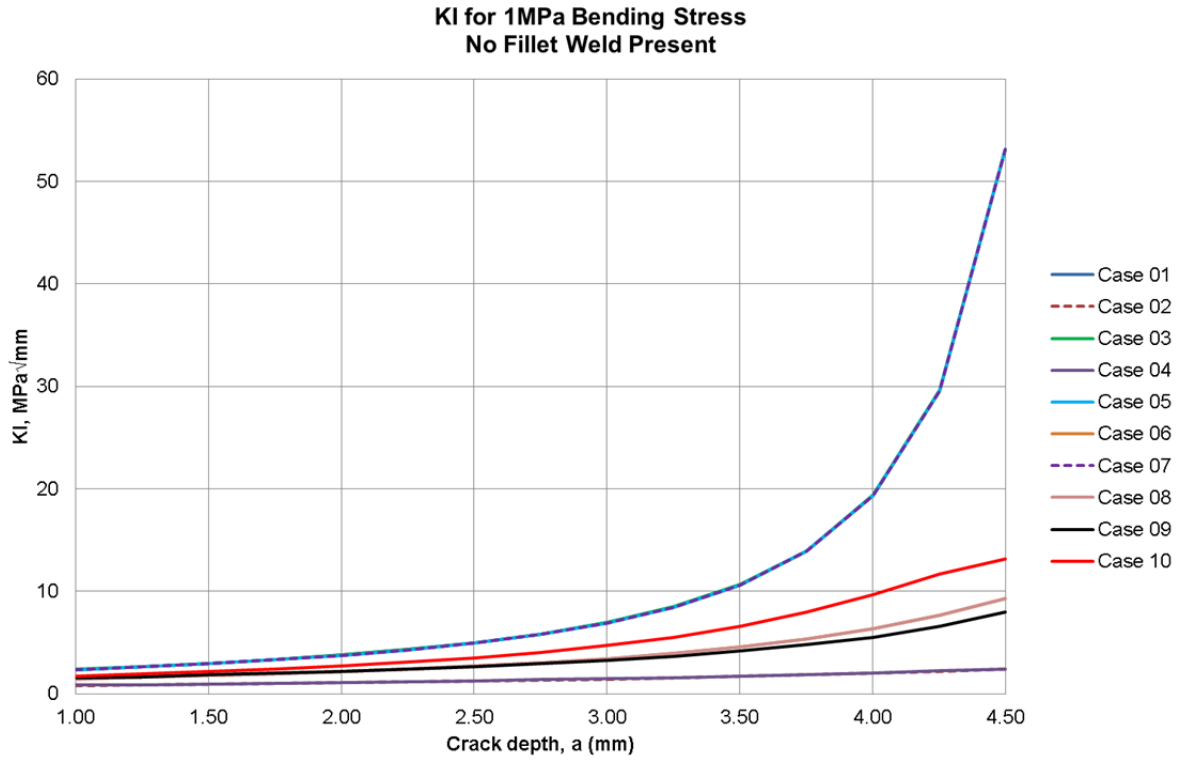

Figure 44 Comparison of stress intensity factors under 1MPa through-wall bending stress without additional internal fillet weld.

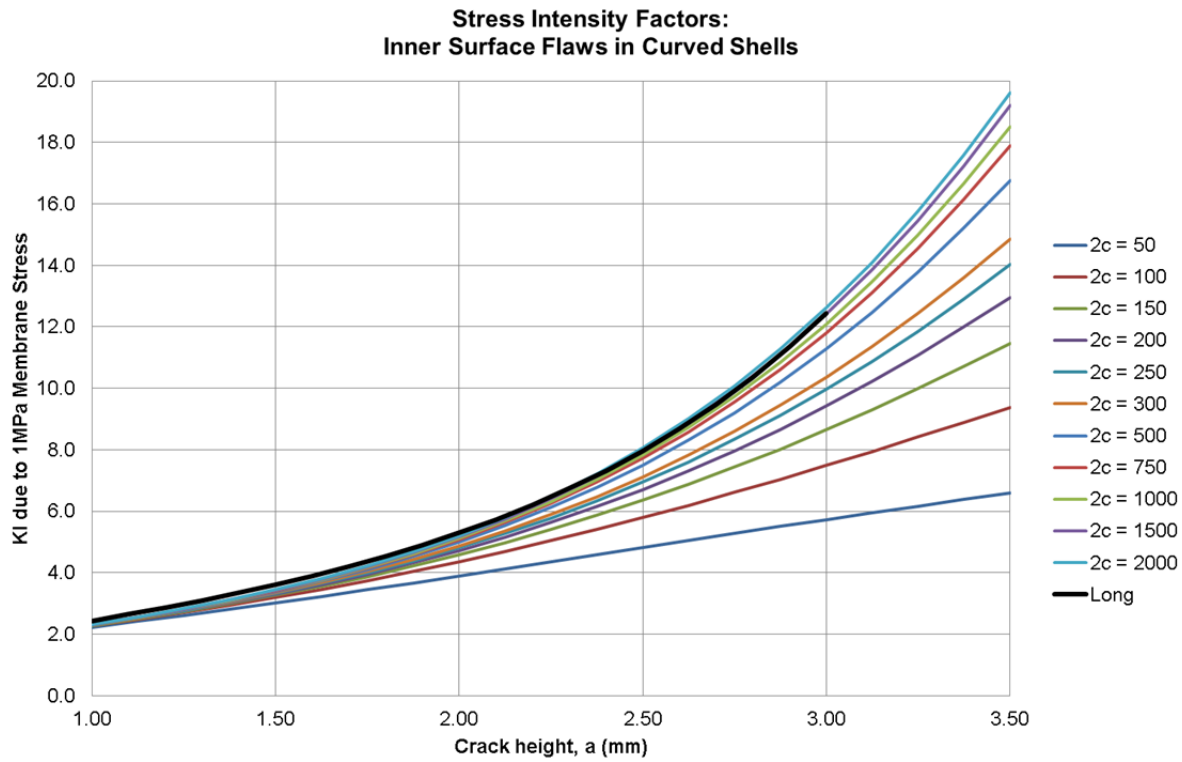

Figure 45 Stress intensity factor solutions for inner surface flaws in curved shells (BS 7910, 2013) under a 1MPa membrane stress.

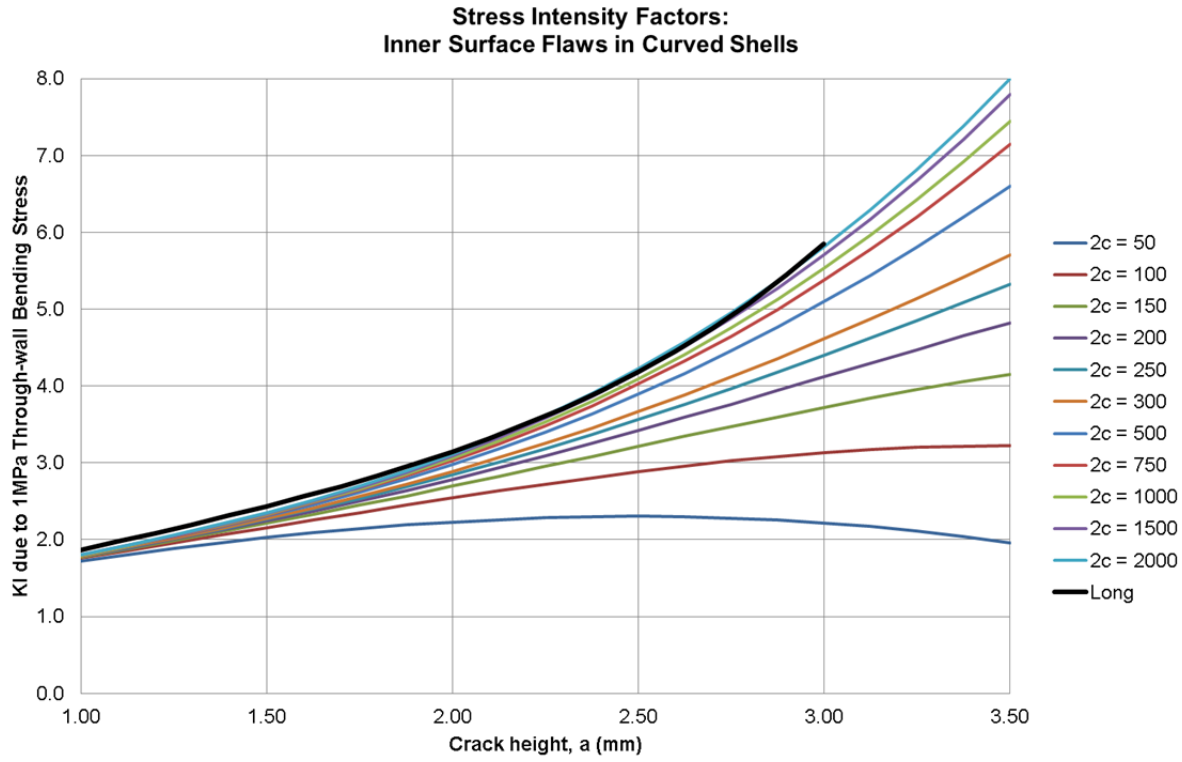

Figure 46 Stress intensity factor solutions for inner surface flaws in curved shells (BS 7910, 2013) under a 1MPa through-wall bending stress.

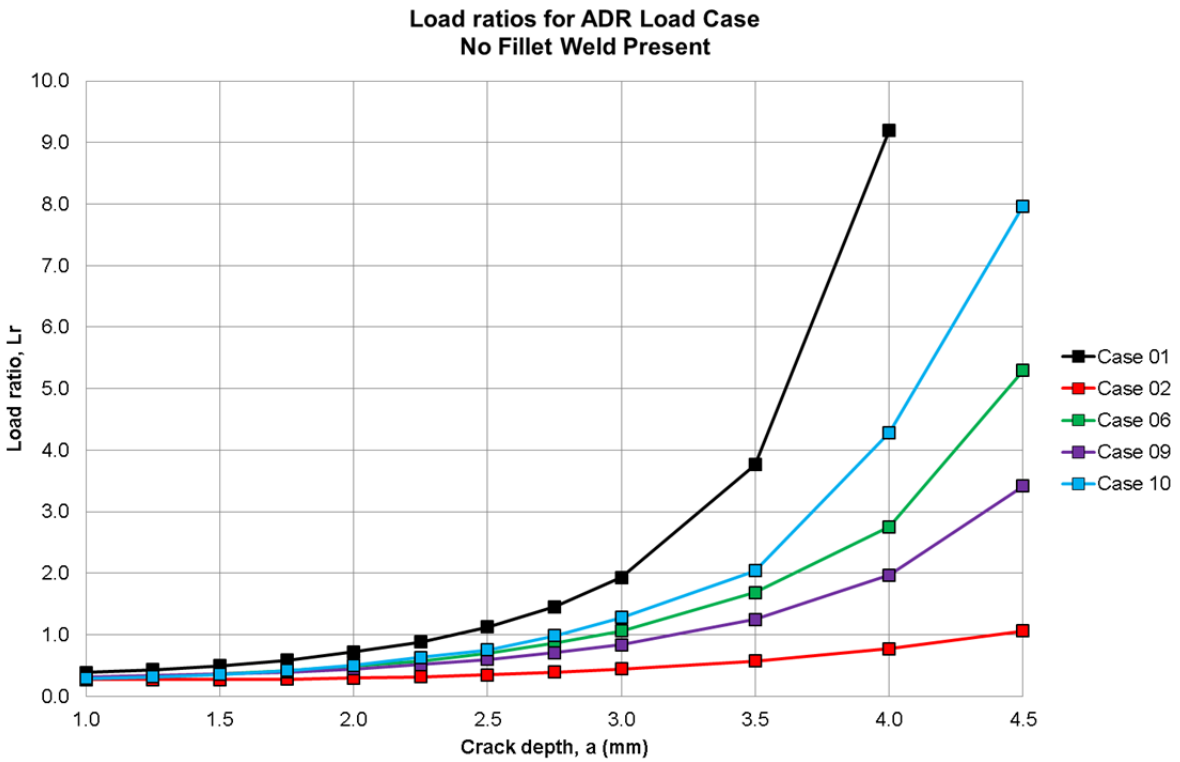

Figure 47 Load ratios for ADR load case without internal fillet weld present. Fully-circumferential flaw.

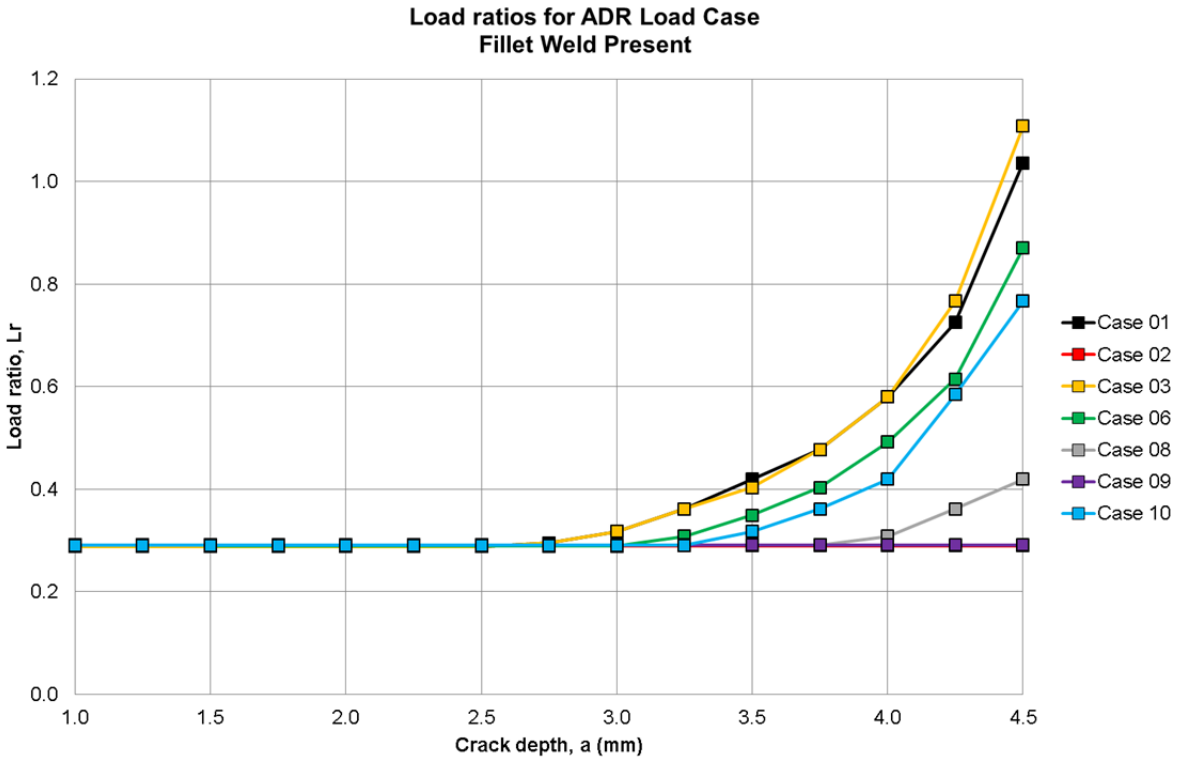

Figure 48 Load ratios for ADR load case with internal fillet weld present. Fully-circumferential flaw.

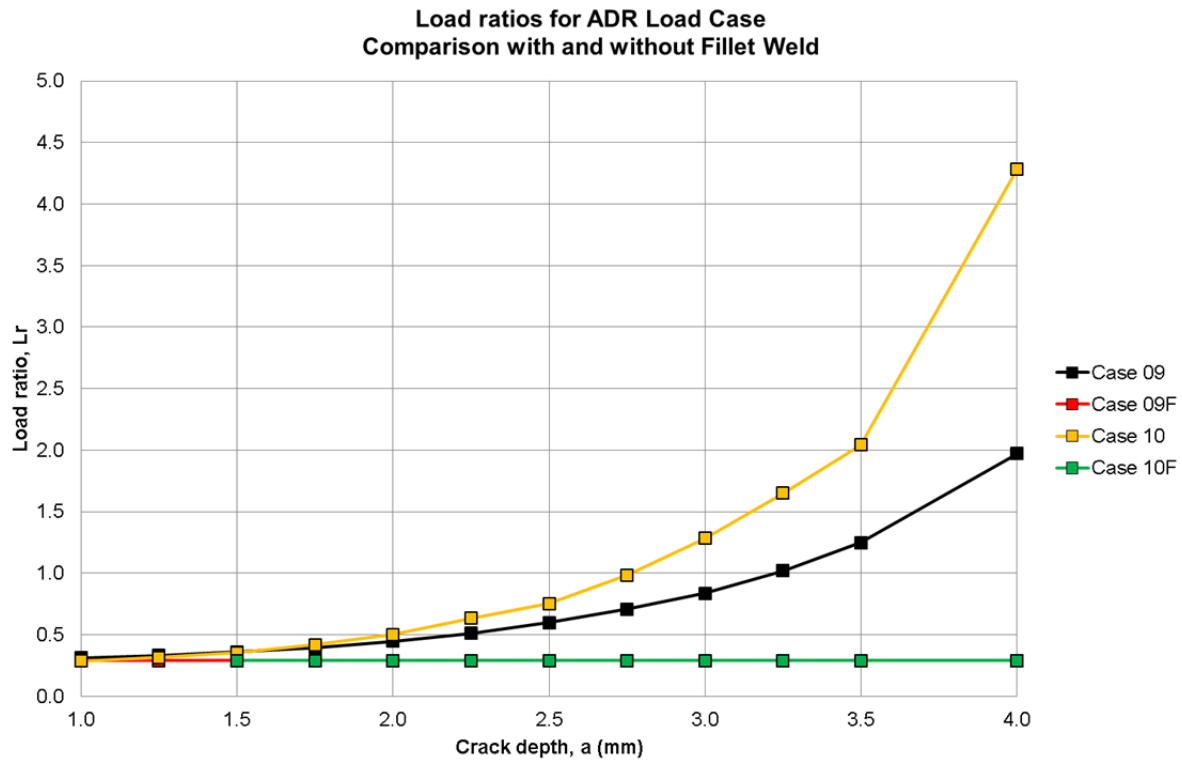

Figure 49 Comparison of load ratios for ADR load case.

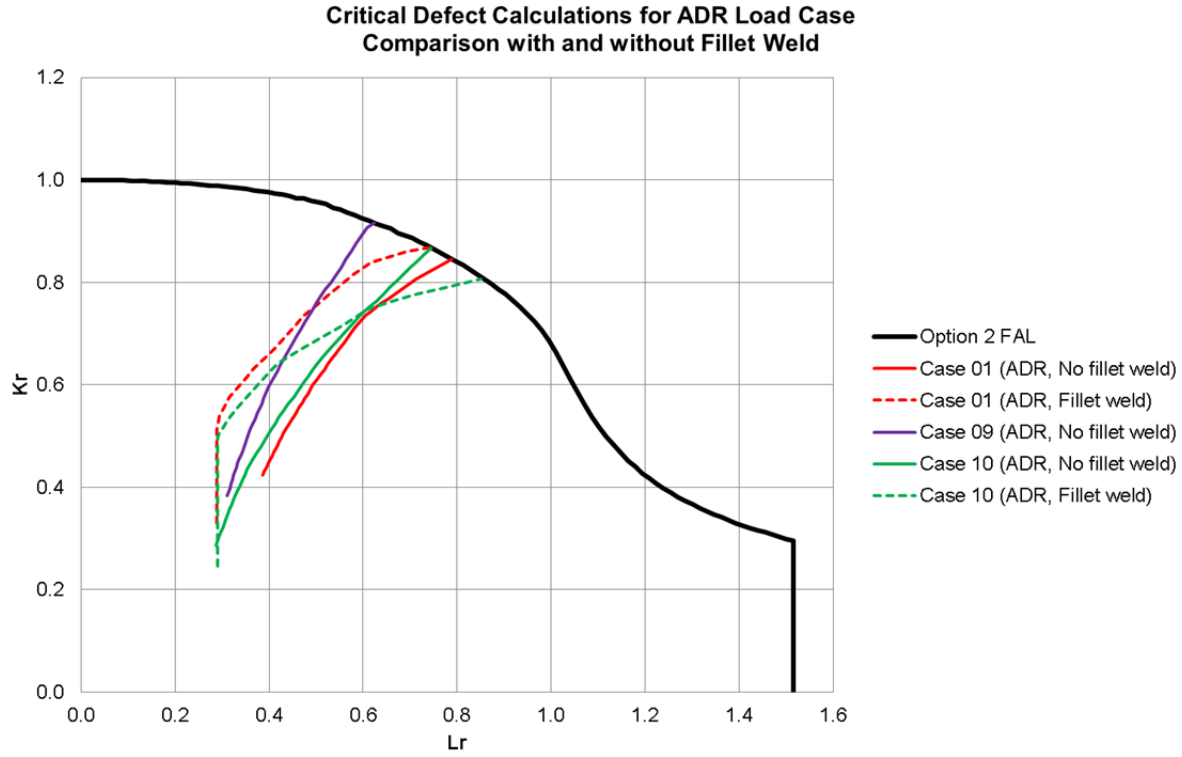

Figure 500 Failure assessment diagram for ADR load case. Initial point of curves is a 1mm defect.

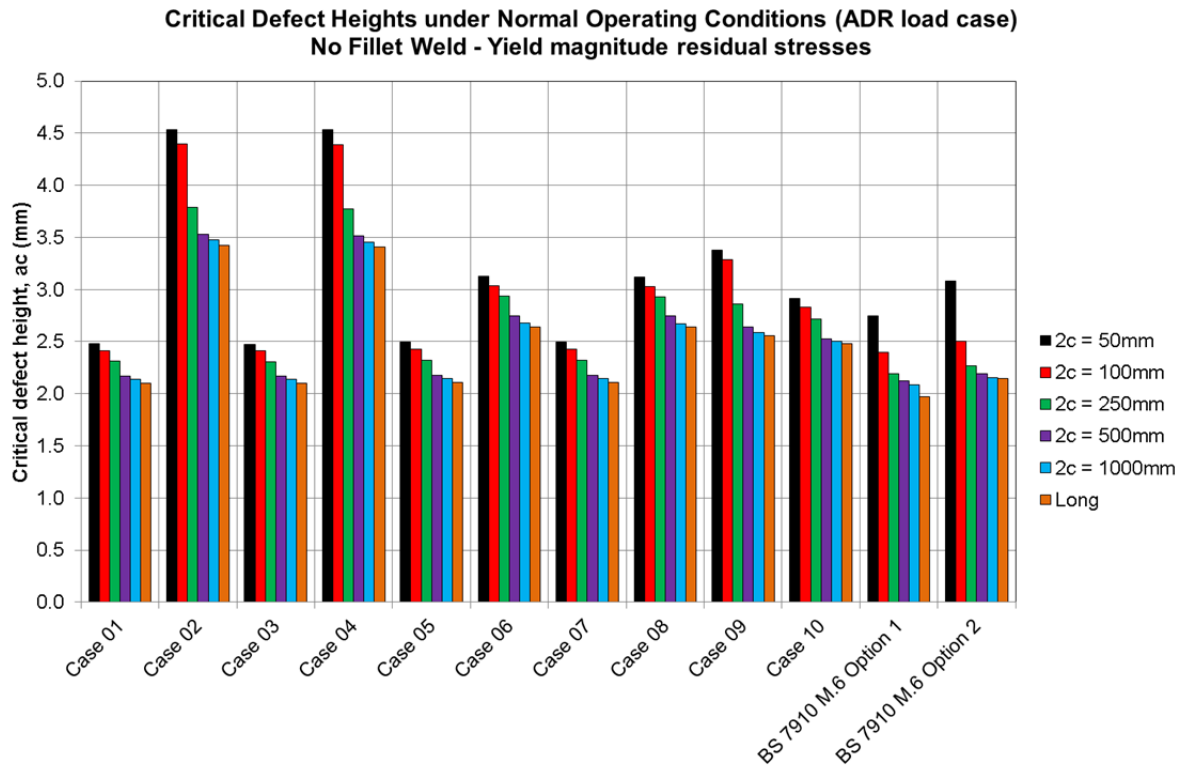

Figure 51 Critical defect heights for the ADR load case without an additional internal fillet weld.

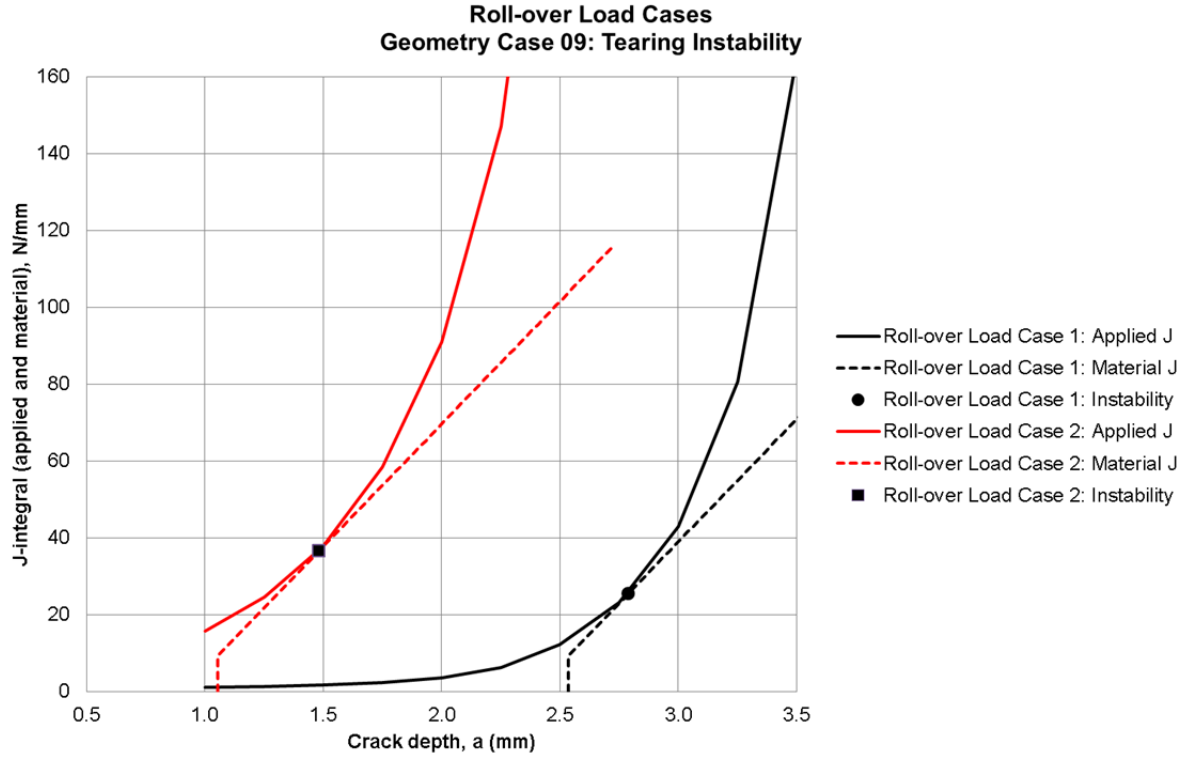

Figure 52 Determination of critical defect size for Geometry Case 09 for the two roll-over load cases.

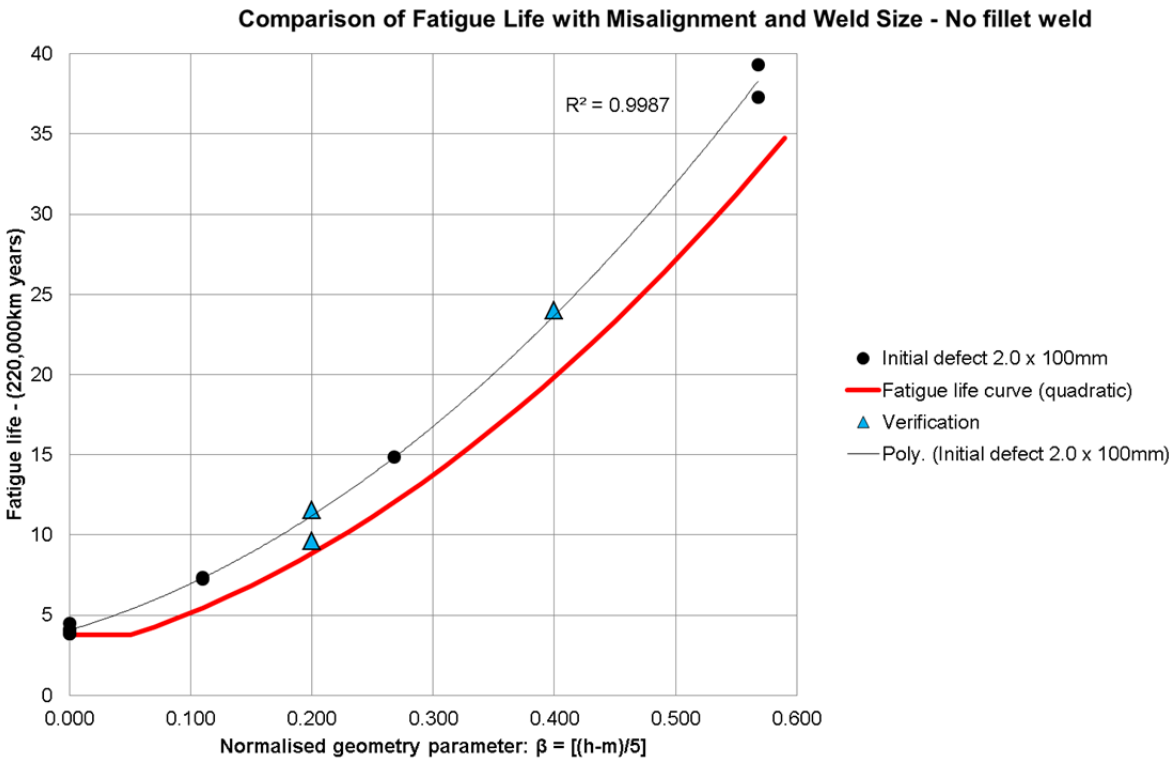

Figure 53 Lower bound fatigue life estimation curve, plotted against the non-dimensional geometry parameter β.

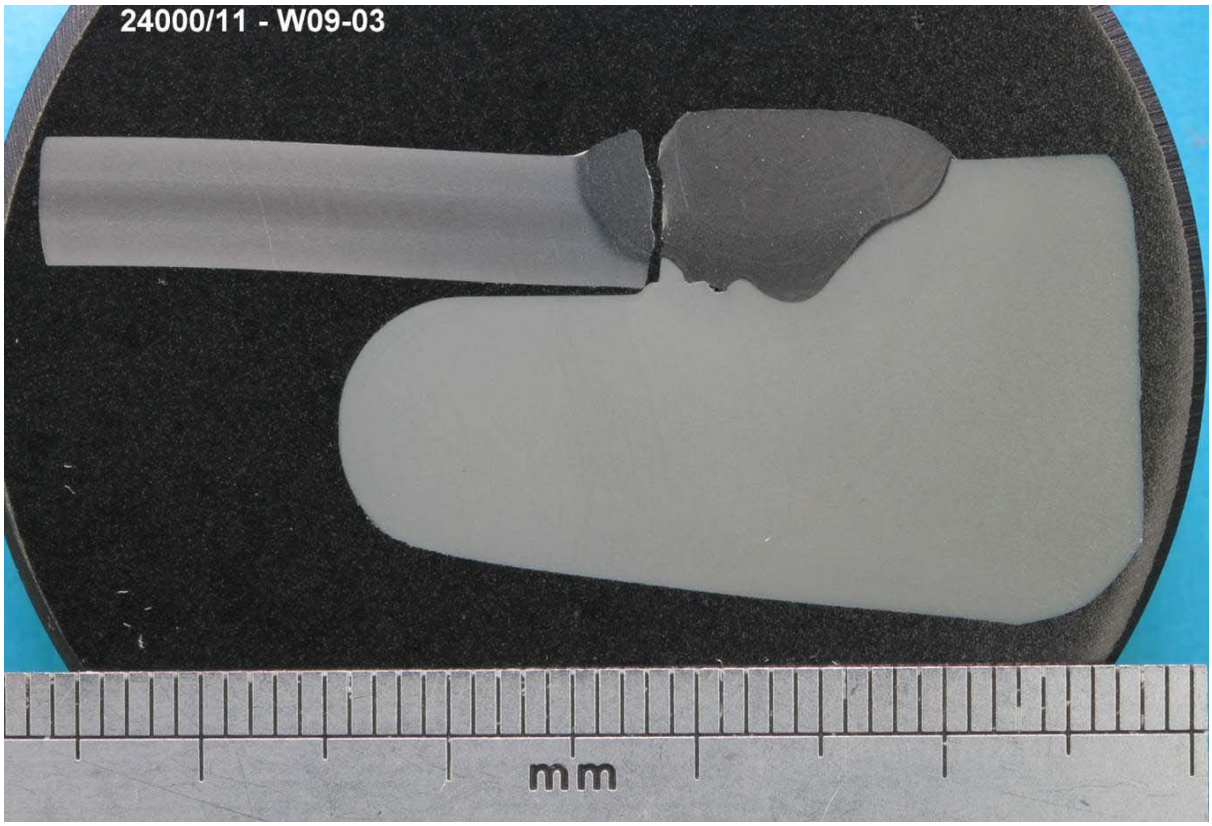

Figure 54 Cross-section of the sample from J2580 that ruptured through-wall thickness as a result of the lack-of-fusion defect at the positioner lip under the topple test experiment performed by HSL. Further details are provided in Appendix I.

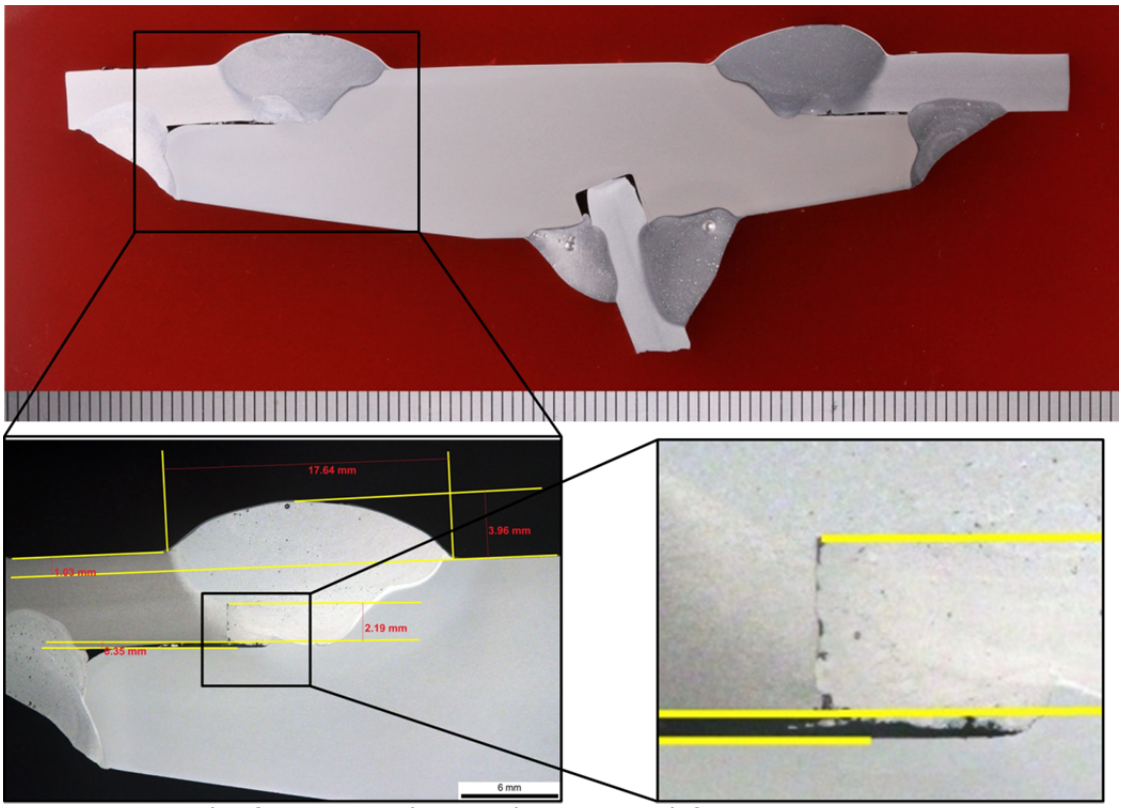

Figure 55 Samples from J3564 showing the 2.19mm defect.

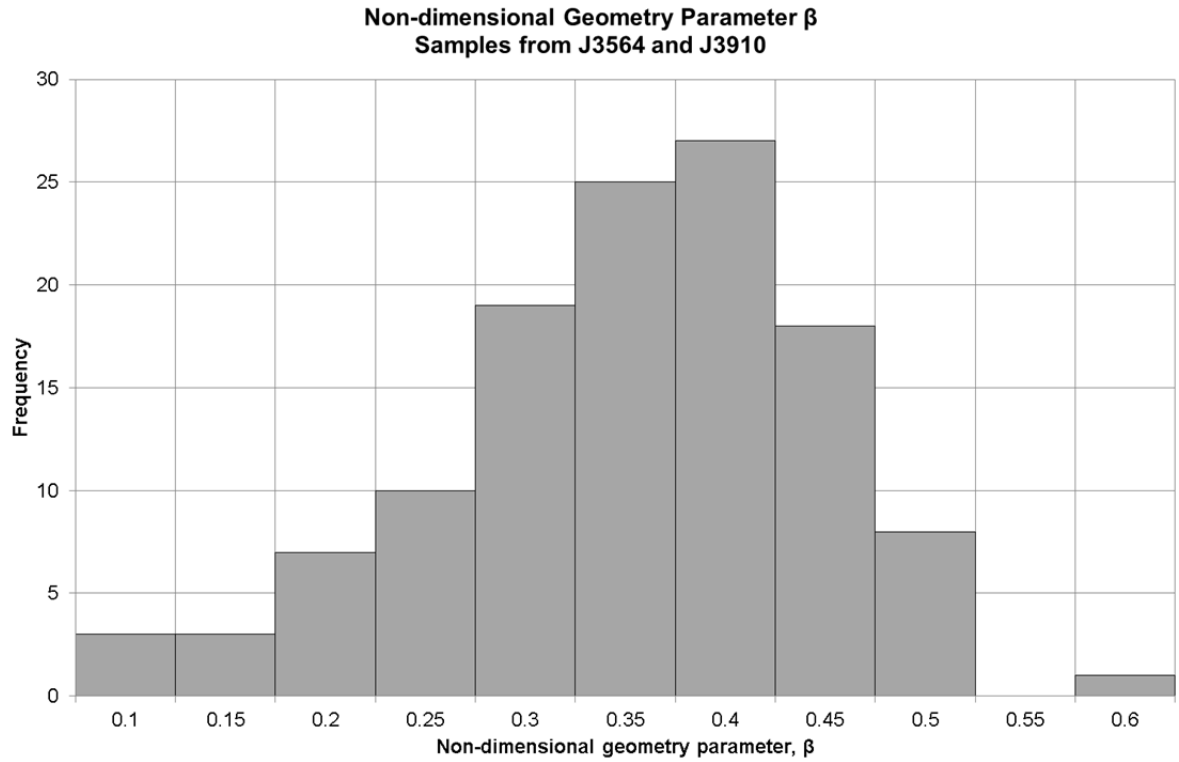

Figure 56 Histogram of non-dimensional geometry parameter β = (h-m)/5 for the J3564 and J3910 data shown in Appendix I. The data follows nearly a Gaussian distribution.

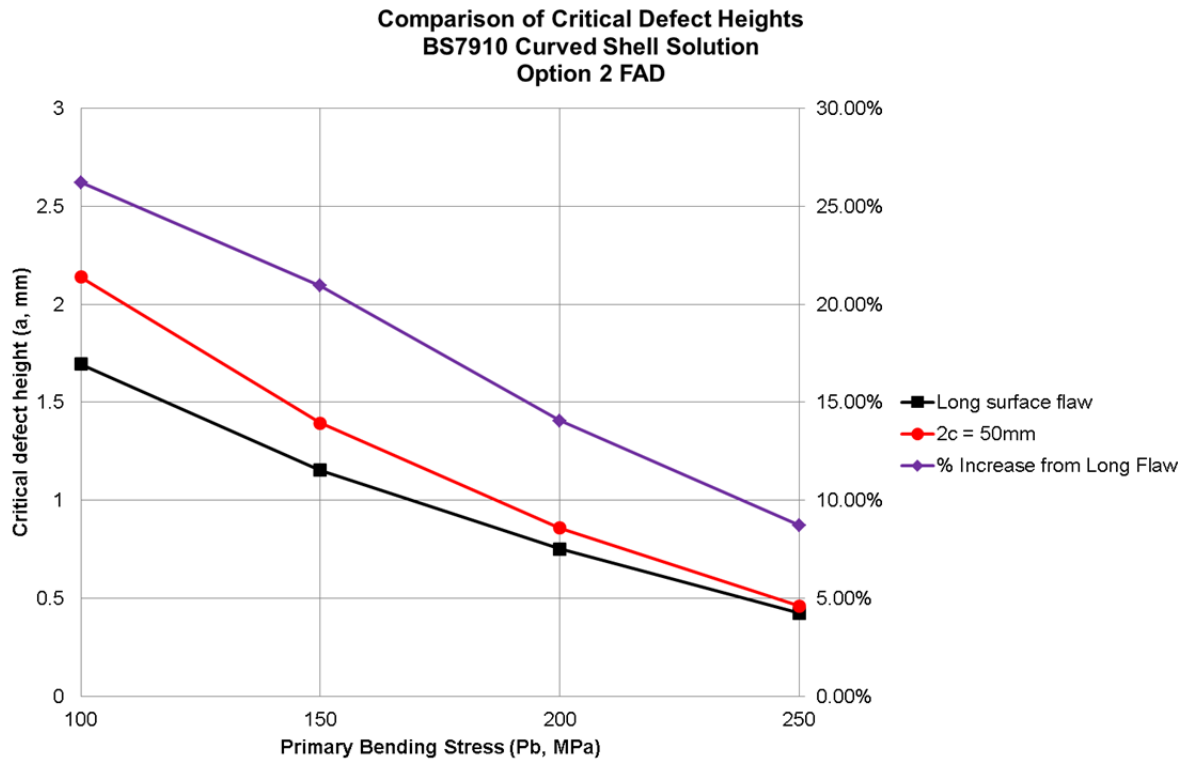

Figure 57 Comparison of critical defect heights for long flaws and finite length, 2c = 50mm, flaws using the BS7910 curved shell solutions under pure bending. Option 2 material specific failure assessment line employed with yield magnitude residual stresses and relaxation enabled.